THE UNIVERSITY *of* EDINBURGH

Synthesis and Characterisation of Luminescent Lanthanide Dyes for Solar Energy Conversion

Martina Congiu

A thesis submitted in fulfilment of the requirements
for the degree of Doctor of Philosophy
to the
University of Edinburgh
2013

Declaration

I hereby declare that this thesis has been entirely composed by myself and that the work described herein is my own except where clearly mentioned either in acknowledgement, reference or text. It has not been submitted in whole or in part for any other degree, diploma or other qualification.

Martina Congiu

February 2013

Giulia Congiu

Giovanni Usala

Acknowledgements

This thesis would have not been possible without the help and support of my supervisor Dr. Neil Robertson, who gave me the opportunity to work in his group. Thank you to Dr. Anita Jones and Tricia for taking me to the magic world of Photophysics. Considering that I graduated as a Medicinal Chemist, I think it was a pretty good journey. Thank you all.

A thank you goes to Prof. Bryce Richards and his research group, old and new, for letting me go to the labyrinthic Heriot-Watt University and use their instruments to carry out my spectroscopic measurements. So, thank you Serena, Thymios, Aruna, Sean, Paolo, Alessandro.

Thank you to Regione Autonoma della Sardegna for funding my research and to the University of Edinburgh for all the support that a postgraduate student can have.

A huge thank you to Robertson lab members, old and new. Especially to Charlotte: for all the kindness, smiles and hugs when I was feeling a bit down, for your chemistry help and for the grammar lessons. To Simon: thanks for helping me in the lab and for your posh English accent, it made my life a lot easier, especially during my first year! To Tracy and Nina: it was a pleasure to work with you and I could not have made it without your help and support. You have been more than just lab mates, thank you girls for your friendship. To Max and Alex: the only two people who actually stopped my conversations giving me grammar tips. Thanks for that, it helped me a lot. And thanks for the laughs and jokes (although it was pretty much Haggis saying something and Lasagna making him repeat it thousand times). To Georg: for the idea of buying Nepresso coffee machine (but Lavazza will always be better! By the way, have you started writing yet?). To Jennifer and Matt: not Robertson lab members but still in the "neighbourhood". To Emiy and Ioanna for the office chats.

For all of this, thanks guys! You made me feel welcomed and part of the group.

A special thank you to the Post Docs of the group and their (apparently) superior knowledge that you managed to obtain once you get a PhD (I will see whether this is true or not in the near future). To Miquel: for the Chemistry tips, I wish you had joined the group before, my lab work would have been much easier. Thanks for every chat we had and for your support especially in these last months of my PhD. I will not mention you are also a gossip expert... Ops, I did it. To Luca: coming from Sardinia it was not enough, I also had to become your Godmother to make this bond stronger! Well, I cannot thank you enough for being my friend these past two years and a half since you arrived I felt less homesick. Saying something in Italian, and saying it again in Sardinian it is a completely different thing, am I right? Thank you Luca.

I am heartily thankful to my best friend Cristina, the pillar of these four years of life in Edinburgh. I would probably have gone crazy without you! Thank you for the food, for the shopping days, for sharing your flat with me, for our (amazingly organised) holidays. I hate you for your never ending late night chats, but I love you for everything else. Thank you Cristina!

Moving away from chemistry I send out my thanks to the Italian connection, here and elsewhere. To Alessandro (*su sposu*) Ceroni, Davide Espa, Roberta Carloni, Mario Buono, Carlo Pirozzi, Rossella Guerrieri, Tiziana Gentilesca, Diana Papini, Manuela Marescotti, Giulia Vargiu, Adriana Gambardella, Giuseppe Cannone, Nicola Festuccia, Luciana Mantovani, Simona Paro, Fabio Pucci, Gabriele Meloni, Antonio Delussu, Rita Meleddu, Marta Montisci, Giorgia Fugallo, Walter Tarantino, Barbara Loddo.

The biggest thank you goes to my parents, who encouraged me during this path and to follow my dreams. To my brother, who decided not to attend university and now he is mocking me because he has a real job, and to my little sister, who keeps stealing my clothes thinking that I am getting old and I do not remember something is missing… I am so lucky to have you as my family.

Last but not least… thank you Scotland! Same number of sheep as in Sardinia, different range of temperature, but still the best choice I have ever made when I decided to move from my lovely island.

Abstract

Lanthanide (III) complexes are used extensively in solar conversion devices, such as Luminescent Solar Concentrators (LSCs) and Luminescent Down-Shifting (LDS) for their peculiar characteristics of narrow band emission, avoidance of re-absorption losses due to large Stokes shift and possibility of high photoluminescence quantum yield (PLQY).

The study has looked into the synthesis of Ln (III) complexes of the general formula: [Ln(hfac)$_3$DPEPO], where DPEPO = bis(2-(diphenylphosphino)phenyl)ether oxide, and hfac = hexafluoroacetylacetonate. The work presented in this thesis focuses on the synthesis, and subsequent photophysical characterisation of these Ln(III) complexes, plus characterisation and spectroscopic study of [Tb(pobz)$_3$(hacim)$_2$], (where Hpobz = phenoxybenzoic acid, and Hacim = acetylacetone imine), yielding results that open new design of functional Ln(III) systems.

Spectroscopic study of Chromium dioxalate and analogous compounds has revealed that with the appropriate design, Cr(III)→Ln(III) energy transfer can be achieved, while study of polyaromatic hydrocarbons (PAH) such as coronene, enable to explore a ligand with better absorption in the whole UV region. These results open attractive perspectives for light-conversion systems, such as LSC devices.

Contents

List of Figures

Chapter 4: Chromium dioxalate and analogue compounds

Chapter 5: $[Tb(pobz)_3(hacim)_2]$ and $[Tb(bz)_3(hacim)_2]$ complexes

List of Tables

Chapter 6: Potassium Coronene Tetracarboxylate salt and its interaction with Europium (III)

Publications

E. Klampaftis, M. Congiu, N. Robertson, B. S. Richards, Luminescent EVA Encapsulation Layers for Enhancing the Short Wavelength Spectral Response and Efficiency of Silicon PV Modules, IEEE Journal of Photovoltaics, 2011, 1, 29-36

Abbreviations

AM	Air mass coefficient
bpy	2,2′-bipyridine
CdTe	Cadmium telluride
DCM	Dichloromethane
DFT	Density functional theory
DPEPO	Bis[2-(diphenylphosphine)phenyl] ether oxide
EtOH	Ethanol
EVA	Ethylvinyl alcohol
Hacim	Acetylacetone imine
Hfac	Hexafluoroacetylacetone
HOMO	Highest occupied molecular orbital
Hpobz	Phenoxybenzoic acid
LDS	Luminescent Down-Shifting
LSC	Luminescent Solar Concentrator
LUMO	Lowest unoccupied molecular orbital
MeOH	Methanol
MLC	Mixed ligand compound
OLEDS	Organic light-emitting diodes
phen	phenanthroline
PLQY	Photoluminescence Quantum Yield
PMMA	Poly(methyl methacrylate)
PVA	Polyvinyl alcohol
RECP	Relativistic effective core potential
TDDFT	Time-dependent density functional theory

Chapter 1: Introduction

1.1 Energy demand

Energy demand is constantly increasing in the modern industrialised world and a 53% increment of energy consumption is predicted from 2008 to 2035 (from 532 EJ (exajoules) to 812 EJ),[1] related to all human activities that modern society requires. Energy consumption is mainly based on fossil fuels, which have a negative impact on the environment.[2] Fossil fuels are organic molecules generated million of years ago by living organisms that were buried under sediments and, through high temperature and pressure, were transformed into compounds with high energetic content.[3] Their use gives rise to several disadvantages. First, fossil fuels are a non-renewable source of energy, so they are limited.[4] We cannot rely completely on them for our future demands, because it will take millions of years for them to re-form, and they will be exhausted faster than new deposits are formed. Secondly, burning fossil fuels means production of different oxides, with carbon dioxide being the main gas responsible for the greenhouse effect, hence global warming and climate change.[5-7] Third, irregular distribution of fossil fuels leads to economical disparity among countries.[2, 5]

Predictions about consumption of fossil fuels are not positive and many concerns in different parts of the world have risen about security and environmental impact due to the use of non-renewable energies.[2] The use of all types of fossil fuel is always

followed by a consequent increase in its price due to their consumption.[5]

Below is a predicted scenario for each:

- Oil still is the most used type of energy source and is expected to grow in usage from 85.7 million barrel per day in 2008 to 97.6 million barrel per day in 2020.[1]
- Coal has been used at a consumption rate of 5.9 Gt/year[8] with an estimated reserve of 800 Gt,[9] with a related huge amount of CO_2 production of 750g per kWh.
- Natural gas use is increasing with a 2.6% increment per year.[1] It is cleaner than other fossil fuels, having a production of CO_2 which is 26% lower than oil and 41% lower than coal.[5]

In order to address problems that arise from energy consumption and global warming, different strategies have been adopted. Nuclear power has been pointed out as a valid opportunity. The nuclear energy per atom that we can obtain is about one million times bigger than that produced from a molecule of fuel. Nevertheless, many problems have arisen such as higher overall lifetime costs, safety, environmental and health consequences and radioactive waste,[4, 10] especially after the accident that occurred in Japan on 11 March 2011, caused by a 9.0 magnitude earthquake followed by a tsunami.

The most appealing possibility is to use renewable energies as power sources, which will lead to prolonging the life of oil and natural gas and which are environmentally

more suitable and reduce the fear of energy security.[7] The European Union set a goal of decreasing greenhouse gases of about 20% by 2020 increasing renewable energy use up to 20% by 2020.[11]

1.2 Solar energy

We usually ask ourselves how long will fossil fuels last and how can we avoid their large-scale use, to reduce carbon dioxide emission. The renewable energy market is constantly in expansion and the renewable share of the total energy supply in 2010 was 16.7% (over the total energy consumption worldwide). Across all renewable industries, wind power had a high impact in 2011 with about 40% of usage, followed by an impressive market growth of solar photovoltaic (PV), with about 30% of usage. Biomass also showed a large improvement especially for heating and transportation (wood pellets, biodiesel and ethanol).[12]

Solar energy (thermal and photovoltaic) is the most promising source that we have; actually, the sun can provide a year of human energy requirements with just one hour of light. In fact the average incident solar radiation (>120,000 TW) goes beyond the power demand of the world population (15 TW)[13]: With a coverage of only 0.16% of the Earth surface, it would be necessary to use 10% efficient solar converters to have 20 TW of power for human activities.[14] Moreover, solar energy is clean and safe, and it is an unlimited source of power; so it is evident that harvesting a small portion of sunlight would help our energy demand with a good

environmental impact.[4]

1.2.1 Solar technologies

Solar technologies aim to actively harvest sunlight and increase the use of solar energy in the modern world. Solar energy needs to be initially captured and converted, then used or stored. Active and passive transformation of solar energy can be achieved: active conversion is mainly accomplished by photovoltaics (PV), while passive collection generally happens in buildings and architectures with thermal and illuminative passive harnessing.[5]

The photovoltaics market is dominated by so called first generation photovoltaics, which were first developed more than 50 years ago by Bell Laboratories (New Jersey),[15] obtaining an efficiency of 4% and improving it to 14% by 1960.[16] One of the most efficient attempts to harvest sunlight has involved the fabrication of silicon *pn*-junction solar cell. In these devices the semiconductor is *p*-doped with boron (which has one less valence electron than silicon) and *n*-doped with phosphorus (which has one more valence electron), in order to allow the carriers to diffuse across the junction.[17] Despite current capital costs, their good efficiency of up to 24.7%,[18, 19] will allow them to become cheaper than fossil fuel electricity, which is already happening in Germany and Italy, where grid-parity has been reached since 2009. [20] Gallium arsenide (GaAs) has also been developed as a material for solar cells but the high level of purity required for this material does not permit its widespread use

despite its good efficiency (18.7%).[21]

To reduce the cost of manufacturing, a second generation of photovoltaics has been introduced, which consist of deposition of a thin film of photo-active material on top of a substrate (rigid or flexible). Materials used are usually amorphous silicon (a-Si, 10% efficiency),[22] copper indium gallium diselenide (CIGS, 19.6%)[23] or cadmium telluride (CdTe, 16.5%).[24]

PVs of third generation still use second generation thin-film technology but aim to reduce costs per Watt.[25, 26] Apart from improving already existing tandem cells (by applying layers of cells one on top of another), third-generation photovoltaics include technologies such as hot-carrier cells (that creates many electron-hole pairs per photon) and thermophotovoltaic conversion devices.[25] 32% efficiency of third-generation PV was reached in 1999 by Karam *et al.*[27] with a thin-film GaInP/GaAs/Ge triple-junction space-PV for satellites (too expensive for terrestrial applications, but with high potential for improvement). Practical application with lower cost is the achievement of Kaneka's 11.7% micromorph a-Si/μc-Si heterostructures.[28]

A portion of the market is also occupied by organic solar cells which can overcome the manufacturing problems of inorganic materials such as high cost deposition of inorganic layers.[29] The research community have widely investigated in organic semiconductor materials such as P3HT (electron donor) and PCBM (electron

acceptor).[30, 31] Their use as active layers in organic photovoltaics have been really successful especially when the two materials are blended.[32] These polymers are easy to synthesised and able to be processed in solution.[31] Therefore, using organic materials could make the manufacturing process cheaper, enabling large-scale production to be available due to an infinite variety of organic compounds, and additional features such as flexibility.[29] The really high absorption coefficient of many organic absorbers (10^5 cm^{-1}) is appealing despite the generally lower charge-carrier mobility and low stability[33, 34]and the prospect of low-cost, large-scale devices has led to significant research in this direction to improve this technology.

As we have discussed, it is possible to improve and implement usage of PV technologies if their cost becomes affordable and their efficiency increases. Since photovoltaic development is mainly based on enhancing material properties, research has been focused on the active layer of PV devices.[35]

1.3 Spectral conversion applied to photovoltaic technology

From Figure 1.1 below we can see the broad wavelength range of the solar electromagnetic spectrum. Specific absorption bands within the atmosphere reduce solar radiation at certain wavelengths. For example, the stratospheric ozone layer prevents a high portion of UV radiation from reaching the Earth. In this context, it is a convention to use air-mass (AM) to define solar radiation, where AM is the optical path length of extraterrestrial light that reaches the Earth through the atmosphere.

AM0 indicates the solar radiation spectrum outside the atmosphere (Figure 1.1 yellow part), while AM1.5 is referred to radiation at sea level (red part), with a solar zenith angle of 48.2°, which is used to characterise terrestrial solar panels.[36]

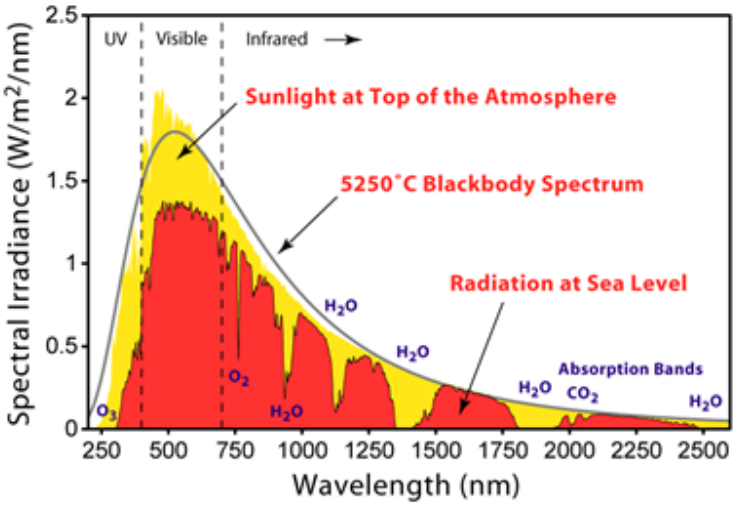

Fig. 1.1. Solar spectrum.[36]

The basic principle of all photovoltaic technology is to harvest sunlight with maximum efficiency while reducing the costs of manufacturing, making solar energy more available to everyone. Systems for spectral conversion belong to third-generation photovoltaics and are mainly focused on Concentrated Photovoltaics (CPV).[37, 38] Different technologies can be mentioned, such as concentrating tracking mirrors or lenses, which focus sunlight onto a small area of PV cell. In this case it is important to dissipate heat produced during performance to avoid degradation of the module.[39] Commercial systems are available (efficiency of about 25%) with opportunities for improvement.[40]

Luminescent Solar Concentrators (LSCs) are another innovative concept, which consist of a thin plastic layer doped with luminescent materials that absorb sunlight at a certain wavelength and re-emit photons at an appropriate wavelength for PV energy conversion.[41, 42]

1.4 Luminescent Solar Concentrators (LSCs)

Developed in the late 1970s, LSCs faced the growing energy needs of the planet by focusing on new low-cost photovoltaic systems, which could replace the more expensive silicon solar cells and meet the environmental concerns about fossil fuel use. LSCs were proposed firstly by Weber and Lambe[43] and others[44] as an attractive feature in renewable energy. In the 1980s interest in these devices decreased a little due to the sudden oil price drop, but the recent situation regarding fossil fuel use, make their research again appealing in different parts of the scientific world.[45]

Different characteristics make the LSC a very promising device. First of all they have a potential low cost production[46, 47] Their adaptability to different architectures, with several colors and shapes, light weight and possible improvement in flexibility, make them attractive devices for building integration and energy saving.[48-51] Moreover, the LSC working principle does not depend on whether the solar radiation is direct or diffuse: they can be used even in those areas where the climate is mostly cloudy and where fixed and tracking mirror concentrators are not suitable.[43, 52, 53]

LSCs still need a photovoltaic portion in order to convert the light into electricity. The advantage of using LSCs is that we have a much smaller portion of photovoltaic converters to be fed by the incoming light trapped and refracted through the doped luminescent layer.[47]

1.4.1 Working principle of LSC

LSCs are optical devices which concentrate the sunlight collected over a large transparent surface of luminescent material, with subsequent transfer to the thin edge of the concentrator, covered by photovoltaic cells.[46] Fig. 1.2 shows the working principle of this system. The incident light is absorbed by a fluorescent dye molecule contained in a large transparent sheet. Once absorbed, the light can be re-emitted at a longer wavelength, possibly without overlapping with the absorption spectrum, and transported through total internal reflection (TIR) to thin photovoltaic cells on the edge of the plate, which convert the concentrated energy into electricity. Of course some loss mechanisms occur during this process, such as front surface reflection (1), transparency of the matrix material (2), self-absorption of emitted light by the dye molecule (3), scattering (4), and escape cone losses at the surfaces.[54]

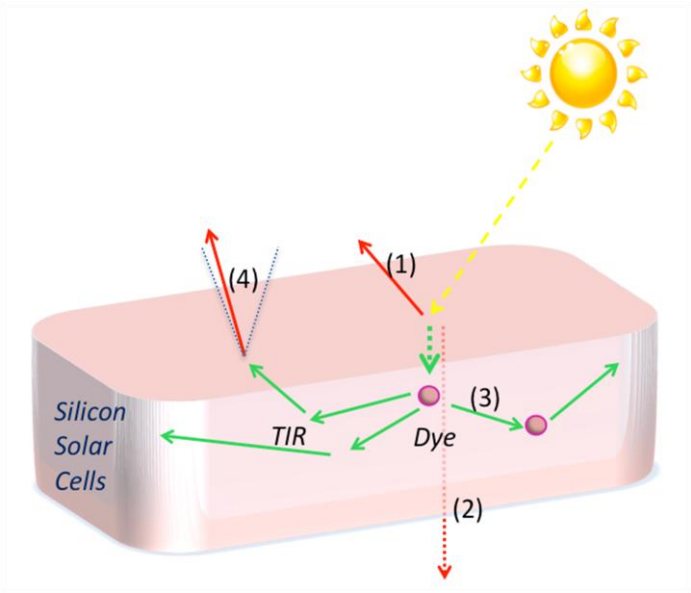

Fig. 1.2. LSC working principle: TIR = Total Internal Reflection; (1) = reflection; (2) = material transparency; (3) = re-absorption; (4) = light scattering.

The transparent material used is crucial in the development of LSCs. The most commonly used waveguides are polymethylmethacrylate (PMMA) and polycarbonate (PC), usually chosen because of low cost, simple preparation, with excellent optical quality. Considering that the light absorbed is trapped in the waveguide, particular attention needs to be given to its refractive index (n): material with refractive index of 1.5-1.6 will allow total internal reflection of about 75% of the photons emitted.[41] PMMA (n = 1.49) and PC (n = 1.59) have been demonstrated to have good transmission characteristics.[55] All polymers will possess some matrix losses related for example to parasitic abosrption by the host polymer,[41] degradation due to exposure to UV light,[56] imperfection of the material surface.[57] Another polymer used is polysiloxane, as it could improve the flexibility of LSCs, but its durability still needs to be improved.[58]

The efficiency of an LSC is determined by different factors as shown by the optical efficiency equation:

$$\eta_{opt} = (1\text{-}R)P_{TIR} \cdot \eta_{abs} \cdot \eta_{PLQY} \cdot \eta_{Stokes} \cdot \eta_{host} \cdot \eta_{TIR} \cdot \eta_{self}$$ [41]

where R is the reflection of solar light at the waveguide surface, P_{TIR} is the total reflection efficiency, η_{abs} is the fraction of light absorbed by the dye, η_{PLQY} is the dye luminescence efficiency, η_{Stokes} represents the fraction of photons lost during re-absorption of emitted photons, η_{host} is the transport efficiency of the matrix, η_{TIR} is the total internal reflection efficiency of the waveguide related to its surface smoothness, η_{self} efficiency of the re-emitted photon.

Apart from all the possible loss mechanisms, the dye is the central element of LSC and in order to have high LSC efficiency, the luminescent dye should satisfy the following requirements:

i) it must have a broadband absorption range < 950nm;

ii) it must exhibit a single emission peak at ≈ 1000nm (optimal conversion wavelength for Si solar cells) ;

iii) it must have a large Stokes' shift to reduce overlap of the absorption and emission spectra;

iv) it must show 100% fluorescent quantum yield;

v) it must be compatible with the collector material;

vi) it must be stable for at least 20 years;

vii) it must not be expensive.

Most of the criteria mentioned above should be met by LSCs to achieve at least a 10% efficiency. Usually both organic and inorganic materials can match some of those requirements but not all.

Organic dyes can usually be stable for many years,[59] with a PLQY of about 100% (perylene dyes[60, 61]) and are cheap and photostable. Rhodamines were studied especially in the first stage of LSC research,[43] while perylene dyes started to be used in the late 1980s.[52, 60] Coumarines are another class of organic dyes that can have a large Stokes shift and high quantum yield over 80%.[62] Unfortunately one of the disadvantages of organic dyes is their limited absorption and a combination of different dyes needs to be used to improve spectral response.[41]

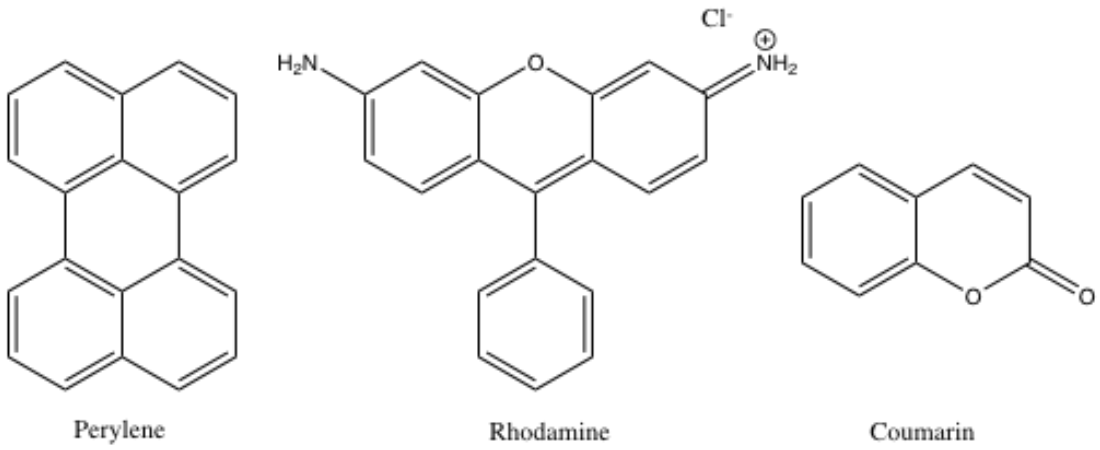

Fig. 1.3. Example of organic dyes.

Quantum Dots are usually more tunable in terms of photophysics due to their size dependent properties.[63] Broad absorption spectra, high absorption coefficient and emission peaks in the near-infrared are also satisfied by some of them[64] (PbS QDs[65, 66]). Unfortunately these dyes are not environmental stable and their photostability

decreases outside the matrix due to oxygen and light sensitivity. Moreover, those available now for use are expensive and not highly efficient.[41]

Rare earth elements are interesting regarding this kind of technology because of their unique characteristics, such as intense emission in the NIR (Yb and Nd), high photostability and low re-absorption of the emitted light (due to a large pseudo-Stokes' shift).[41] Their main disadvantage is poor absorption efficiency, which can be enhanced using organic ligands.[67, 68] Another problem occurring with lanthanide ions is quenching of their luminescence in the presence of high-energy vibrations of bonds, such as C-H, O-H and N-H. Deuteration or fluorination can reduce this.[68, 69]

Chromium(III) is also an interesting element to use for LSC. Its higher spectral absorption than lanthanide ions has been used already for doping Nd and Yb-doped glasses, giving rise to energy transfer.[52, 70]

1.5 Luminescent Down-Shifting (LDS) devices

Innovative designs have been applied to PV in order to harvest sunlight more efficiently and overcome device limitations.[71] The first appearance of Luminescent Down-Shifting (LDS) was in the 1970s,[43, 44] by Hovel[72] were they actually described it as an independent layer on top of a pre-existing PV device. The addition of this extra layer enables reduction of problems and costs in manufacturing, because there is no need to disrupt the already existing and efficient photovoltaic device.[73] The

LDS technique consists of a polymer host matrix layer in which the luminescent dye is incorporated. The down-shifting process of non-absorbable photons occurs when those photons are converted to photons that better match the spectral response of a particular solar cell.[74]

Poor spectral response at wavelengths shorter than 510 nm of some solar cells can be overcome by using a Luminescent Down-Shifting (LDS) layer to improve their efficiency in that part of the spectrum. It has been proven that for solar cells based on CdTe we have a huge loss of absorption at wavelengths shorter than 500 nm.[75] With a LDS layer, which can absorb below 500 nm and re-emit above this wavelength, the solar cell can perform better at its maximum efficiency.[76] The figure below shows that using a perylene-based dye, it is possible to exploit the short wavelength spectrum to improve CdTe efficiency.[73]

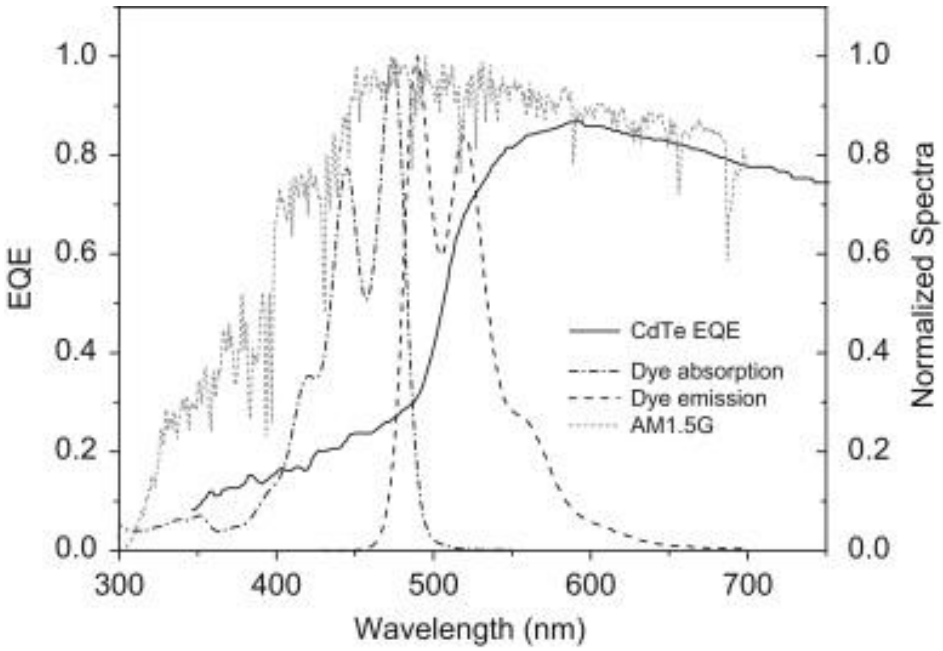

Fig. 1.4. Representation of the LDS method. Normalized emission and absorption bands of a fluorescent organic dye (BASF Lumogen-F Yellow 083)[77], AM1.5G solar spectrum[78] and the EQE of a production line CdTe PV module[79] (figure taken from Klampaftis *et al.* [73])

The additional layer on top of a PV module is a polymer doped with the luminescent dye. Once the dye absorbs the light (1) it is re-emitted and will be directly conveyed to the solar cell (2), or it can be reflected by the air/LDS interface and then directed to the cell (3), or it can be re-absorbed (4) and re-emitted (5) by another luminescent dye.

Some losses occur via escape cone (6) or sideways (7). It is possible that some light not absorbed by the dye will hit the cell directly (8).[73]

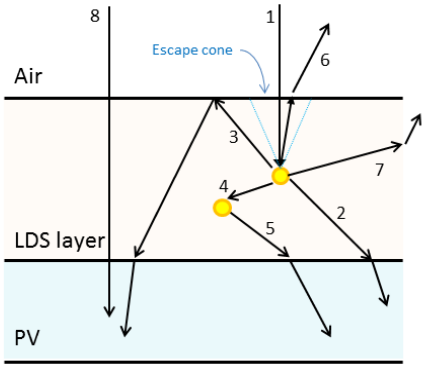

Fig. 1.5. LDS diagram; see text for details.

1.6 Why use Lanthanides

Lanthanide chemistry has seen widespread use in different fields, such as biochemical studies,[68, 80] therapeutical applications,[81] as well as photonic and electronic materials,[68, 82-84] promoted by attractive photophysical properties: long-lived excited states and narrow band emission.[69, 85-88] Energy levels within each lanthanide ion are determined according to their $4f^n$ electronic configuration. These energies are predominantly determined by interelectronic repulsion and spin-orbit

coupling, with ligand field effects playing a negligible role because of 5s and 5p electrons that shield the inner 4f electrons.

Transitions between f-f states are parity forbidden, which means that lanthanide complexes have low absorption coefficients ($\varepsilon < 10$ M^{-1} cm^{-1}) and radiative lifetimes on the millisecond time scale. Absorption and emission spectra of lanthanide(III) ions are quite characteristic with sharp narrow bands that differ from other inorganic systems and that usually are not dependent on the surrounding environment.

Europium(III) and Terbium(III) are the most common lanthanides studied because they emit in the visible region, while for NIR emission, Neodymium(III) and Ytterbium(III) have been widely investigated.

Europium emission comprises the transitions $^5D_0 \rightarrow {}^7F_J$ with J=0, 1, 2, 3, and 4. The most intense transitions arise from $^5D_0 \rightarrow {}^7F_{1,2,4}$ with $^5D_0 \rightarrow {}^7F_2$ being the most sensitive to the environment effect and change in structure. Accordingly, this transition is known as the hypersensitive peak (around 613 nm).[89] The magnetic dipole transition, $^5D_0 \rightarrow {}^7F_1$, instead is independent of the ion surroundings and can be used as an "internal reference" for emission.[90]

Terbium has $^5D_4$ as emissive state and the most common transitions in its case are $^5D_4 \rightarrow {}^7F_J$, with J=6, 5, 4, 3, 2, 1 and 0. The most intense transition is to $^7F_5$, occurring at

about 542 nm. The band attributed to the transition $^5D_4 \rightarrow {}^7F_4$ is sensitive to the ligands present around the metal ion. Emission lifetimes are in the range of 0.4-5 ms.[80]

In the case of NIR emitters, Neodymium(III) is well-know in the Nd-YAG laser, used especially in biological applications, as well as for lasers and optical devices in telecommunication systems.[91] Compared to Eu and Tb, emission intensity of Nd in solution is weak due to vibrational quenching, which is the predominant non-radiative decay that quenches its emission.[92]

Ytterbium is another lanthanide that allows exploitation of the long wavelength NIR range of the spectrum. Its emission peak comes from the transition $^2F_{5/2} \rightarrow {}^7F_{7/2}$ at 980 nm.[93] It is apparent that since the emissive states of NIR emitting lanthanides are much lower in energy than Eu and Tb, an increased variety of chromophores may be used to sensitise them (see below).[94]

By introducing an appropriate chromophore (usually referred to as an "antenna") it is possible to increase the complex's absorbance in the visible and UV regions.[85, 95] The antenna effect is an energy conversion process which involves a ligand able to collect the light and an emitting metal ion. Usually such ligands are highly π-conjugated systems, aromatic or hetero-aromatic, with high molar absorption coefficients. Once the ligand singlet-excited state has been reached, it may convert to a triplet state by intersystem crossing. The triplet energy level needs to be slightly above the emissive lanthanide state for the latter to accept efficiently the energy

from the chromophore. Excitation of the coordinated metal centre is then possible by way of energy transfer from the triplet state of the ligand to the excited state of the lanthanide. The overall efficiency of this photoluminescence process depends on different factors; the intensity of the ligand photon absorption, the efficiency of the ligand-to-metal energy transfer and the efficiency of the metal luminescence.[95]

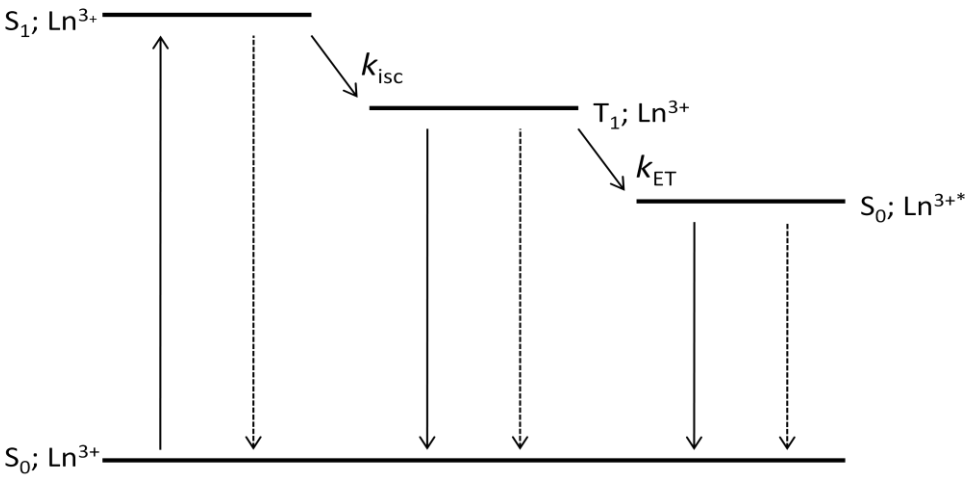

Fig. 1.6. Photophysical diagram showing the main processes in luminescent complexes. S_0 = sensitizer ground state; Ln^{3+} = lanthanide ion; S_1 = sensitiser excited singlet state; Ln^{3+*} = lanthanide ion excited state; T_1 = sensitizer triplet energy state; k_{isc} = intersystem crossing rate; k_{ET} = rate of energy transfer.

Since the 4f electrons of the lanthanides are shielded by 5s and 5p electrons, they are not available for covalent bonds with the ligands. Hence electrostatic interactions mostly determine the geometry of the molecule, alongside any steric factors concerning the ligand and the metal ion. For this reason, lanthanide complexes with the same ligands are often isostructural, although the size steadily decreases across the series and differences may occur between the early and the late lanthanide ions. Coordination numbers that vary from 6 to 12 are not uncommon, but the most

frequently observed coordination number is usually 8 or 9. Behaving as hard Lewis acids, lanthanide cations usually bind anionic ligands such as carboxylates, phosphates, phosphonates and β-diketonates.

The total photoluminescence quantum yield (PLQY) of the molecule upon photoexcitation of the ligand (Φ_{tot}) is the product of the efficiency of ligand sensitisation (η_{sens}), the efficiency of the energy transfer process (η_{ET}) and the intrinsic luminescence efficiency of the Ln ion (Φ_{Ln}). To achieve high luminescence efficiency, it is necessary to suppress radiationless transitions caused by vibrational excitation of the surrounding environment; for example by preventing solvating molecules from strongly coordinating to the metal centre in its first coordination sphere, therefore reducing the presence of high frequency oscillators such as C-H and O-H bonds. On that account, ligand design is crucial to create highly emissive complexes, because the influence on the 4f electrons by interaction with the surrounding ligands can modify the electronic transitions of the lanthanide ion.

In summary, the synthesis of lanthanide complexes for solar conversion technologies is a great advantage due to their peculiar characteristics, such as large Stokes shift, which avoid any self absorption; possibility of good light harvesting and high PLQY using different ligands as antenna; possibility to emit in the NIR for their use in LSC technology; ability to emit in the visible reagion of the spectrum for application in LDS technology.

1.7 Chapters outline

The molecules described in Chapter 3 of this thesis are designed following the "antenna" approach for ligand sensitisation.

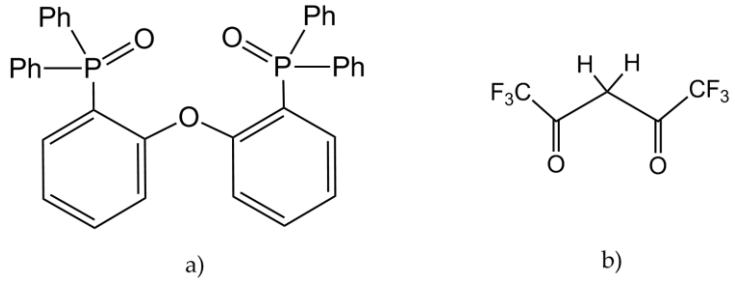

Fig. 1.7. Ligands used in [Ln(hfac)$_3$DPEPO]; a) DPEPO, bis(2-(diphenylphosphino)phenyl)ether oxide; b) hfac, hexafluoroacetylacetonate.

Using β-diketonates as a ligand, light harvesting can be tuned according to the substituents present in the ligand itself as well as allowing ligand-to-metal energy transfer. Excitation at around 300 nm,[96] due to its intense π-π* transition, have made β-diketonates an important antenna.[85]

In the literature[97-101], the synthesis of lanthanide complexes with β-diketonates and phosphine oxides as ligands has been studied, due to the ability of phosphine oxide ligands to prevent coordination of solvent molecules and their intrinsic low-frequency vibrations due to the presence of P=O. In this context, the complex [Eu(hfac)$_3$DPEPO][102] was studied, where DPEPO = bis(2-(diphenylphosphino)phenyl)ether oxide, and hfac = hexafluoroacetylacetonate. This complex was found to have an unprecedentedly high value of PLQY in polymethylmethacrylate (PMMA). The DPEPO ligand was previously used by Xu *et al.* [100] due to its good coordination ability and for giving more rigidity to the

complex. The DPEPO ligand contributed to maximise the photoluminescence efficiency, giving a value of $\Phi_{Ln} = 0.8$ in PMMA.[102]

To further probe the origins of this exceptional PLQY, in Chapter 3 we extend the study to analogues of [Eu(hfac)$_3$DPEPO], using Tb^{3+}, Nd^{3+}, Yb^{3+} and Gd^{3+}, with attention to the ligand's role within the molecule and in the energy transfer process, the luminescence efficiency of the lanthanide centres and the resulting total PLQY. Tb^{3+}, like Eu^{3+}, is a technologically-important visible emitter; Yb^{3+} and Nd^{3+} enable the study to be extended to near-IR emitters; and Gd^{3+} enables specific insights to be made into the excited ligand energy levels.

Chapter 4 is focused on a different approach to lanthanide sensitisation. Chromium oxalate molecules are synthesised and studied in this section because of their high emissive potential and because the oxalate ligand has no C-H bonds, which are known to be highly quenching. Cr(III) and Ln(III) also have optical similarity, which at a first sight could be redundant, but actually the low-lying Cr(^{2}E) excited level can be a good energy donor for efficient sensitisation of lanthanide ions emitting in the NIR region.[103]

Chapter 5 is focused on studying the photophysical properties of other terbium complexes with potential for LDS application: Tb(pobz)$_3$(hacim)$_2$ – compound **10** and Tb(bz)$_3$(hacim)$_2$ – compound **11** (with pobz = phenoxybenzoic acid and bz = benzoic acid). The particular feature of these complexes is the insolubility of their precursors (Tb(pobz)$_3$ and Tb(bz)$_3$), which have a high emission quantum yield as

studied before by Eliseeva *et al*.[68]

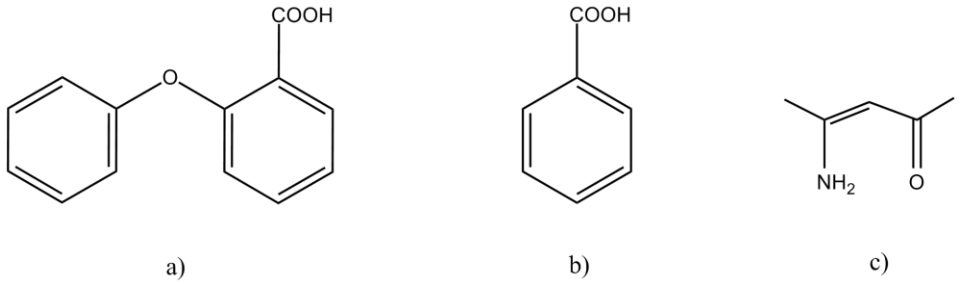

Fig. 1.8. Ligands used for compounds **10** and **11**. a) phenoxybenzoic acid (pobz); b) benzoic acid (bz); c) acetylacetone imine.

An annealing process was hence performed to study the separation of the complexes from their neutral ligand, acetylacetone.

Chapter 6 is dedicated to the study of a coronene salt, potassium coronene tetracarboxylate salt (compound **12**), as a potential ligand for lanthanide complexes. The highly-conjugated structure makes it a good candidate as "antenna", due to its high molar extinction coefficient. This system could be applied to LDS technology because it showed a good energy transfer to a visible-emitting lanthanide.

1.8 References

1. http://www.eia.gov/forecasts/ieo/more_highlights.cfm#world. *International Energy Outlook 2011*. [Last access 16th October 2012].
2. Armaroli, N. and Balzani, V., *Energy & Environmental Science*, 2011. **4**(9): p. 3193.
3. Berner, R.A., *Nature*, 2003. **426**(6964): p. 323.
4. Lewis, N.S. and Nocera, D.G., *PNAS*, 2006. **103**(43): p. 15729.
5. Armaroli, N. and Balzani, V., *Energy for a sustainable world*. 2011: Wiley-VCH.
6. Panwar, N., Kaushik, S., and Kothari, S., *Renew. Sust. Energ. Rev.*, 2011. **15**(3): p. 1513.
7. Eisenberg, R. and Nocera, D.G., *Inorg. Chem.*, 2005. **44**(20): p. 6799.
8. http://www.worldcoal.org/. *THE COAL RESOURCE - A Comprehensive Overview of Coal*. [Last access 15th October 2012].
9. http://www.bp.com. *BP Statistical Review of World Energy June 2012*. [Last access 15th October 2012].
10. Guidolin, M. and Guseo, R., *Technological Forecasting and Social Change*, 2012.
11. da Graça Carvalho, M., *Energy*, 2012. **40**(1): p. 19.
12. http://www.ren21.net/. *RENEWABLES 2012 Global Status Report*. [Last access 15th October 2012].
13. Ducat, D.C. and Silver, P.A., *Curr. Opin. Chem. Biol.*, 2012. **16**(3–4): p. 337.
14. Balzani, V., Credi, A., and Venturi, M., *ChemSusChem*, 2008. **1**(1-2): p. 26.
15. Green, M.A., *Prog. Photovolt. Res. Appl.*, 2005. **13**(5): p. 447.
16. Rappaport, P., *Proc. Natl. Acad. Sci. U. S. A.*, 1961. **47**(8): p. 1303.
17. Johansson T.B., K.H., Reddy .K.N., Williams R. *ERS, 1992.* **4**(3) art. 6.
18. Zhao, J., Wang, A., Green, M.A., and Ferrazza, F., *Appl. Phys. Lett.*, 1998. **73**(14): p. 1991.
19. Green, M.A., Emery, K., Hishikawa, Y., Warta, W., and Dunlop, E.D., *Prog. Photovolt. Res. Appl.*, 2012. **20**(1): p. 12.
20. www.epia.org/. *Global market outlook for photovoltaics until 2014 - May 2010 update*. [Last Access 16th October 2012].
21. Venkatasubramanian, R., O'Quinn, B., Hills, J., Sharps, P., Timmons, M., Hutchby, J., Field, H., Ahrenkiel, R., and Keyes, B. *18.2%(AM1. 5) efficient GaAs solar cell on optical-grade polycrystalline Ge substrate*. 1996: IEEE.
22. Benagli, S., Borrello, D., Vallat-Sauvain, E., Meier, J., Kroll, U., Hötzel, J., Bailat, J., Steinhauser, J., Marmelo, M., and Monteduro, G., *Solar Energy*, 2009(September): p. 21.
23. Repins, I., Contreras, M.A., Egaas, B., DeHart, C., Scharf, J., Perkins, C.L., To, B., and Noufi, R., *Prog. Photovolt. Res. Appl.*, 2008. **16**(3): p. 235.
24. Wu, X., Keane, J., Dhere, R., DeHart, C., Duda, A., Gessert, T., Asher, S., Levi, D., and Sheldon, P. *16.5%-efficient CdS/CdTe polycrystalline thin-film solar cell*. 2001: James & James Ltd.: London.
25. Green, M.A., *Prog. Photovolt. Res. Appl.*, 2001. **9**(2): p. 123.
26. Conibeer, G., *Mater. Today*, 2007. **10**(11): p. 42.
27. Karam, N.H., King, R.R., Cavicchi, B.T., Krut, D.D., Ermer, J.H., Haddad, M., Li, C., Joslin, D.E., Takahashi, M., Eldredge, J.W., Nishikawa, W.T., Lillington, D.R., Keyes, B.M., and Ahrenkiel, R.K., *Electron Devices, IEEE Transactions on*, 1999. **46**(10): p. 2116.
28. Yoshimi, M., Sasaki, T., Sawada, T., Suezaki, T., Meguro, T., Matsuda, T., Santo, K., Wadano, K., Ichikawa, M., Nakajima, A., and Yamamoto, K. *High efficiency thin film*

silicon hybrid solar cell module on 1 m/sup 2/-class large area substrate. in *Photovoltaic Energy Conversion, 2003. Proceedings of 3rd World Conference on*. 2003.
29. Goetzberger, A., Hebling, C., and Schock, H.W., *Mat. Sci. Eng. R.*, 2003. **40**(1): p. 1.
30. Planells, M. and Robertson, N., *Eur. J. Org. Chem.*, 2012. **2012**(26): p. 4947.
31. Mayer, A.C., Scully, S.R., Hardin, B.E., Rowell, M.W., and McGehee, M.D., *Mater. Today*, 2007. **10**(11): p. 28.
32. Dennler, G., Scharber, M.C., and Brabec, C.J., *Adv. Mater.*, 2009. **21**(13): p. 1323.
33. Hoppea, H. and Sariciftci, N.S., *J. Mater. Res*, 2004. **19**(7): p. 1925.
34. Dimitrakopoulos, C.D. and Mascaro, D., *IBM J. Res. Dev.*, 2001. **45**(1): p. 11.
35. Bagnall, D.M. and Boreland, M., *Energy Policy*, 2008. **36**(12): p. 4390.
36. http://en.wikipedia.org/wiki/Solar_radiation. [Last access 17th September 2012].
37. Van Sark, W., DonegV°, C.D.M., Harkisoen, C., Kinderman, R., van Roosmalen, J., Schropp, R., and Lysen, E. *Improvement of spectral response of solar cells by deployment of spectral converters containing semiconductor nanocrystals*. 2004.
38. Richards, B. and McIntosh, K.R. *Ray-tracing simulations of luminescent solar concentrators containing multiple luminescent species*. 2006.
39. Royne, A., Dey, C.J., and Mills, D.R., *Sol. Energy Mater.*, 2005. **86**(4): p. 451.
40. http://www.soitec.com/en/solar-energy/. *Leading the solar energy revolution with Concentrator Photovoltaic (CPV) technology*. [Last access 16th October 2012].
41. Debije, M.G. and Verbunt, P.P.C., *Advanced Energy Materials*, 2012. **2**(1): p. 12.
42. Swanson, R.M., *Prog. Photovolt. Res. Appl*, 2000. **8**(1): p. 93.
43. Weber, W.H. and Lambe, J., *Appl. Opt.*, 1976. **15**: p. 2299.
44. Goetzberger, A. and Greube, W., *Appl. Phys. A: Mater. Sci. Process.*, 1977. **14**(2): p. 123.
45. Bende, E., Slooff, L., Burgers, A., Van Sark, W., and Kennedy, M. *Cost & efficiency optimisation of the fluorescent solar concentrator*. 2008.
46. Hernandez-Noyola, H., Potterveld, D.H., Holt, R.J., and Darling, S.B., *Energy Environ. Sci.*, 2012. **5**(2): p. 5798.
47. Beattie, N., Themistokleous, T., Zoppi, G., Forbes, I., and Miles, R., 2012.
48. Chemisana, D., *Renewable Sustainable Energy Rev.*, 2011. **15**(1): p. 603.
49. Benemann, J., Chehab, O., and Schaar-Gabriel, E., *Sol. Energy Mater.*, 2001. **67**(1–4): p. 345.
50. Oliver, M. and Jackson, T., *Energy*, 2001. **26**(4): p. 431.
51. Wiegman, J.W.E. and van der Kolk, E., *Sol. Energy Mater.*, 2012. **103**(0): p. 41.
52. Reisfeld, R., *Inorg. Chim. Acta*, 1987. **140**: p. 345.
53. Carrascosa, M., Unamuno, S., and Agullo-Lopez, F., *Appl. Opt.*, 1983. **22**(20): p. 3236.
54. Rowan, B.C., Wilson, L.R., and Richards, B.S., *IEEE J. Sel. Top. Quantum Electron.*, 2008. **14**(5): p. 1312.
55. Polishuk, P., *Comm. Mag., IEEE*, 2006. **44**(9): p. 140.
56. White, J.R., *Comptes Rendus Chimie*, 2006. **9**(11,Äì12): p. 1396.
57. Thomas, W.R.L., Drake, J.M., and Lesiecki, M.L., *Appl. Opt.*, 1983. **22**(21): p. 3440.
58. Buffa, M., Carturan, S., Debije, M., Quaranta, A., and Maggioni, G., *Sol. Energy Mater.*, 2012. **103**: p. 114.
59. Earp, A.A., Smith, G.B., Franklin, J., and Swift, P., *Sol. Energy Mater.*, 2004. **84**(1–4): p. 411.
60. Seybold, G. and Wagenblast, G., *Dyes Pigm.*, 1989. **11**(4): p. 303.
61. Wilson, L. and Richards, B., *Appl. Opt.*, 2009. **48**(2): p. 212.
62. Baumberg, I., Berezin, O., Drabkin, A., Gorelik, B., Kogan, L., Voskobojnik, M., and Zaidman, M., *Polym. Degrad. Stab.*, 2001. **73**(3): p. 403.

63. Gallagher, S., Norton, B., and Eames, P., *Sol. Energy*, 2007. **81**(6): p. 813.
64. van Sark, W., Meijerink, A., and Schropp, R., 2012.
65. Etgar, L., Moehl, T., Gabriel, S., Hickey, S.G., Eychmüller, A., and Grätzel, M., *ACS Nano*, 2012. **6**(4): p. 3092.
66. Shcherbatyuk, G., Inman, R., Wang, C., Winston, R., and Ghosh, S., *Appl. Phys. Lett.*, 2010. **96**: p. 191901.
67. Moudam, O., Rowan, B.C., Alamiry, M., Richardson, P., Richards, B.S., Jones, A.C., and Robertson, N., *Chem. Comm.*, 2009(43): p. 6649.
68. Eliseeva, S.V. and Bünzli, J.C.G., *Chem. Soc. Rev.*, 2010(39): p. 189.
69. Bünzli, J.C.G., *Spectrosc. Prop. Rare Earths Opt. Mater.*, 2005: p. 462.
70. Cantuel, M., Bernardinelli, G., Imbert, D., Bunzli, J.-C.G., Hopfgartner, G., and Piguet, C., *Dalton Trans.*, 2002(9): p. 1929.
71. Richards, B.S., *Sol. Energy Mater.*, 2006. **90**(15): p. 2329.
72. Hovel, H.J., Hodgson, R.T., and Woodall, J.M., *Sol. Energy Mater.*, 1979. **2**(1): p. 19.
73. Klampaftis, E., Ross, D., McIntosh, K.R., and Richards, B.S., *Sol. Energy Mater.*, 2009. **93**(8): p. 1182.
74. Klampaftis, E. and Richards, B.S., *Prog. Photovolt. Res. Appl*, 2011. **19**(3): p. 345.
75. Demtsu, S. and Sites, J. *Quantification of losses in thin-film CdS/CdTe solar cells*. 2005: Ieee.
76. Danos, L., Parel, T., Markvart, T., Barrioz, V., Brooks, W.S.M., and Irvine, S.J.C., *Sol. Energy Mater.*, 2012. **98**(0): p. 486.
77. http://www.performancechemicals.basf.com/ev-wcms-in/internet/en_GB/portal/show-content_cps/function:evproducts:/multilist/basic/4704/4732. [Last access 16th October 2012].
78. http://rredc.nrel.gov/solar/spectra/am1.5/. *Reference Solar Spectral* [Last access 16th October 2012].
79. Demtsu, S.H. and Sites, J.R. *Quantification of losses in thin-film CdS/CdTe solar cells*. in *Photovoltaic Specialists Conference, 2005. Conference Record of the Thirty-first IEEE*. 2005.
80. Elbanowski, M. and Ma kowska, B., *J. Photochem. Photobiol. A*, 1996. **99**(2-3): p. 85.
81. Fricker, S.P., *Chem. Soc. Rev.*, 2006. **35**(6): p. 524.
82. Kilbourn, B.T., *Inorg. Chim. Acta*, 1987. **140**: p. 335.
83. Kido, J. and Okamoto, Y., *Chem. Rev*, 2002. **102**(6): p. 2357.
84. de Bettencourt-Dias, A., *Dalton Trans.*, 2007. **2007**(22).
85. Raj, D.B.A., Biju, S., and Reddy, M.L.P., *Dalton Trans.*, 2009. **2009**(36): p. 7519.
86. Leonard, J.P. and Gunnlaugsson, T., *J. Fluor.*, 2005. **15**(4): p. 585.
87. Werts, M.H.V., Jukes, R.T.F., and Verhoeven, J.W., *Phys. Chem. Chem. Phys.*, 2002. **4**(9): p. 1542.
88. Wilson, L.R., Rowan, B.C., Robertson, N., Moudam, O., Jones, A.C., and Richards, B.S., *Appl. Opt.*, 2010. **49**(9): p. 1651.
89. Klampaftis, E., Congiu, M., Robertson, N., and Richards, B.S., *Photovoltaics, IEEE Journal of*, 2011. **PP**(99): p. 1.
90. Werts, M.H.V., Jukes, R.T.F., and Verhoeven, J.W., *Phys. Chem. Chem. Phys.*, 2002. **4**(9): p. 1542.
91. Weber, J.K.R., Felten, J.J., Cho, B., and Nordine, P.C., *Nature*, 1998. **393**(6687): p. 769.
92. Hasegawa, Y., Wada, Y., and Yanagida, S., *J. Photochem. Photobiol. C*, 2004. **5**(3): p. 183.

93. Beeby, A., Dickins, R.S., Faulkner, S., Parker, D., and Williams, J.A.G., *Chem. Commun.*, 1997(15): p. 1401.
94. Faulkner, S., Pope, S.J.A., and Burton,ÄêPye, B.P., *App. Spectrosc. Rev.*, 2005. **40**(1): p. 1.
95. Armelao, L., Quici, S., Barigelletti, F., Accorsi, G., Bottaro, G., Cavazzini, M., and Tondello, E., *Coord. Chem. Rev.*, 2010. **254**: p. 487.
96. Pawlowski, V., Strasser, A., and Vogler, A., *ZEITSCHRIFT FUR NATURFORSCHUNG B*, 2003. **58**(10): p. 950.
97. Klink, S.I., Hebbink, G.A., Grave, L., Oude, A.P.G.B., van, V.F.C.J.M., and Werts, M.H.V., *J. Phys. Chem. A*, 2002. **106**(15): p. 3681.
98. Bauer, H., Blanc, J., and Ross, D.L., *J. Am. Chem. Soc.*, 1964. **86**(23): p. 5125.
99. Pietraszkiewicz, M., KÅ‚onkowski, A., Staniszewski, K., Karpiuk, J., and Bianketti, S.a., *J. Alloys Compd.*, 2004. **380**(1-2): p. 241.
100. Xu, H., Wang, L.H., Zhu, X.H., Yin, K., Zhong, G.Y., Hou, X.Y., and Huang, W., *J. Phys. Chem. B*, 2006. **110**(7): p. 3023.
101. Xu, H., Yin, K., and Huang, W., *Chem. Eur. J*, 2007. **13**(36): p. 10281.
102. Moudam, O., Rowan, B.C., Alamiry, M., Richardson, P., Richards, B.S., Jones, A.C., and Robertson, N., *Chem. Comm.*. 2009. p. 6649.
103. Aboshyan-Sorgho, L., Cantuel, M., Petoud, S., Hauser, A., and Piguet, C., *Coord. Chem. Rev.*, 2012. **256**(15â€“16): p. 1644.

Chapter 2: Experimental techniques

The information gained through this thesis work was based on different experimental techniques. Spectroscopy measurements details will be discussed in the appropriate experimental section of each chapter. General basic knowledge behind absorption and emission spectroscopy will be discussed further in this chapter.

2.1 Absorption Spectroscopy

Absorption spectroscopy has been used in this work to gain an understanding about the electronic energy changes in the synthesised compounds. When radiation hits the molecule, its electron can take energy from the incident photon and increase its energy level to a higher electronic state. The absorption of a photon has hence occurred, according to and respecting certain selection rules.

In a solution, we can define the quantity of photons absorbed through the absorbance (A) and according to the Beer-Lambert[1] Law

$$A = \varepsilon c l$$

Absorbance is proportional to the concentration (c) of the absorbing species, to the path length (l) of the cuvette and to the molar extinction coefficient (ε). Deviation from the linear dependence of absorbance on concentration (according to Beer-Lambert Law) could be caused by aggregation of material at high concentration or by the presence of different absorbing species.

The probability of a molecule to absorb the light is regulated by the selection rules and a clear assumption is that we should have some spatial overlap between the ground state wavefunction and the excited state wavefunction in order to have electronic transition (as it is shown in Figure 2.1).

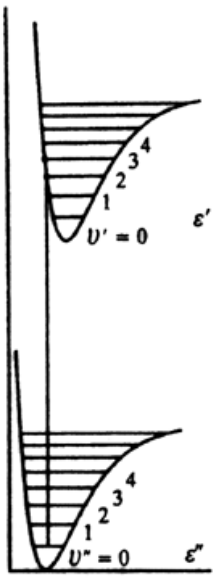

Fig. 2.1. General electronic transition diagram.

We know that an electromagnetic wave, such as light, can induce an electric or magnetic moment. When the difference between the wavefunction of the final state and the wavefuction of the initial state is the same as the frequency induced by the electric or magnetic moment, it means that molecule and the field are resonant. The transition between these two states is governed by the transition dipole moment (R_{if}), given by the equation below:

$$R_{if} = \int \psi_f^* \hat{\mu} \psi_i d\tau$$

where Ψ_f is the wavefunction in the final state, Ψ_i is the wavefunction in the initial state and μ is the dipole moment operator.

The total wavefunction can be separated into electronic, rotational and vibrational parts:

$$R_{if} = \int \psi^*_{e,f} \hat{\mu} \psi_{e,i} d\tau \int \psi^*_{s,f} \psi_{s,i} d\tau \int \psi^*_{n,f} \psi_{n,i} d\tau$$

First of all the Born-Oppenheimer approximation allow us to assume that electronic transitions are so rapid that nuclear coordinates cannot be displaced, hence motion of electrons can be separated from nuclei motion. With this approximation, vibrational and rotational transitions don't change during optical transition, and the product of the initial and final wavefunction with the dipole moment operator must be totally symmetric for the transition to occur.

Secondly, we can refer to selection rules in order to determine which transitions are allowed.

- Symmetry-forbidden transition: For a molecule with an inversion centre, transitions between the same atomic orbitals are forbidden. For example. since *p* orbitals have *u* symmetry, the transition dipole moment is the triple product of *uxuxu* which has *u* symmetry, therefore transition is forbidden. Note however, that absorption can be weakly observed in asymmetric molecules or in symmetric molecules where vibronic coupling may allow departure from perfect symmetry.

- Spin-forbidden transition: different multiplicity states transitions are not allowed (singlet-triplet, triplet-singlet transitions), although wavefunctions of different multiplicity can have weak interactions due to spin-orbit coupling. Spin-orbit coupling is also responsible for intersystem crossing (isc) and it varies with the atomic number (it is proportional to Z^4 where Z is the atomic number). This explains why we can observe it in compounds with heavy atoms.
- Δl = +/- 1 (Orbital Rule - Laporte): during spectroscopic transitions the angular momentum cannot change by more than one unit.

2.2 Emission Spectroscopy

Figure 2.2 shows a general energy diagram, which depicts the process of light absorption and emission.

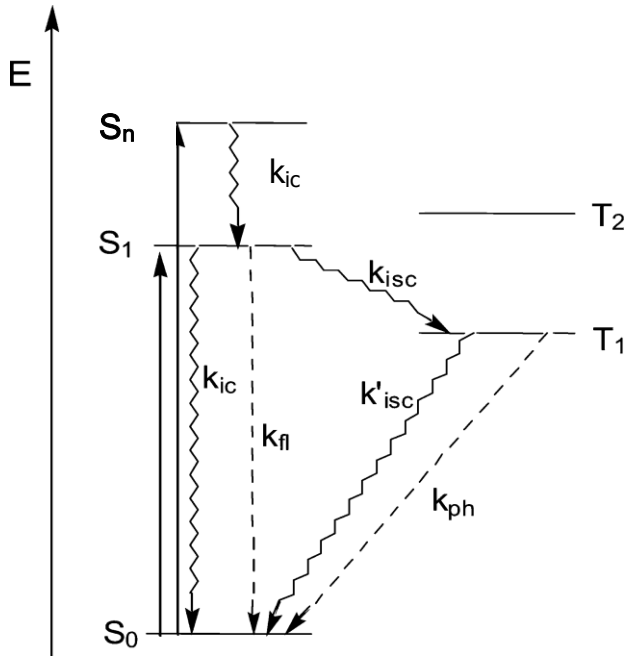

Fig. 2.2. Jablonski diagram of energy levels

Upon excitation of the molecule, an electron is promoted from the ground state (S_0) to an excited level (S). According to the energy absorbed, the electron is promoted to a particular excited level (S_1,… S_n), and from these states energy can be dissipated through different deactivation processes.

Emission of light within a molecule occurs when the molecule returns from its excited energy level to the ground state, providing that no thermal energy losses happen. According to the photochemistry notation in the diagram (Fig. 2.1), we already defined that S_0 is the singlet ground state, S_1 and S_n are the different excited states of the same molecule. T_1 and T_2 are instead the triplet excited states. Having as an example a singlet ground state (S_0), the electronic states of molecules are defined in terms of the spin multiplicity of the state, which is given by 2S+1, where S is the total spin. For a singlet (S), there are no unpaired electrons, S=0, and the spin multiplicity is one.

Fluorescence and phosphorescence are two types of possible photoluminescence that can occur after excitation of the molecule. [2]

2.2.1 Fluorescence

Conventionally, fluorescence is defined as a radiative transition between two energy levels with the same multiplicity. Upon absorption of light after radiation, the molecule is excited from the ground state (S_0, which is normally the only state

significantly occupied at room temperature) to an upper spin-allowed excited state (S_n). From the excited state it can undergo an internal conversion and decay to the lowest excited state between the different vibrational levels (S_1), which is the only emissive level of a given multiplicity (Kasha's rule). This is typical for organic molecules but not obeyed 100% of the time. The energy lost is released as a photon with an energy that matches the difference between the energy levels involved.

2.2.2 Phosphorescence

Another photoluminescence process related to fluorescence is phosphorescence. Once the molecule is excited, the photon can be reemitted as phosphorescence after intersystem crossing occurs, creating a higher spin multiplicity with aligned spin parallel, called triplet (T_1). The phosphorescence is therefore defined as a radiative process occurring between states with different spin multiplicity, so in T_1 the energy decays again to the ground state, emitting a photon. Since it is formally forbidden, it is a significantly less favourable process that typically occurs at a slower rate compared to the fluorescence emission. The difference between these two processes is then highlighted by the timescale at which they occur: 10^{-4} to 10^{2} seconds for phosphorescence and 10^{-9} to 10^{-6} seconds for fluorescence.

2.2.3 Photoluminescence quantum yield and lifetime

Photoluminescence quantum yield (PLQY) and emission lifetime are two properties we can measure by emission spectroscopy.

PLQY is the efficiency of the luminescence process and it is given by the number of photons emitted over the number of photons absorbed

$$PLQY = \frac{\text{n. of photons emitted}}{\text{n. of photons absorbed}}$$

PLQYs were determined by absolute measurement, using a Horiba Jobin Yvon integrating sphere.[3] The integrating sphere provides an average over all angles of illumination, which means that it is able to average the emitted light over all directions. Once the absorption spectrum of the sample is measured, it is possible to determine an appropriate excitation wavelength to measure the PLQY. We need to measure the area under the excitation and emission spectra of the sample (L_C and E_C), plus the area under the excitation and emission spectra without any sample in the sphere (L_A and E_A). E_A needs to be measured in order to account for detector dark counts and any emission from the sphere itself (overall background spectrum). The PLQY is then given by

$$PLQY = \frac{E_C - E_A}{L_A - L_C}$$

Each area is calculated by the sum of the photon count rate multiplied by the wavelength of the entire spectrum (from the raw spectral data):

$$E_C = \sum E_C(\lambda)\Delta\lambda$$

(taking E_C as an example). Since integrating spheres are nowadays commercially available and used, measurements taken with this method are easily repeatable.

Lifetime is a measure of the time that takes to the excited state of a molecule to decay to the ground state. It usually follows first order kinetics and it is given by the following formula

$$\tau = \frac{1}{k_{obs}}$$

where k_{obs} is the rate constant of decay of the excited state.

The rate constant of decay is defined by the contribution of both radiative (k_r) and non-radiative (k_{nr}) deactivation pathways, as below

$$\tau = \frac{1}{k_r + k_{nr}}$$

Non-radiative deactivation is the process by which a molecule returns to the ground state without emission of light. This can be due to collisional or vibrational quenching occurring within the molecule and in relation to the environment (for example, solvent molecules). The general behaviour of the excited state of a fluorophore is described by the rate equation:

$$\frac{dn(t)}{dt} = -kn(t) + f(t)$$

where n is the number of the excited elements at the time t, k is the deactivation process rate constant, $f(t)$ is a function of time describing the course of the excitation.

At t=0

$$\frac{dn(t)}{dt} = -kn(t)$$

If we integrate the equation, we have the lifetime, which is the time that the excited population of a fluorophore takes to decay to 1/e,

$$\frac{n(t)}{n_0} = e^{-t/\tau}$$

So the decay of intensity as a function of time is given by

$$I_t = \alpha e^{-t/\tau}$$

where I_t is the intensity at time t, and α is the pre-exponential factor.

2.3 References

1. http://imgbase-scd-ulp.u-strasbg.fr/displayimage.php?album=53&pos=405&lang=english. *Photometria sive de Mensura et Gradibus Luminis, Colorum et Umbrae*. [Last access 20th September 2012].
2. Dexter, D.L., Klick, C.C., and Russell, G.A., *Phys. Rev.*, 1955. **100**(2): p. 603.
3. Wilson, L.R. and Richards, B.S., *Appl. Opt.*, 2009. **48**(2): p. 212.

Chapter 3: [Ln(hfac)$_3$DPEPO] complexes

3.1 Introduction

The increasing interest in Lanthanide chemistry is due to the unique properties of these metal ions. Their long-lived excited states together with narrow band emission, makes them appealing and researchers have been studying them for their use in different areas, such as bioluminescent probes in biochemistry,[1] as well as light-emitting materials in various optical devices.[2]

The work in this chapter is focused on the study of [Ln(hfac)$_3$DPEPO] complexes, with Ln = Eu, Tb, Nd, Yb and Gd as central metal ion, describing their synthetic route and their photophysical properties, in order to better understand the mechanism behind their luminescent behaviour. The design of these molecules was first presented in a communication by Moudam, in which the europium complex was photophysically characterised. It was found that its luminescent properties were quite exceptional, with a photoluminescent quantum yield (PLQY) of 0.8.[3] The exclusive properties of lanthanides derive from their $4f^n$ electronic configuration. The f-f transitions are parity forbidden with the consequent low molar extinction coefficient of lanthanide complexes, in the range of 1-10 $M^{-1}cm^{-1}$. In order to overcome the low light absorption of the lanthanide compounds, the idea of using "antenna" ligands has been introduced: a chromophore able to absorb light and

then transfer energy to the lanthanide ion, which ideally would have its excited state level below the excited triplet level of the antenna chromophore.[4] For this reason, we used two ligands able to promote this energy transfer mechanism and we discuss the synthesis and photophysical behaviour of the complexes in this chapter. DPEPO (bis(2-(diphenylphosphino)phenyl)ether oxide) was first used as a bidentate ligand by Xu[5], as a ligand with good coordination properties to lanthanides and able to give more rigidity to the complex. Hfac (hexafluoroacetylacetonate) belongs to the β-diketone class and it is well known as an important antenna for lanthanide complexes.[6] The main aim of new designs for lanthanide complexes is to achieve high photoluminescence quantum yield (PLQY, Φ_{tot}), which can be explained as the conversion efficiency of the absorbed light into emitted photons. It depends on the efficiency of ligand sensitisation (η_{sens}) and the intrinsic luminescence efficiency of the lanthanide ion (Φ_{Ln}).

$$\Phi_{tot} = \eta_{sens} \cdot \eta_{ET} \cdot \Phi_{Ln}$$

Photoluminescence can be quenched by radiationless transitions due to the presence of high frequency oscillators like C-H, N-H or O-H, hence avoiding the presence of molecules such as water around the lanthanide ions is essential.

In this work, due to the exceptional PLQY of [Eu(hfac)$_3$DPEPO] we extend the study to analogues with Tb^{3+}, Nd^{3+}, Yb^{3+} and Gd^{3+}, focusing on the role of the different ligands in the energy transfer process, the luminescence efficiency of the lanthanide centres and the resulting total PLQY.

3.2 Results and discussion

The two-step reaction scheme in Fig. 3.1 shows that the molecules were synthesised by stirring the appropriate stoichiometric amounts of the starting materials. The new complex series has the general formula [Ln(hfac)$_3$DPEPO], with Ln = Tb^{3+}, Nd^{3+}, Yb^{3+}, Gd^{3+} (Fig. 3.2).

The intermediate [Ln(hfac)$_3$(H_2O)$_2$] and the complex [Ln(hfac)$_3$DPEPO] were synthesised following the procedure used for the Eu analogue as outlined in the Experimental section. The DPEPO ligand was synthesised following a literature method.[5]

$$Hfac + KO^tBu + LnCl_3{\cdot}6H_2O \xrightarrow[2)\ 3h,\ RT]{1)\ 1h,\ 60\ °C,\ N_2} Ln(hfac)_3(H_2O)_2$$

$$Ln(hfac)_3(H_2O)_2 + DPEPO \xrightarrow[1)\ 1h,\ 60\ °C,\ N_2\\ 2)\ 3h,\ RT]{water,\ ethanol} Ln(hfac)_3DPEPO$$

Fig.3.1. Reaction scheme for the compounds studied.

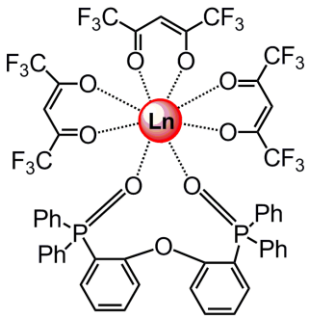

Fig. 3.2. General structure of [Ln(hfac)$_3$(DPEPO)]: Ln = Eu (**1**); Tb (**2**); Yb(**3**); Nd (**4**); Gd (**5**).

All the molecules were fully characterised by ^{1}H-NMR, elemental analysis, mass

spectrometry, UV/Vis, steady-state and time-resolved emission spectroscopy. DFT calculations were performed on the Eu complex, which, together with determination of the $Gd(hfac)_3$DPEPO X-ray crystal structure, gave additional insight into the photophysical processes.

3.2.1 NMR studies

All the complexes were analysed by ^{1}H-NMR in *d*-chloroform solution. Although the peaks in the spectra were broadened by the paramagnetism of the lanthanide ions, it was possible to identify the molecule for comparison with similar complexes found in the literature.[5]

Evidence of the complexation of lanthanides by DPEPO was confirmed by ^{1}H NMR. As shown in Fig. 3.3 the DPEPO NMR spectrum, obtained in *d*-chloroform solution, has two ranges of peaks at higher frequency: the first range between 7.75 and 7.60 ppm, and the second one from 7.55 ppm to 7.22 ppm. They should be attributed to the four phenyl groups bonded to the phosphorus and the proton at the 1 position in the diphenyl ether group. In addition to these peaks, two triplets at 7.19 ppm and at 7.11 ppm are assigned to the protons at the 2 and 3 position in the diphenyl group, whereas the doublet of doublets at 6.07 ppm is attributable to the proton at the 4 position which couples with the phosphorus atom. When the DPEPO is complexed with the lanthanide (Eu complex in Fig. 3.4), a signal shift is observed due to the deshielding effect of the paramagnetic Lanthanide ion. It is to notice that

the shift in δ depends essentially on the angle and distance according to (3 $\cos^2\theta$–1)/r^3. The mixed peaks of the phenyl groups are shifted to high frequency and the proton of the hfac group appears at 5.29ppm.

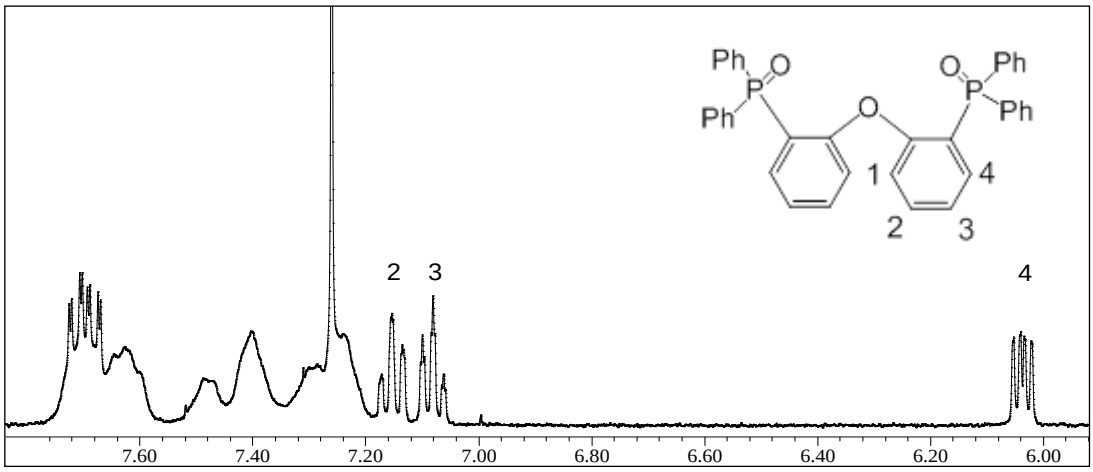

Fig. 3.3. ^{1}H NMR spectrum (300 MHz) for DPEPO ligand in Chloroform.

The paramagnetic nature of lanthanides is a complicating factor for NMR interpretation because the signal is usually broadened by the molecular relaxation caused by the electronic magnetic moment. For this reason, interpretation of the NMR spectra (Fig. 3.4-3.7) was not possible to achieve in detail. The peak between 5.5-6 ppm in each spectrum can be readily assigned to the hfac proton. Although we were able to integrate this peak, which is the most distinct peak in the spectrum, the other peaks were not possible to assign due to the paramagnetic phenomenon resulting in very broad signals that cannot be accurately integrated.

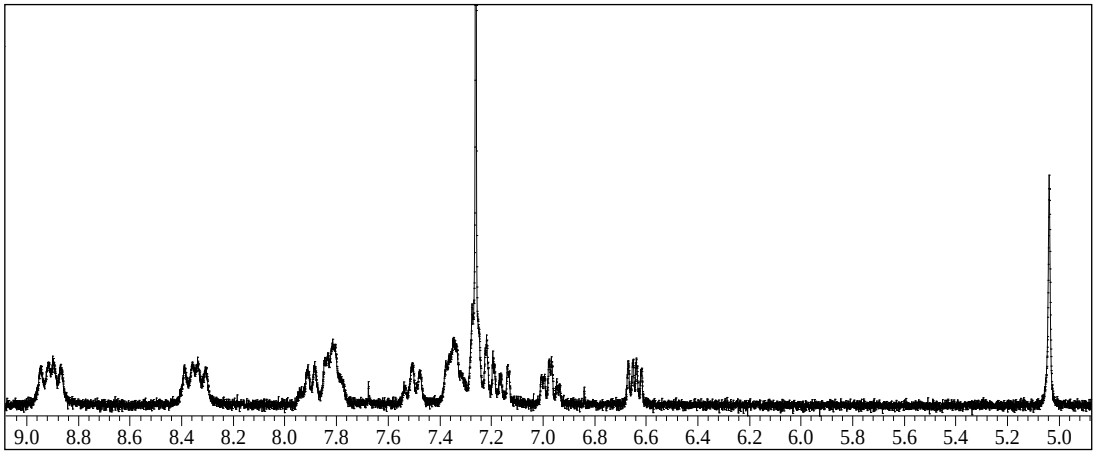

Fig. 3.4. ^{1}H NMR spectrum (300 MHz) for [Eu(hfac)$_3$(DPEPO)] in Chloroform.

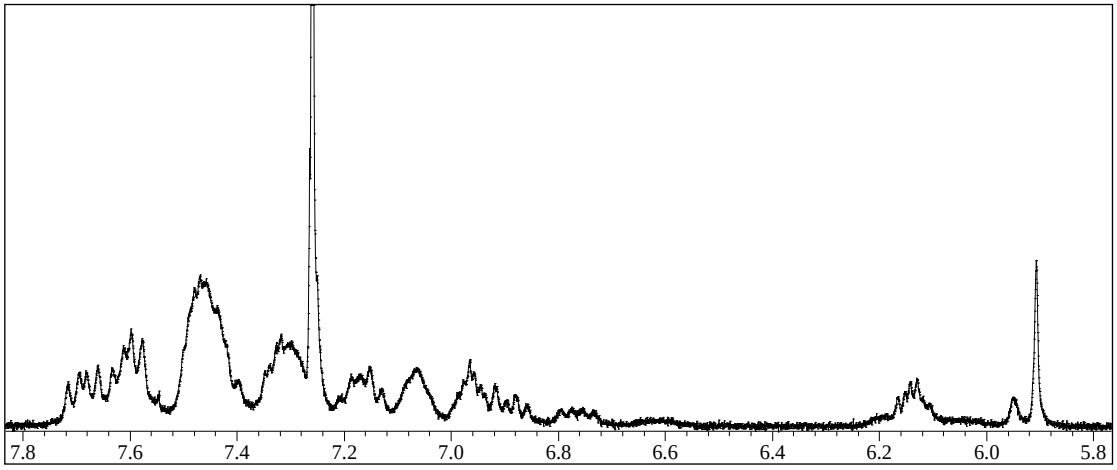

Fig. 3.5. ^{1}H NMR spectrum (300 MHz) for [Tb(hfac)$_3$(DPEPO)] in Chloroform.

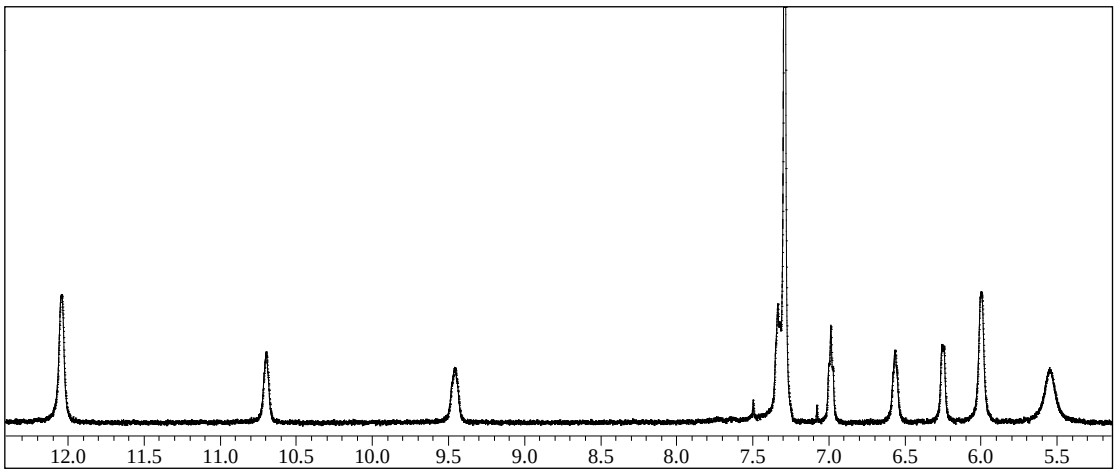

Fig. 3.6. ^{1}H NMR spectrum (300 MHz) for [Yb(hfac)$_3$(DPEPO)] in Chloroform.

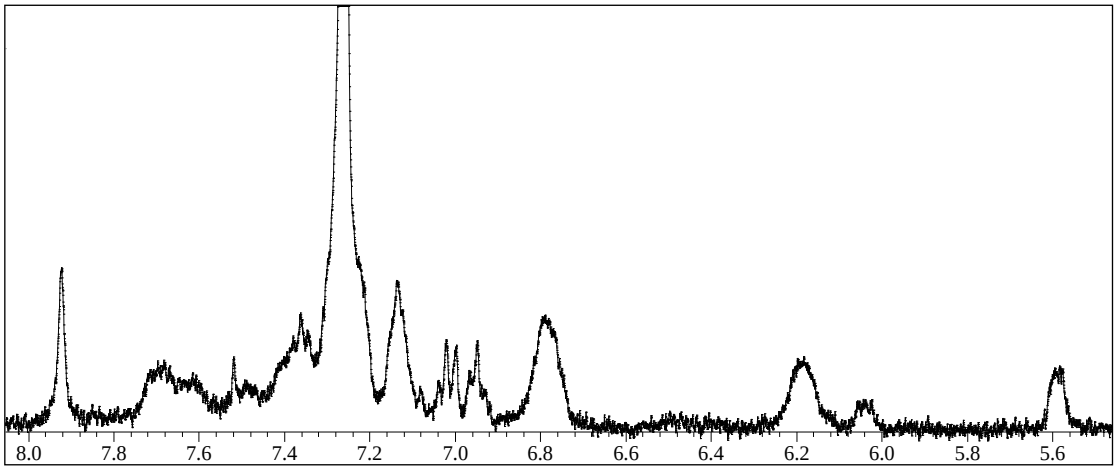

Fig. 3.7. ^{1}H NMR spectrum (300 MHz) for [Nd(hfac)$_3$(DPEPO)] in Chloroform.

3.2.2 Gadolinium structure analysis

The single crystal structure was obtained for complex **5**, [Gd(hfac)$_3$DPEPO] (Fig. 3.8) allowing us a better insight into the structure of the molecule. In Fig. 3.9 the same crystal structure is observed from a different viewing angle with H, F and phenyl groups removed for clarity.

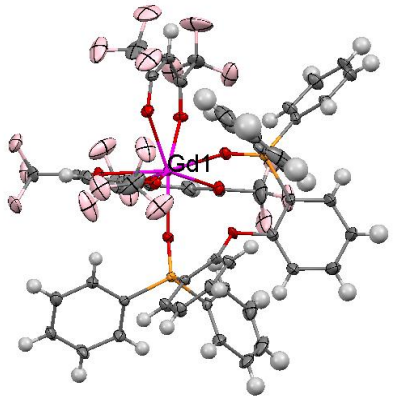

Fig. 3.8. X-ray structure of [Gd(hfac)$_3$(DPEPO)] (**5**) with thermal ellipsoids drawn at the 30% probability level

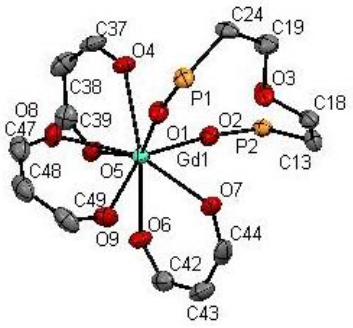

Fig. 3.9. Ortep representation of the structure of **5** with thermal ellipsoids drawn at the 30% probability level. For clarity,the complex has H and F atoms and phenyl groups removed.

The system crystallized with two molecules in the asymmetric unit with the expected eight-coordinate environment of the Gd(III) centre, which excludes other ligands such as H_2O, which for the Eu, Tb, Nd and Yb complexes might increase non-radiative decay of the excited state through coupling with high-energy O-H oscillators. (For clarity, only one molecule of $[Gd(hfac)_3(DPEPO)]$ is shown in Fig 3. 8 and Fig 3.9). Gd and Eu complex structures typically differ only by the ionic radius of the metal ion, therefore this similarity allows us to be confident that discussing Gd data is also relevant to the Eu complex and its analogues.

Gd(1) is coordinated to two oxygen atoms [O(1) and O(2)] of the DPEPO ligand and its coordination sphere is completed by the other six oxygen atoms belonging to the three hfac ligands. It is notable that the ether oxygen [O(3)] of the DPEPO ligand does not coordinate the Gd as the distance between these two atoms Gd(1)-O(3) is too large (3.686 Å). More rigidity to the complex is given by the DPEPO ligand due to its bulky structure, which is expected to stabilise the molecule reducing the relaxation from the excited state. Despite the widespread interest in Ln complexes

with β-diketonate and phosphine oxide ligands, there are no other structurally-determined species of similar structure in the literature.[7] The only analogous structure of Gd to compare with **5** is a $[Gd(hfac)_3(H_2O)_2]$ unit, from crystals of $[Re(CO)_3Cl(dpq)][Gd(hfac)_3(H_2O)_2]\cdot C_6H_6$.[8] The Gd ion coordination geometry with hfac is in general agreement with that of **5** (Table 1). The average Gd···O bond length in **5** is 2.403 Å, similar to the average bond for the Gd-β-diketone unit (2.364 Å) shown by Kennedy *et al*.[8] This value can be compared to Eu analogues in which the average Ln···O bond length for β-diketonate complexes vary from 2.395 Å ($[Eu(hfac)_3(bpyO_2)]\cdot 0.5C_6H_6$[9]) to 2.430 Å ($Eu(hfac)_3(dmbipy)(H_2O)$[10]).

Comparing the $[Gd(hfac)_3(H_2O)_2]$[8] structure with $[Gd(hfac)_3DPEPO]$ highlights the influence of a bulky ligand like DPEPO introduced to the molecule. In $[Gd(hfac)_3(H_2O)_2]$ by Kennedy *et al*., the Gd atom is eight-coordinate forming two planes created in one case by two hfac ligands and the other by two molecules of water and the other hfac[8]. On the contrary, for **5** the introduction of phosphine oxide ligand compresses the hfac ligands and forces them to a different spatial arrangement. Analysing the hfac-metal portion of both the $[Gd(hfac)_3(H_2O)_2]$ fragment and the $[Gd(hfac)_3DPEPO]$ complex the angles formed by the O-hfac atoms and Gd are more compressed for **5**, with an average O···Gd···O angle of 70.88° for $[Gd(hfac)_3DPEPO]$ and 72.28° for $[Gd(hfac)_3(H_2O)_2]$.

The origin of this difference is apparent when we consider the angle between O(1)···Gd(1)···O(2) that measures 103.4° in complex **5** and $H_2O(1)\cdots Gd(1)\cdots OH_2(2)$

angle in $[Gd(hfac)_3(H_2O)_2]$ with 74.3°. Gd(1) in our complex **5** has still an 8 coordination geometry but the bulky bidentate DPEPO ligand is slightly compressing the hfac ligands.

A further difference is found comparing O(1)···Gd(1)···O(2) and O(101)···Gd(101)···O(102) angles in the two asymmetric units of $[Gd(hfac)_3DPEPO]$: a particular spatial arrangement is observed, reducing the angle O(101)···Gd···O(102) by 13.53°(from 103.4° to 89.87°).

Table 1 Selected bond lengths (Å) and angles (◦) for the complex $Gd(hfac)_3DPEPO$

Bond lengths/Å			
Gd(1)-O(1)	2.281(5)	Gd(101)-O(101)	2.298(5)
Gd(1)-O(2)	2.304(5)	Gd(101)-O(102)	2.264(4)
Gd(1)-O(3)	3.686(5)	Gd(101)-O(103)	3.935(4)
Gd(1)-O(4)	2.444(5)	Gd(101)-O(104)	2.376(5)
Gd(1)-O(5)	2.385(5)	Gd(101)-O(105)	2.438(5)
Gd(1)-O(6)	2.381(5)	Gd(101)-O(106)	2.414(5)
Gd(1)-O(7)	2.420(5)	Gd(101)-O(107)	2.376(5)
Gd(1)-O(8)	2.403(4)	Gd(101)-O(108)	2.365(5)
Gd(1)-O(9)	2.418(5)	Gd(101)-O(109)	2.425(5)
Angles/◦			
O(8)-Gd(1)-O(9)	69.21(17)	O(108)-Gd(101)-O(109)	72.15(18)
O(4)-Gd(1)-O(5)	71.51(16)	O(105)-Gd(101)-O(104)	69.96(19)
O(6)-Gd(1)-O(7)	71.93(16)	O(107)-Gd(101)-O(106)	70.53(15)
O(1)-Gd(1)-O(2)	103.41(17)	O(101)-Gd(101)-O(102)	89.87(17)

3.2.3 UV/Vis Gadolinium complex Absorption Spectroscopy

Photoluminescence properties were studied for a series of Gd complexes, comprising the ligands DPEPO, hfac or both, to identify the singlet and triplet

energy levels of the ligands in order to further our understanding of the origin of the emission. Note that the Gd $^6P_{7/2}$ emissive level is too high in energy to be sensitised by the antennae, therefore the emission spectra of the Gd complexes originate from the triplet ligand states due to the heavy atom effect, which increases the spin-orbit coupling and the rate of intersystem crossing. This effect is shown by the large spectral shift between excitation and emission. Spectra were recorded in degassed DCM solution at 77 K. Due to this difference in photophysics, the Gd complex is discussed separately from Eu, Tb, Nd and Yb.

Gd cannot be directly excited by energy transfer from the ligands due to its high-energy first excited state, hence it can give useful information about the excited-state energies of the ligands bound to it. To understand the contribution of both hfac and DPEPO ligands to the photophysical behaviour of the new complexes, UV/Vis absorption measurements of the Gd complex **5**, related Gd complexes and free DPEPO ligand were recorded (Fig. 3.10).

Firstly, we studied the UV/Vis absorption in DCM solution of the free ligand: DPEPO (green line) shows an absorption onset around 302 nm (33000 cm^{-1}) and λ_{max} = 292 nm (34500 cm^{-1}, ε = 4300 M^{-1} cm^{-1}). $[Gd(hfac)_3(H_2O)_2]$ (black line) has a broader absorption than DPEPO shifting the λ_{max} to 298 nm (33500 cm^{-1}, ε = 6400 M^{-1} cm^{-1}) and onset at 345 nm (28900 cm^{-1}). $[Gd(DPEPO)(NO_3)_3]$ absorption spectrum (blue line) follows same shape as the DPEPO ligand but has broader absorption with onset equal to $[Gd(hfac)_3(H_2O)_2]$ (λ_{max} = 292 nm (34500 cm^{-1}, ε = 10200 M^{-1} cm^{-1}).

Finally [Gd(hfac)$_3$DPEPO] absorption (red line) overlaps with all three previous spectra with λ_{max} = 294 nm (33700 cm^{-1}, ε = 20200 M^{-1} cm^{-1}). The onset is the same as the [Gd(DPEPO)(NO$_3$)$_3$] and [Gd(hfac)$_3$(H$_2$O)$_2$]. The overlap of the [Gd(hfac)$_3$DPEPO] complex with respect to the single absorption spectrum of the complex [Gd(hfac)$_3$(H$_2$O)$_2$] and DPEPO indicates a synergic effect due to both ligands absorption contribution.

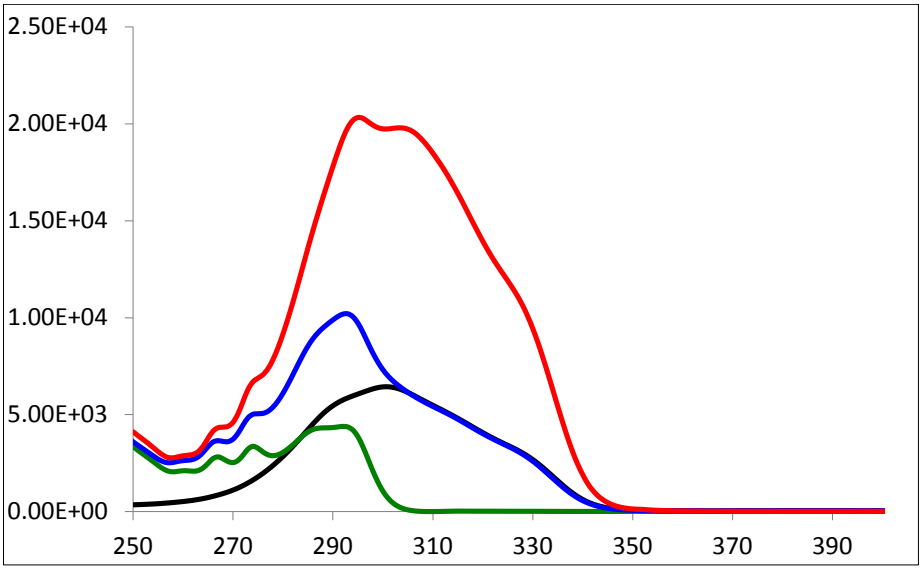

Fig. 3.10. UV/Vis absorption spectra of DPEPO ligand (green line), Gd(hfac)$_3$(H$_2$O)$_2$ (black line), [Gd(DPEPO)(NO$_3$)$_3$] (blue line), Gd(hfac)$_3$DPEPO (red line) in DCM at room temperature.

The analysis of the excitation and emission spectra of [Gd(DPEPO)(NO$_3$)$_3$] and [Gd(hfac)$_3$(H$_2$O)$_2$] revealed the singlet and triplet energy levels of the DPEPO and hfac ligands respectively (Fig. 3.11). The triplet energy level of [Gd(DPEPO)(NO$_3$)$_3$] and [Gd(hfac)$_3$(H$_2$O)$_2$] are measured from the high-energy onset of the emission curve and found at 27600 cm^{-1} (362 nm) and at 22300 cm^{-1} (449 nm) respectively. The singlet energy levels, derived from the onset of the absorption spectrum, are at 345 nm (28900 cm^{-1}) for both hfac and DPEPO.

The presence of the two different ligands in the environment of the Gd ion is

important for the photoluminescence properties. The synergic effect first observed in the UV/Vis spectra is reproduced in Fig. 3.11, in which the [Gd(hfac)$_3$DPEPO] excitation spectrum is broadened compared with [Gd(hfac)$_3$(H$_2$O)$_2$] by about 1600 cm^{-1}. Also, the lowest triplet level of the complex [Gd(hfac)$_3$DPEPO] is clearly localised on the hfac ligand, since the emission spectrum of the complex is almost identical to the hfac ligand emission. The [Gd(hfac)$_3$DPEPO] excitation spectrum looks slightly distorted and it could indicate saturation, but the solutions measured were in the optimal range of absorption (0.1 with 5x10^{-6} M concentration). Lower concentration did not give accurate measurements because emission could not be observed. A possible inner filter effect could account for the unexpected peak shape, however this does not affect the key conclusions and these studies provide a framework for understanding the ligand energetics of all the analogous complexes prepared in the series.

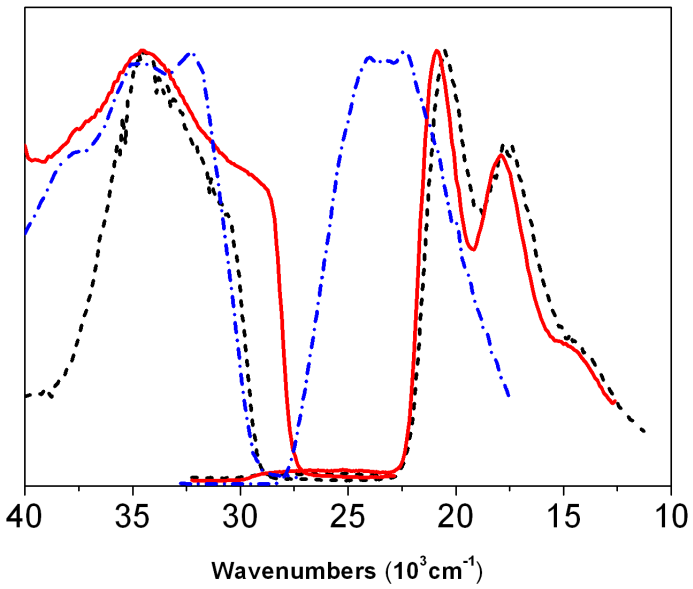

Fig. 3.11. Normalised excitation and emission spectra of [Gd(hfac)$_3$(H$_2$O)$_2$] (black dotted line), [Gd(hfac)$_3$DPEPO] (red solid line) and [Gd(DPEPO)(NO$_3$)$_3$] (blue dash dot line) in DCM at 77 K.

3.2.4 Computational studies

In order to gain more insight into the excited-state properties for this family of complexes, a theoretical investigation of [Eu(hfac)$_3$(DPEPO)] was carried out at the DFT level. The europium complex was studied because of the high quantum yield measured previously. The DFT methodology has been shown in the literature to be a reliable approach to address this type of problem.[11, 12] In particular, the use of f-in-core RECP was used as an appropriate method. First of all, geometry optimisation of the [Eu(hfac)$_3$(DPEPO)] complex was carried out without any symmetry constraints on both the singlet and triplet spin states (Fig. 3.12).

Although the crystal structure was obtained for a smaller lanthanide centre (Gd), the optimised structure compares well with the experimental one. In particular, the Ln-O1/Ln-O2 bond lengths are reproduced within 0.05 Å and the Ln-O4/Ln-O5 ones by 0.03 Å (the optimised bond lengths being longer than the experimental ones as expected when using f-in-core RECPs[13]). This agreement demonstrates the ability of the methodology to accurately reproduce the structure of europium complexes. Information about ligand excitation can be obtained by analysing the geometry of the triplet state. Indeed, in the triplet state, the geometry of the DPEPO ligand remains unchanged whereas one hfac ligand is clearly affected. In particular, the C-C bonds of one of the hfac ligands are elongated by 0.02 Å with respect to the other two. This corresponds to an occupation of the π^* orbital of the hfac ligand, indicating that the excitation is primarily located on it. Hence, TDDFT calculations were carried out to confirm this. The lowest excitation computed at the TDDFT level

corresponds to a singlet-triplet excitation (with three degenerate triplets, one located on each hfac ligand) involving the HOMO and LUMO orbitals that are located on the hfac ligand (Fig. 3.13). Moreover, the triplet energy level is computed to be 20950 cm^{-1} which is in excellent agreement with the phosphorescence spectrum of the $[Gd(hfac)_3(H_2O)_2]$ complex, demonstrating that the excitation is located on the hfac ligand. Thus, all the theoretical analyses are pointing toward an excitation located on the hfac ligand.

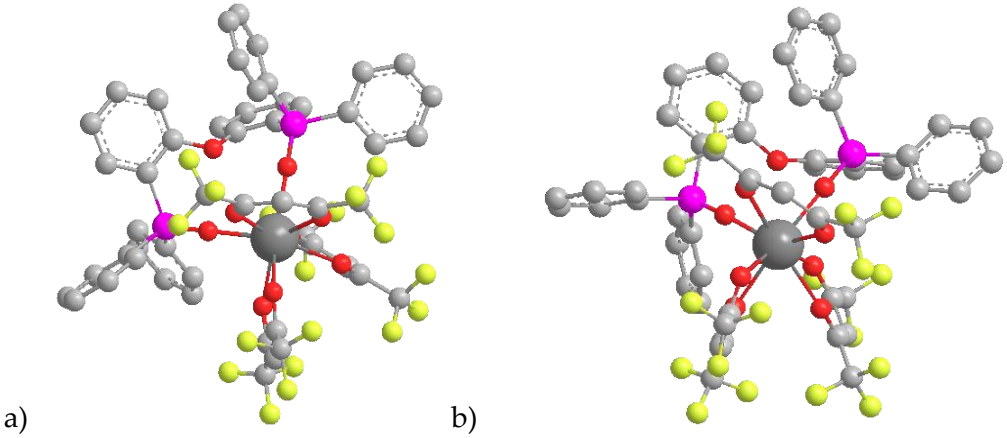

a) b)

Fig. 3.12. Optimised structures of the singlet spin state (a) and of the triplet spin state (b) of the $[Eu(hfac)_3(DPEPO)]$.

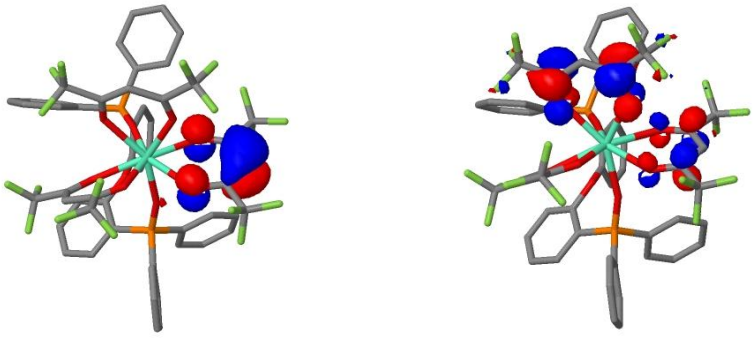

a) b)

Fig. 3.13. Molecular orbitals involved in the excitation of the $[Eu(hfac)_3(DPEPO)]$ complex. a) HOMO, b) LUMO

3.2.5 Photoluminescence studies

Compound **2**, **3** and **4** were used to record absorption, excitation and emission spectra at room temperature, in DCM dilute solutions. Fig. 3.14 and 3.15 show the absorption and excitation spectra. For clarity, the curves are offset along the y-axis.

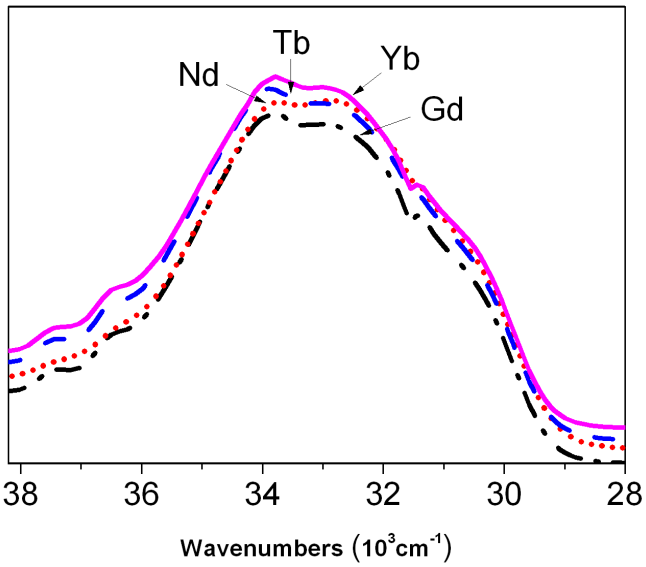

Fig. 3.14. Normalised UV/Vis absorption spectra of the [Ln(hfac)$_3$DPEPO] complexes: [Yb(hfac)$_3$DPEPO] (pink solid line); [Tb(hfac)$_3$DPEPO] (blue dashed line); [Nd(hfac)$_3$DPEPO] (red dotted line); [Gd(hfac)$_3$DPEPO] (black dash dot line) in DCM at room temperature.

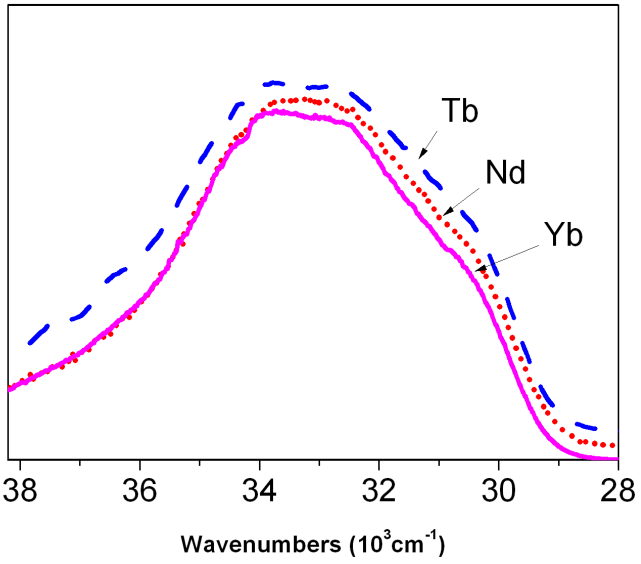

Fig. 3.15. Normalised excitation spectra of the emissive compounds: [Yb(hfac)$_3$DPEPO] (pink solid line); [Tb(hfac)$_3$DPEPO] (blue dashed line); [Nd(hfac)$_3$DPEPO] (red dotted line) in DCM at room temperature.

Excitation and absorption spectra are essentially superimposable and it was also clearly observed that the emission spectrum is independent of the excitation wavelength. Upon UV excitation, narrow emission bands typical of lanthanide complexes were observed (Fig. 3.16). The four main emission bands of the Tb^{3+} complex **2** originate from $^5D_4 \rightarrow {}^7F_j$ (with j = 6,5,4,3): 20400 cm^{-1} (488 nm), 18400 cm^{-1} (544 nm), 17200 cm^{-1} (581 nm), 16200 cm^{-1} (619 nm). The Nd^{3+} complex **3** has three narrow emission bands at 885 nm (11300 cm^{-1}, $^4F_{3/2} \rightarrow {}^4I_{9/2}$), 1063 nm (9400 cm^{-1},$^4F_{3/2} \rightarrow {}^4I_{11/2}$) and 1336 nm (7500 cm^{-1}, $^4F_{3/2} \rightarrow {}^4I_{13/2}$), and the Yb^{3+} complex **4** has an emission due to the $^2F_{7/2} \rightarrow {}^2F_{5/2}$ transition at 980 nm (10200 cm^{-1}).

From these measurements, energies of the emissive lanthanide states were determined as follows: Tb = 20400 cm^{-1} (488 nm), Yb = 10200 cm^{-1} (980 nm), Nd = 11300 cm^{-1} (885 nm), Eu = 16300 cm^{-1} (613 nm; Eu value was taken from previous work[3]) (Fig. 3.16). These values were taken by measuring the wavenumbers at the highest-energy peak for each complex.

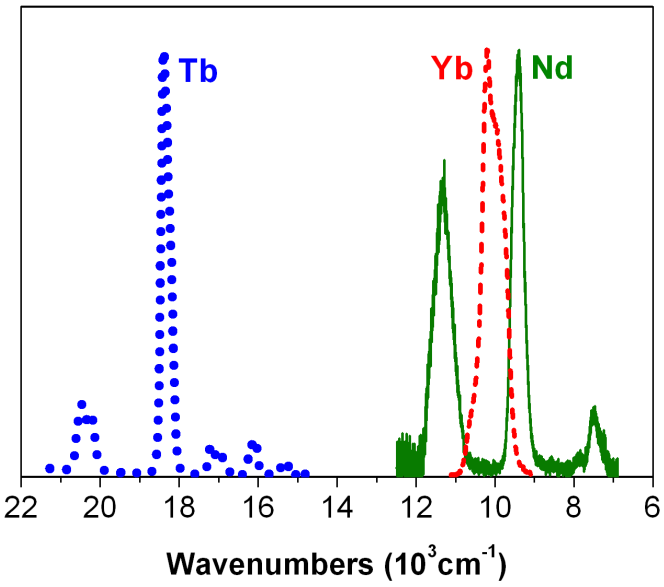

Fig. 3.16. Normalised emission spectra of the emissive compounds: [Yb(hfac)$_3$DPEPO] (red dashed line); [Tb(hfac)$_3$DPEPO] (blue dotted line); [Nd(hfac)$_3$DPEPO] (green solid line) in DCM at room temperature. A Peltier cooled R2658P Hamamatsu photomultiplier was used for Tb compound and a liquid nitrogen cooled Hamamatsu R5509-72 NIR photomultiplier was used for Nd and Yb compounds.

Table 2 reports the spectral properties (wavelengths of the absorption band and the emission transitions and pseudo-Stokes' shifts, $\Delta\upsilon_s$, calculated from the maxima in the absorption and emission spectra) and the photoluminescence quantum yields of the studied compounds. The measurements were recorded in DCM solution at room temperature. The PLQYs reported are averages of at least four independent measurements with a relative error of 10%, taken with an integrating sphere. No concentration effect on the PLQY was observed in the range of absorbance 0.1 – 0.4 at λ_{exc}.

The fluorescence decay times were measured at a fixed wavelength for each compound, both excitation and emission. Data are an average of at least three

measurements in DCM solution at room temperature and given in Table 3. From the ratio of the measured lifetime to the radiative lifetime, the Φ_{Ln} values for the complexes are estimated as: Tb ≤ 50%, Nd ≤ 1%, Yb ≤ 2%, Eu = 78% . However, the differing values of τ_R reported for Tb[14, 15], Nd[16, 17] and Yb[38, 40, 41] in different recent studies (Table 2) illustrates the uncertainty in the resulting Φ_{Ln} values often considered and reported in literature as Φ_{tot} . Note that an important exception to this regards Eu complexes, for which the $^5D_0 \rightarrow {}^7F_1$ magnetic dipole transition is independent of the coordination sphere and can be used as a standard for the dipole strength, allowing τ_R to be accurately determined for any given Eu complex.[36]

Table 2 Spectral and photophysical properties of the investigated compounds in DCM

compound	λ_{exc} (nm)	λ_{em} (nm)	$\Delta\tilde{\nu}_S$ (cm-1)	PLQY(%)
$Tb(hfac)_3DPEPO$	274^{sh}, <u>295</u>, 304^{sh}	489, 493^{sh}, <u>545</u>, 582, 590^{sh}, 620	13400, <u>15500</u>	5.5
$Nd(hfac)_3DPEPO$	<u>295</u>, 304	885, <u>1063</u>, 1257, 1336	22600, <u>24500</u>	1.1
$Yb(hfac)_3DPEPO$	274^{sh}, <u>295</u>, 304^{sh}	943^{sh}, <u>981</u>, 1005	23700	1.9
$Eu(hfac)_3DPEPO$[3]	<u>340</u>	578, 592, <u>613</u>, 650, 697	31250	76

Table 3 Radiative and natural lifetime of the investigated compounds in DCM at fixed wavelength of emission and excitation

compound	λ_{exc} (nm)	λ_{em} (nm)	τ_R (ms)	Lifetime (ms)
$Tb(hfac)_3DPEPO$[14, 15]	295	543	5.1,[14] 1.9[15]	0.95
$Nd(hfac)_3DPEPO$[16, 17]	266	1080	0.25,[16] 0.613[17]	0.027
$Yb(hfac)_3DPEPO$[15, 17, 18]	266	980	1.3,[15] 1.2,[17] 1.2[18]	0.022
$Eu(hfac)_3DPEPO$[19]	320	613	1.11[19]	0.86

Efficient sensitisation of lanthanides requires careful control regarding the singlet excited state and the triplet excited state. For example, europium complexes typically have an emission at 610 nm (16300 cm^{-1}); the achievement of efficient sensitisation requires the ligand triplet energy level to be at least 2500 cm^{-1} higher (~19000 cm^{-1}) and hence its singlet energy level must be around 24000 cm^{-1} if it is assumed to be typically around 5000 cm^{-1} higher than the triplet level, namely 416nm.[20] Accordingly it is difficult to sensitise Eu efficiently with visible light-absorbing ligands. When the molecule is excited by UV light, both the DPEPO and hfac ligands undergo to the transition from the ground state to the singlet excited state. A triplet energy level is then reached via intersystem crossing.

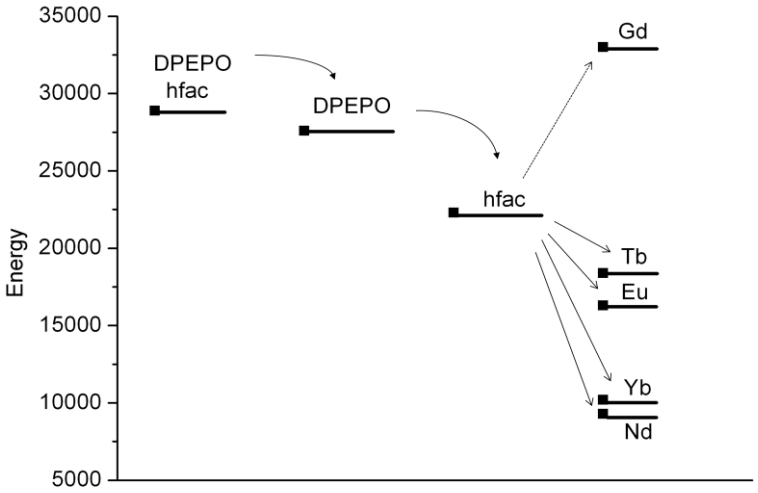

Fig. 3.17: Energy level diagram of the studied compounds

The energy transfer to the lanthanide clearly occurs from the hfac ligand, as shown through the emission spectra of the Gd complexes and the computational study of the Eu complex **1**. Theoretically, the Tb compound also has an excited energy level (20466 cm^{-1}, 488 nm) able to be sensitised by the triplet state of the antenna (22260 cm^{-1}, 449 nm), however in this case, we do not observe a high PLQY. The PLQY of the Tb complex (5.1%) is lower compared with the one measured before for Eu (80%). A reason for this unexpected behaviour could be the longer radiative lifetime for the Tb complex, which could encourage an energy back transfer from the excited state of the lanthanide to the triplet state of the antenna ligand. Moreover, the proximity of the two excited energy levels involved is another factor that can encourage back energy transfer from the triplet state. The presence of some ligand luminescence was detected in the spectrum at a wavelength below 480 nm (20800 cm^{-1}), which means that the efficiency of the total energy transfer from the triplet state of the antenna to the excited state of the lanthanide is incomplete, leading to ligand luminescence that competes with the emission process of the Tb centre (Fig. 3.18). This is additional evidence of incomplete energy transfer to the Tb excited level.

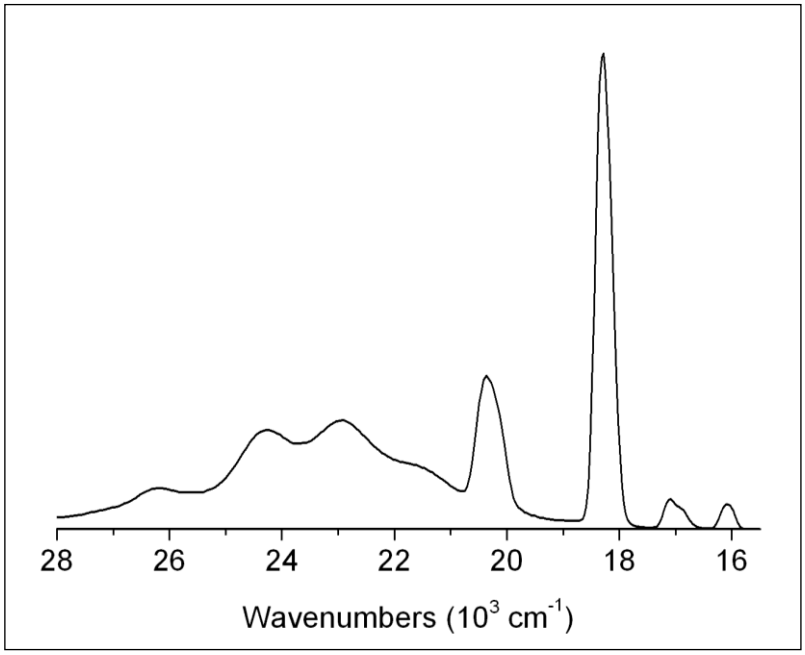

Fig. 3.18. Emission spectrum with ligand phosphorescence of $Tb(hfac)_3(DPEPO)$.

Nd and Yb energy levels are quite low (11300 cm^{-1} and 10204 cm^{-1}), therefore a faster relaxation to the ground state is more likely to happen after the energy transfer from the triplet state of the antenna takes place. This leads to a low PLQY, which is typical for Nd[21, 22] (0.45% and 0.33% reported) and Yb[23] complexes (1.28%), because they are particularly sensitive to deactivation by radiationless pathways. The presence of high-vibration-energy bonds such as C-H accelerate the quenching of PLQY due to the overlap between the Frank-Condon wavefunctions of the f excited state and an overtone of the C-H oscillator.[24, 25] A possible approach to overcome this problem would be deuteration or fluorination of the ligands, because they would then possess lower energy vibrations of the bonds.

3.3 Conclusions

In this chapter, we have addressed the structural and photophysical properties of [Ln(hfac)$_3$DPEPO] complexes. The reported compounds were fully characterised and we gained a better insight into factors controlling energy transfer within the Eu complex, the role of the hfac and DPEPO ligands and the interaction between them. Some synergic effects between the two ligands were shown in the absorption properties, in which a broader absorption spectrum of the complex itself is shown with respect to the single ligand absorptions. Furthermore, we clearly have a better understanding of the overall photoluminescence process, underlined by the photoluminescence spectroscopy analysis. Both emission and computational studies agreed on the fact that the energy transfer to the Lanthanide ion upon excitation of the molecule is likely to come from the hfac ligand, which has the lowest triplet excited state directly able to transfer its energy to the lanthanide ion. Although many details about the structure and the energy transfer process are now clearly described, some improvements on the general molecular structure can be addressed.

An extensively conjugated π-electrons system could be used to shift the excitation energy of the ligand to a longer wavelength, possibly without lowering efficiency of energy transfer and hence the photoluminescence quantum yield. Specifically, the DPEPO ligand could be modified with ancillary groups on the diphenyl phosphine part of the molecule. Provided the excited triplet of the modified DPEPO remains

above the energy of the excited hfac, the energy transfer process should remain efficient. In order to increase the intrinsic quantum yield of the lanthanide ions, deuteration or halogenation of the ligands could be applied to reduce the presence of high frequency oscillators, which are responsible for quenching the emission efficiency. In particular, deuteration of the hfac ligand might be expected to enhance the quantum yield since this proton is in close proximity to the lanthanide centre.

3.4 Experimental section

Materials

H_2O, acetone, ethanol and hexane (analytical grade from Acros) were degassed and used without further purification. KO^tBu, 1,1,1,5,5,5-Hexafluoroacetylacetone, $EuCl_3 \cdot 6H_2O$, $TbCl_3 \cdot 6H_2O$, $NdCl_3 \cdot 6H_2O$, $YbCl_3 \cdot 6H_2O$, $GdCl_3 \cdot 6H_2O$ and $Gd(NO_3)_3 \cdot 6H_2O$ were purchased from Sigma-Aldrich. The ligand Bis(2-diphenylphosphino)phenyl) ether oxide and $Gd(DPEPO)(NO)_3$ were synthesised according to a published procedure.[5]

Synthesis of Ln(diketonate)$_3$(H_2O)$_2$ compounds

All the compounds were synthesised according to the following procedure:

3 mmol of potassium tert-Butoxide were added to a solution of 3 mmol hexafuoroacetylacetone in water (20 ml). The mixture was stirred until dissolution of the reagents and 1 mmol of europium trichloride was added to afford white precipitate. Then the mixture was left to stir under a flux of nitrogen for 3 h at 60 °C, and at room temperature for another hour.

The precipitate was filtered off, washed with cold water (100 ml) and hexane (5 ml), and stored under vacuum until dryness. The comound was further purified by recrystallisation from acetone/hexane and obtained as a powder.

$Eu(hfac)_3(H_2O)_2$

Europium tris(hexafluorocaetylacetonate) dihydrate (375 mg).

Yield: 46%. ESI MS (MeOH): m/z = 809.07 (M^+)

Found: C, 23.73; H, 0.87. Calc. for $C_{15}H_7EuF_{18}O_8$: C, 22.27; H, 0.37%

$Tb(hfac)_3(H_2O)_2$

Terbium tris(hexafluorocaetylacetonate) dihydrate (428 mg).

Yield: 52%. ESI MS (MeOH): m/z = 815 (M^+)

Found: C, 23.48; H, 0.40. Calc. for $C_{15}H_7F_{18}O_8Tb$: C, 22.08; H, 0.86%

$Yb(hfac)_3(H_2O)_2$

Ytterbium tris(hexafluorocaetylacetonate) dihydrate (720 mg).

Yield: 84%.

Found: C, 21.64; H, 0.78. Calc. for $C_{15}H_7F_{18}O_8Yb$: C, 21.70; H, 0.85%

$Nd(hfac)_3(H_2O)_2$

Neodymium tris(hexafluorocaetylacetonate) dihydrate (425 mg).

Yield: 53%. ESI MS (MeOH): m/z = 801 (M^+)

Found: C, 22.32; H, 0.79. Calc. for $C_{15}H_7F_{18}O_8Nd$: C, 22.48; H, 0.88%

$Gd(hfac)_3(H_2O)_2$

Gadolinium tris(hexafluorocaetylacetonate) dihydrate (709 mg).

Yield: 40%. ESI MS (MeOH): m/z = 607 ($M - C_5HF_6O_2$)

Found: C, 23.21; H, 0.4. Calc. for $C_{15}H_7F_{18}GdO_8$: C, 22.12; H, 0.87%

Synthesis of Ln(diketonate)$_3$(DPEPO) compounds

Eu, Tb, Yb and Nd compounds were synthesised according to the following procedure:

1 mmol of Ln(hfac)$_3$(H$_2$O)$_2$ was added to a DPEPO solution in water:ethanol (1:1) (10ml:10ml) to afford white precipitate. The mixture was left to stir at 60 °C for 1 h under a flux of nitrogen, then for 3 h at room temperature. The white precipitate was filtered off and washed with cold water (100 ml) and hexane (5 ml) and left under vacuum until dryness. The comound was further purified by recrystallisation from acetone/hexane and obtained as a powder.

Eu(hfac)$_3$(DPEPO) – compound 1

Europium tris(hexafluorocaetylacetonate) (2-(diphenylphosphino)phenyl)ether oxide (175 mg).

Yield: 71%. ESI MS (MeOH): m/z = 1347 (M^-)

^{1}H NMR (300 MHz, CDCl$_3$): δ 5.04 (s, 3H), 6.64 (dd, 2H, J_{H-H} = 7.5, J_{P-H} = 5.0), 6.97 (tr, 2H, J = 7.5 Hz), 7.18 (dd, J = 7.5 Hz, 3H), 7.35 (m, 4H), 7.38 (m, 4H), 7.76-7.86 (m, 4H), 7.90 (d, 2H, J = 7.5 Hz), 8.35 (dd, 4H, J = 7.5 Hz), 8.91 (dd, 4H, J = 7.5 Hz).

Found: C, 45.92; H, 1.85. Calc. for $C_{51}H_{34}EuF_{18}O_9P_2$: C, 45.49; H, 2.54%

Tb(hfac)$_3$(DPEPO) – compound 2

Terbium tris(hexafluorocaetylacetonate) (2-(diphenylphosphino)phenyl)ether oxide (157 mg).

Yield: 63%. ESI MS (MeOH): m/z = 1389 (M - $C_5HF_6O_2$)

Found: C, 47.29; H, 1.82. Calc. for $C_{51}H_{34}F_{18}O_9P_2Tb$: C, 47.29; H, 2.31%

$Yb(hfac)_3(DPEPO)$ – compound 3

Ytterbium tris(hexafluorocaetylacetonate) (2-(diphenylphosphino)phenyl)ether oxide (208 mg).

Yield: 54%. ESI MS (MeOH): m/z = 1159 ($M-C_5H_2F_6O_2$)

Found: C, 44.71; H, 2.13. Calc. for $C_{51}H_{34}F_{18}O_9P_2Yb$: C, 44.88; H, 2.29%

$Nd(hfac)_3(DPEPO)$ – compound 4

Neodymium tris(hexafluorocaetylacetonate) (2-(diphenylphosphino)phenyl) ether oxide (361 mg).

Yield: 62%. ESI MS (MeOH): m/z = 1128 ($M-C_5H_2F_6O_2$)

Found: C, 48.03; H, 1.33. Calc. for $C_{51}H_{34}F_{18}NdO_9P_2$: C, 45.85; H, 2.34%

$Gd(hfac)_3$DPEPO – compound 5

Gadolinium tris(hexafluorocaetylacetonate) (2-(diphenylphosphino)phenyl)ether oxide (363 mg).

Yield: 77%. ESI MS (MeOH): m/z = 1142 ($M-C_5H_2F_6O_2$)

Found: C, 45.38; H, 2.25. Calc. for $C_{51}H_{34}F_{18}GdO_9P_2$: C, 45.41; H, 2.32%

$Gd(DPEPO)(NO_3)_3$

Gadolinium (2-(diphenylphosphino)phenyl)ether oxide tri-nytrate (277 mg). A 1.0 mmol portion of DPEPO was dissolved in 50 ml of ethanol. A 1.0 mmol portion of $Gd(NO_3)_3(H_2O)_6$ in 0.1 ml of water was added in solution dropwise under stirring and the solution was heated to refluxing for 2 h. White precipitates were formed. The resulting solution was filtered and a white powder was obtained.

Yield: 58%.

IR (KBr) ν_{max}/cm^{-1}: 1589, 1567, 1461, 1437, 1380, 1300, 1229, 1154, 1135, 1081, 879, 720,

695 cm^{-1}.

Found: C, 47.60; H, 3.00; N, 4.53. Calc. for $C_{36}H_{28}GdN_3O_{12}P_2$: C, 47.32; H, 3.09; N, 4.60%

Photoluminescence and lifetime details

The emission and excitation spectra of compounds **2**, **3** and **4** were measured using an Edinburgh Instruments FS920 spectrometer. Excitation light from a 450 W Xenon lamp was delivered via double monochromators to the sample chamber and emission was detected either by a Peltier cooled R2658P Hamamatsu photomultiplier or a liquid nitrogen cooled Hamamatsu R5509-72 NIR photomultiplier. The photoluminescence quantum yields were determined by absolute measurement, by using a Horiba Jobin Yvon integrating sphere[26]. All measurements were performed at room temperature in dichloromethane (DCM, spectroscopic grade from Fisher Scientific). Dilute solutions (absorbance 0.1- 0.2 at the excitation wavelength, λ_{exc}) were used for emission measurements. The photoluminescence quantum yields were measured in air-equilibrated solutions. Absorption spectra were obtained by a Varian Cary 50 Scan spectrophotometer in DCM solution. Excited-state lifetime data in the visible were measured using a Fluoromax-P spectrofluorimeter (Horiba-Jobin-Yvon) in DCM (77 °K) and fitted to exponential functions using an iterative non-linear least squares algorithm in the 'Solver' facility in Microsoft Excel.

Computational details

The analysis were carried out by Laurent Maron from the Institut National des Sciences Appliquées, Toulouse (France). Calculations were made at the DFT level of theory using the hybrid functional B3PW91.[27, 28] Geometry optimizations were carried out without any symmetry restrictions; the nature of the *extrema* (*minima* and transition states) was verified with analytical frequency calculations. All the computations were performed with the Gaussian 03 suite of programs.[29] Europium and fluorine were represented with a Stuttgart–Dresden pseudo-potential in combination with its adapted basis set.[30, 31] The basis set has been augmented by *f* function (◎ = 1.0) for Eu and a set of *d* functions for F[32]. Carbon, nitrogen, oxygen and hydrogen atoms have been described with all electrons 6–31G(*d*,*p*) double–ζ quality basis sets.[33] TDDFT methods were also performed to define the nature of the triplet states.

Crystallographic details

$Gd(hfac)_3DPEPO$ **(5)** complex was obtained by slow evaporation from acetone/hexane and the structure determined by single-crystal X-ray crystallography by Anna Collins. Crystal data are provided in Table 4.

Table 4 Crystal data, collection, and structure refinement parameters for the complex Gd(hfac)$_3$DPEPO (complex **5**)

Empirical formula	$C_{51}H_{31}F_{18}GdO_9P_2$
M_r/g mol^{-1}	1348.96
Crystal system	Orthorhombic
Space group	P b c a
Cryst size/mm^3	0.14 × 0.22 × 0.61
T/K	150
a/ Å	24.6540(8)
b/ Å	22.2370(7)
c/ Å	39.1070(12)
a/◦	90
b/◦	90
γ /◦	90
V/Å^3	21439.7
Z	16
ρ_{calcd}/Mg m^{-3}	
μ/mm^{-1}	1.414
F(000)	10640
R_1 [$I > 2\sigma(I)$]	0.0471
wR_2 [$I > 2\sigma(I)$]	0.0471
R_1 (all data)	0.1028
wR_2 (all data)	0.0542
Number of reflections	
Number of independent reflections	
R_{int}	
GOF	1.2141

3.5 References

1. Bunzli, J.-C.G., *Chem. Lett.*, 2009. **38**(2): p. 104.
2. Eliseeva, S.V. and Bünzli, J.C.G., *Chem. Soc. Rev.*, 2010(39): p. 189.
3. Moudam, O., Rowan, B.C., Alamiry, M., Richardson, P., Richards, B.S., Jones, A.C., and Robertson, N., *Chem Comm*. 2009. p. 6649.
4. Bünzli, J.C.G., Andre, N., Elhabiri, M., Muller, G., and Piguet, C., *J. Alloys Compd.*, 2000. **303**: p. 66.
5. Xu, H., Wang, L.H., Zhu, X.H., Yin, K., Zhong, G.Y., Hou, X.Y., and Huang, W., *J. of Phys Chem B*, 2006. **110**(7): p. 3023.
6. Kido, J. and Okamoto, Y., *Chem. Rev*, 2002. **102**(6): p. 2357.
7. Allen, F., *Acta Cryst.*, 2002. **58**(3 Part 1): p. 380.
8. Kennedy, F., Shavaleev, N.M., Koullourou, T., Bell, Z.R., Jeffery, J.C., Faulkner, S., and Ward, M.D., *Dalton Trans.*, 2007(15): p. 1492.
9. Eliseeva, S.V., Pleshkov, D.N., Lyssenko, K.A., Lepnev, L.S., Bulˆnzli, J.-C.G., and Kuzmina, N.P., *Inorg. Chem.*, 2011. **50**(11): p. 5137.
10. De Silva, C.R., Maeyer, J.R., Wang, R., Nichol, G.S., and Zheng, Z., *Inorg. Chim. Acta*, 2007. **360**(11): p. 3543.
11. Gutierrez, F., Tedeschi, C., Maron, L., Daudey, J.-P., Poteau, R., Azema, J., Tisnes, P., and Picard, C., *Dalton Trans.*, 2004(9): p. 1334.
12. Gutierrez, F., Tedeschi, C., Maron, L., Daudey, J.-P., Azema, J., Tisnès, P., Picard, C., and Poteau, R., *Journal of Molecular Structure: THEOCHEM*, 2005. **756**(1-3): p. 151.
13. Maron, L. and Eisenstein, O., *J. Phys. Chem. A*, 2000. **104**(30): p. 7140.
14. Duhamel-Henry, N., Adam, J.L., Jacquier, B., and Linarès, C., *Opt. Mater.*, 1996. **5**(3): p. 197.
15. Aebischer, A., Gumy, F., and Bunzli, J.-C.G., *Phys. Chem. Chem. Phys.*, 2009. **11**(9): p. 1346.
16. Klink, S.I., Grave, L., Reinhoudt, D.N., van Veggel, F.C.J.M., Werts, M.H.V., Geurts, F.A.J., and Hofstraat, J.W., *J. Phys. Chem. A*, 2000. **104**(23): p. 5457.
17. Werts, M.H.V., Jukes, R.T.F., and Verhoeven, J.W., *Phys. Chem. Chem. Phys.*, 2002. **4**(9): p. 1542.
18. He, H., Sykes, A.G., May, P.S., and He, G., *Dalton Trans.*, 2009(36): p. 7454.
19. McIntosh, K.R., Lau, G., Cotsell, J.N., Hanton, K., Bätzner, D.L., Bettiol, F., and Richards, B.S., *Prog. Photovol: Res. Appl.*, 2009. **17**(3): p. 191.
20. Biju, S., Raj, D.B.A., Reddy, M.L.P., and Kariuki, B.M., *Inorg. Chem.*, 2006. **45**(26): p. 10651.
21. Zhang, J. and Petoud, S., *Chem. Eur. J.*, 2008. **14**(4): p. 1264.
22. Vasquez Lopez, M., Eliseeva, S.V., Blanco, J.M., Rama, G., Bermejo, M.R., Vazquez, M.E., and Bunzli, J.C.G., *Eur. J. Inorg. Chem.*, 2010: p. 4532.
23. Sun, L.N., Yu, J.B., Zheng, G.L., Zhang, H.J., Meng, Q.G., Peng, C.Y., Fu, L.S., Liu, F.Y., and Yu, Y.N., *Eur. J. Inorg. Chem.*, 2006(19): p. 3962.
24. Bünzli, J.-C.G. and Eliseeva, S.V., *J. Rare Earths*. **28**(6): p. 824.
25. Monguzzi, A., Milani, A., Lodi, L., Trioni, M.I., Tubino, R., and Castiglioni, C., *New J. Chem.*, 2009. **33**(7): p. 1542.
26. Wilson, L.R. and Richards, B.S., *Appl. Opt.*, 2009. **48**(2): p. 212.
27. Becke, A.D., *Chem. Phys*, 1993. **98**(1): p. 5648.
28. Burke, K.P., J. P.; Yang, W., *Electronic Density Functional Theory: Recent Progress and New Directions*, 1998.

29. Frisch, M.J.T., G. W.; Schlegel, H. B.; Scuseria, G. E.; Robb, M. A.; Cheeseman, J. R.; Zakrzewski, V. G.; Montgomery, J. A.; Stratman, R. E.; Burant, J. C.; Dapprich, S.; Millam, J. M.; Daniels, A. D.; Kudin, K. N.; Strain, M. C.; Farkas, O.; Tomasi, J.; Barone, V.; Cossi, M.; Cammi, R.; Mennucci, B.; Pomelli, C.; Adamo, C.; Clifford, S.; Ochterski, J.; Petersson, G. A.; Ayala, P. Y.; Cui, Q.; Morokuma, K.; Malick, D. K.; Rabuck, A. D.; Raghavachari, K.; Foresman, J. B.; Cioslowswi, J.; Ortiz, J. V.; Baboul, A. G.; Stefanov, B. B.; Liu, G.; Liashenko, A.; Piskorz, P.; Komaromi, I.; Gomperts, R.; Martin, R.; Fox, D. J.; Keith, T.; Al-Laham, M. A.; Peng, C. Y.; Nanayakkara, A.; Gonzalez, C.; Challacombe, M.; Gill, P. M. W.; Jonhson, B.; Chen, W.; Wong, M. W.; Andres, J. L.; Head-Gordon, M.; Replogle, E. S.; Pople, J. A., *Gaussian 03, Revision D-02*, in *Gaussian 03, Revision D-02*, I. Gaussian, Pittsburgh PA, Editor. 2003.
30. Dolg, M., Stoll, H., and Preuss, H., *Theoretical Chemistry Accounts: Theory, Computation, and Modeling (Theoretica Chimica Acta)*, 1993. **85**(6): p. 441.
31. Bergner, A., Dolg, M., Kuchle, W., Stoll, H., and Preus, H., *Mol. Phys.*, 1993. **80**(6): p. 1431.
32. Maron, L. and Teichteil, C., *Chem. Phys.*, 1998. **237**(1-2): p. 105.
33. Hariharan, P.C. and Pople, J.A., *Theor Chem Accounts Theor Comput Model Theor Chim Acta*, 1973. **28**(3): p. 213.

Chapter 4: Chromium dioxalate and analogue compounds

4.1 Introduction

Chromium photophysics has been a central topic in transition metal photochemistry since the 1960s and despite all the research efforts so far, interest continues to be present especially regarding investigation of excited states and primary photochemical processes.[1]

Chromium (III) has a d^3 configuration and it is considered to have an ideal octahedral geometry only in a few ionic crystals,[2] but we can still usefully consider hexacoordinated Cr(III) complexes to be close enough to the O_h geometry. In this situation we have two orbital subsets, t_{2g} and e_g, filled according to Hund's Rule. The quartet ground level $^4A_{2g}$ has electronic configuration $(t_{2g})^3$, which also generates two doublet levels, $^2T_{1g}$ and ^2E_g. With the optical promotion of an electron into the e_g orbital, the new configuration is $(t_{2g})^2(e_g)^1$ with preservation of the spin. This leads to associated quartet excited states with labels $^4T_{2g}$ and $^4T_{1g}$. (Fig. 4.1)

Absorption of light is observed when the transitions $^4A_{2g} \rightarrow {}^4T_{2g}$ and $^4A_{2g} \rightarrow {}^4T_{1g}$ occur. The first excited state of Cr^{3+} is a mix between ^2E and $^4T_2$ states, which means that their interaction is related to the spin-orbit coupling and that they are close enough to both be populated according to the temperature of the system[3-5] Relaxation by

vibration can happen from the higher excited state $^4T_{1g}$ to $^4T_{2g}$ and fluorescence might be possible from $^4T_{2g}$, if it is the lowest excited state, to the ground state, according to the environmental condition such as ligand field strength and temperature, although emission under normal conditions is rarely observed. Intersystem crossing between $^4T_{2g}$ and ^2E_g takes place at a very high efficiency and rate, and emission from the ^2E_g level is observed frequently in rigid systems at low temperature.[6]

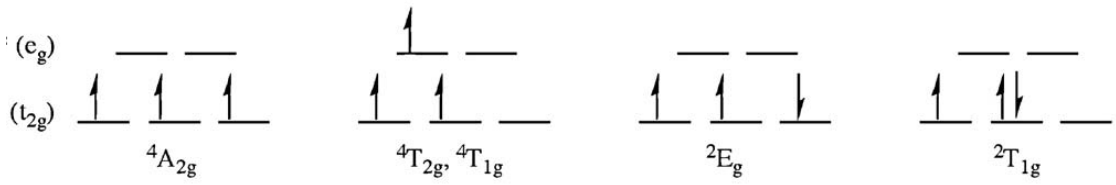

a)

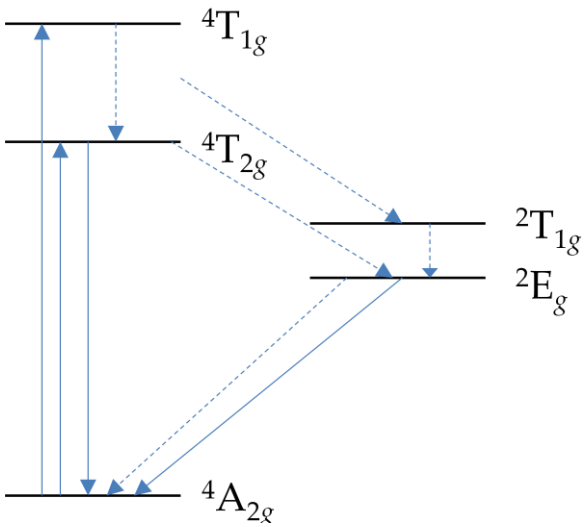

b)

Fig. 4.1. a) Electronic states related to octahedral geometry and b) energy level diagram. Full arrows represent radiative processes and dotted arrows represent non-radiative processes.

The photochemistry of Cr(III) has been widely investigated and collected in different reviews. The review by Kirk[7] extensively covers the literature up to 1998, whereas some developments are reviewed by Kane-Maguire up to 2006.[8] Becquerel was the first scientist who built a phosphoroscope, enabling him to measure the emission spectra of some Cr(III) solids (in which Cr(III) was an inpurity) and also ruby's luminescence lifetime.[9] In 1940 the interest in chromium increased and gave rise to studies into its crystal field theory,[10] hence the first detailed research on Cr(III) luminescence[11] and its photophysics by different research groups.[12-14] Forster and DeArmond studied and published in 1961[11] a paper on Cr(acetylacetonate)$_3$ and $[Cr(urea)_6]^{3+}$, in which emission of the two was measured and revealed that $[Cr(urea)_6]^{3+}$ emission consists of broad and sharp emission bands, in which broad fluorescence can only being observed when the $^4T_{2g}$ level is below the ^2E_g level. The sharp lines belong instead to phosphorescence emission, originating from ^2E_g.

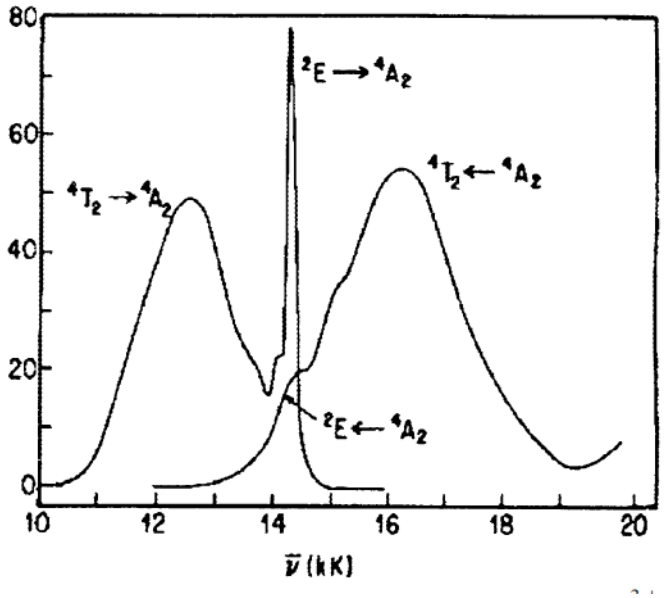

Fig. 4.2. Absorption and emission spectra of $Cr(urea)_6^{3+}$ reproduced from Porter and Schläfer.[15]

Other different ligands were then explored: $Cr(acac)_3$[16, 17], $[Cr(bpy)_3]^{3+}$, $[Cr(phen)_3]^{3+}$ [18, 19] and $[Cr(CN)_6]^{3-}$ [20]. All these studies were carried out to relate the different environment around chromium to its photophysical and photochemistry processes.

Several heteropolymetallic compounds containing Cr(III) and Ln(III) ions have been investigated, attempting to understand important interactions between the metals.[4, 21, 22] Chromium is electronically interesting for being used as an energy donor in this kind of assembly, especially for polymetallic complexes such as Cr-Ln (Ln = Yb, Nd, Er, Ho, Tm).[4] A large interest in Near-Infrared (NIR) lanthanide emission and how to improve its efficiency has developed in different areas such as luminescent probes for biological purposes[23-26] or optic fibres for telecommunication.[25, 27]

Our interest in Cr(III) complexes highlights the similarities between lanthanide and chromium ions: both of them have long-lived excited states and narrow emission bands. Such Ln(III) optical properties are due to the 4f shielded valence electrons and the forbidden f→f transition. On the other hand, similar optical properties of Cr(III) depend on both low-lying excited state levels $Cr(^2E)$ and $Cr(^2T_1)$, which have the same $(t_{2g})^3$ configuration as $Cr(^4A_2)$. The luminescence properties of Cr(III) and Ln(III) give rise to the fact that a possible d→f energy transfer could occur when using chromium complexes as an antenna for photoexcitation of lanthanide ions. For these reasons, we chose to analyse chromium dioxalate as a suitable bridging ligand for bimetallic complexes in d→f energy transfer. As well as acting as a

bridge, quenching of luminescence could be minimised because of fewer high-energy vibrational modes within the oxalate group than in other ligands with C-C bonds (such as hfac).

4.2 Results and discussion

Reported in this work is the study of PPh_4[Cr(2,2′-bipyridine)dioxalate]·H_2O (compound **7**) and its analogue PPh_4[Cr(2,2′-phenanthroline)dioxalate]·H_2O (compound **8**), prepared following a procedure by Lescouëzec et al.[28] Although these have been previously reported, electronic characterisation was restricted to their magnetic properties. The original preparation was modified in order to increase the solubility of the compound and we also isolated NH_4[Cr(4,4′-dinonyl-2,2′-bipyridine)dioxalate]·H_2O (compound **9**).

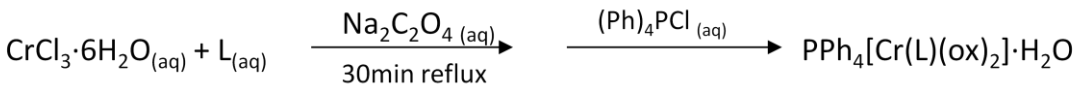

Fig. 4.3. Reaction scheme for compound **7** and **8** (L=bpy; phen)

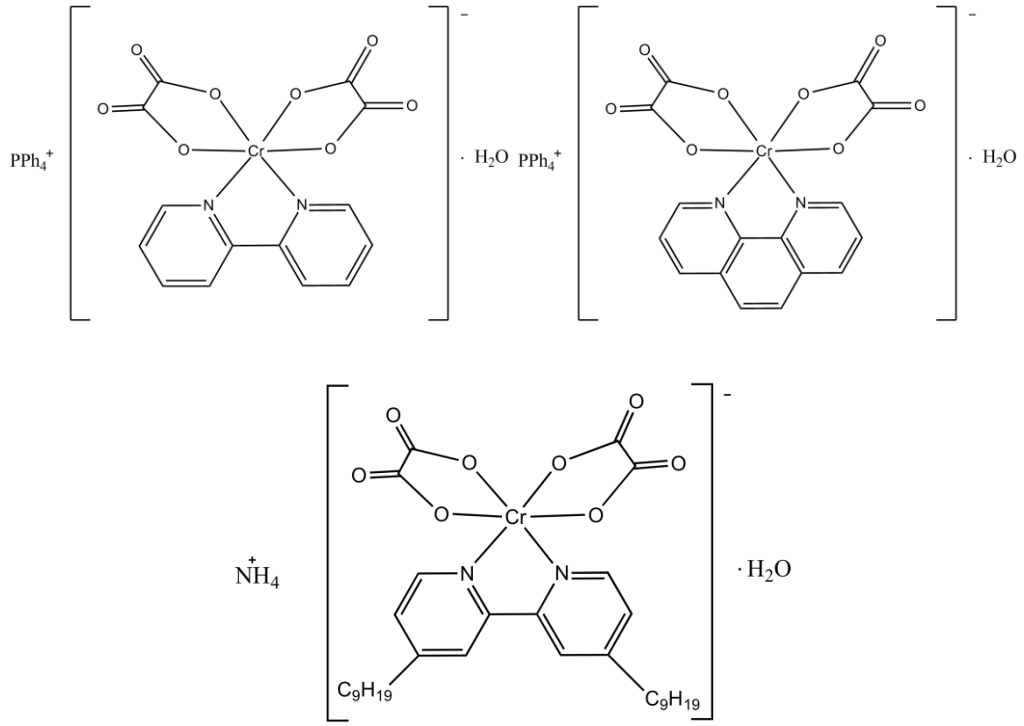

Fig. 4.4. Molecular structure of compounds **7**, **8** and **9**.

Compounds **7** and **8** were obtained by dissolving stoichiometric amounts of chromium chloride and ligand (L = bipyridine; phenanthroline) in the minimum amount of water and stirred. Then, sodium oxalate was added to the mixture and refluxed for 30 minutes. After filtration, a concentrated solution of tetraphenylphosphonium chloride was added to the filtrate and the solid was allowed to crystallise at room temperature. Their solubility in most organic solvents was poor: they were soluble only in methanol after heating and sonication. To increase the solubility of the above mentioned compounds, the original preparation was modified changing the counter ion (NH_4PF_6 instead of $P(Ph)_4PCl$). Also alkyl chains (C_9H_{19}) were added to the bipyridine ligand in the 4,4′ positions. With this preparation it was possible to isolate a more soluble complex, NH_4[Cr(4,4′-dinonyl-2,2′-bipyridine)dioxalate]·H_2O (compound **9).**

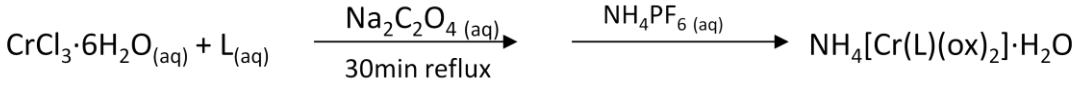

Fig. 4.5. Reaction scheme for compound **9** (L=4,4′-dinonyl-bpy)

4.2.1 UV/Vis Absorption Spectroscopy

Solutions of the Cr(III) complexes in methanol were used to measure absorption spectra. Compound **7** and **8** are insoluble in most solvents and slightly soluble in methanol, thus sonication of the solutions was necessary to dissolve the compounds properly. Compound **9** is quite soluble in ethanol, methanol and dichloromethane.

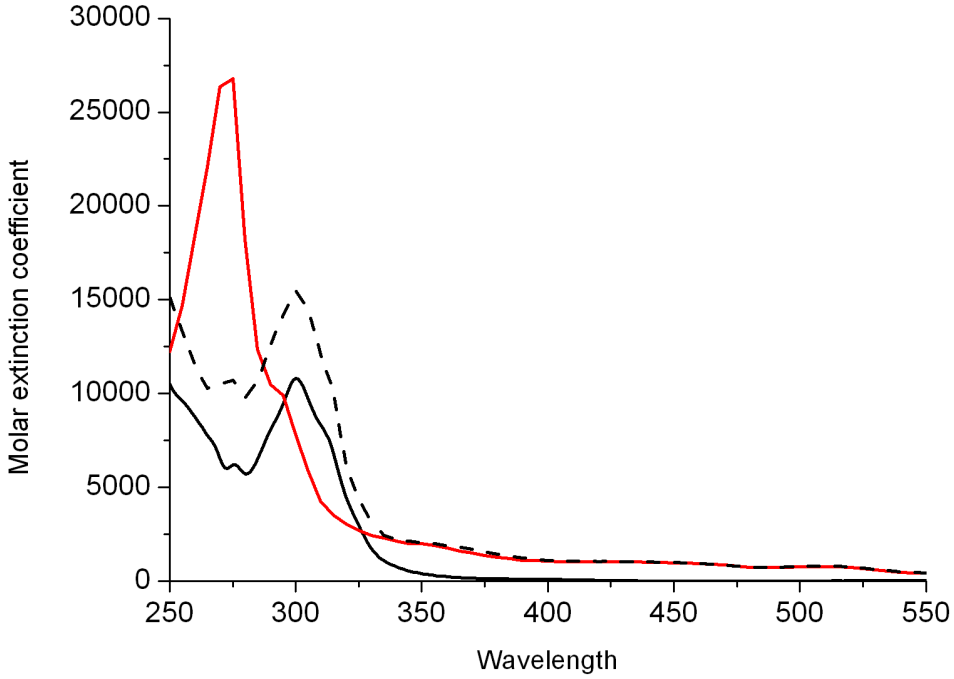

Fig. 4.6. UV/Vis absorption spectra of the studied compounds: compound **7** (dashed black line), compound **8** (red continuous line) and compound **9** (black continuous line).

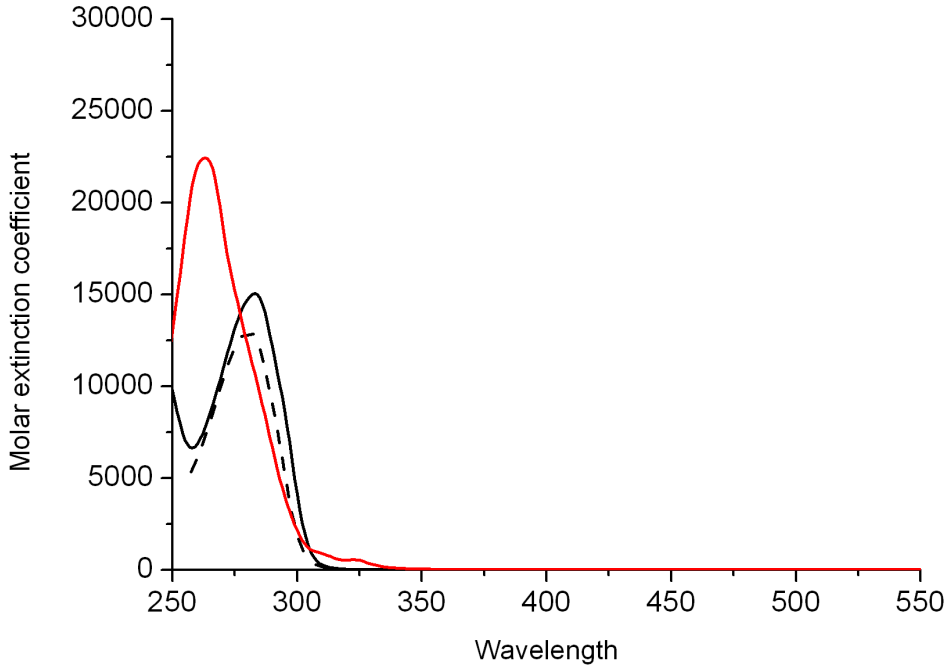

Fig. 4.7. UV/Vis absorption spectra of the related free ligands: 2,2′-bipyridine (dashed black line), 2,2′-phenanthroline (red continuous line) and 4,4′-dinonyl-2,2′-bipyridine (black continuous line).

Table 1 Absorption wavelengths and molar extinction coefficient of the studied compounds (in methanol) and related ligands (methanol for 2,2′-bipyridine and 2,2′-phenanthroline, chloroform for 4,4′-dinonyl-2,2′-bipyridine

Compounds	Compounds $\lambda_{max}/\varepsilon$	Ligands $\lambda_{max}/\varepsilon$
Compound **7**	300 nm/15500 $M^{-1}cm^{-1}$	281 nm/13000 $M^{-1}cm^{-1}$
Compound **8**	275 nm/26700 $M^{-1}cm^{-1}$	263 nm/22400 $M^{-1}cm^{-1}$
Compound **9**	300 nm/10800 $M^{-1}cm^{-1}$	283 nm/15000 $M^{-1}cm^{-1}$

Absorption wavelengths and molar extinction coefficient of the studied compounds and free ligands are shown in Fig. 4.6 and Fig. 4.7, and reported in the table above. The spectra show essentially ligand centred transitions with little perturbation from the metal present. There is a general trend of red-shifting of about 10-20 nm for each complex spectrum compared to the uncomplexed ligand. A poorly resolved band for each complex around 530 nm is assigned to a Cr(III) centred d-d transition, which is Laporte forbidden and with much lower molar extinction coefficient (~ 30-110 $M^{-1}cm^{-1}$) compared to the ligand centred transitions. Possibly some light scattering due to undissolved material is also detected for compounds **7** and **8**, since we mentioned before their solubility was poor and heating plus sonication was necessary before taking any measurement.

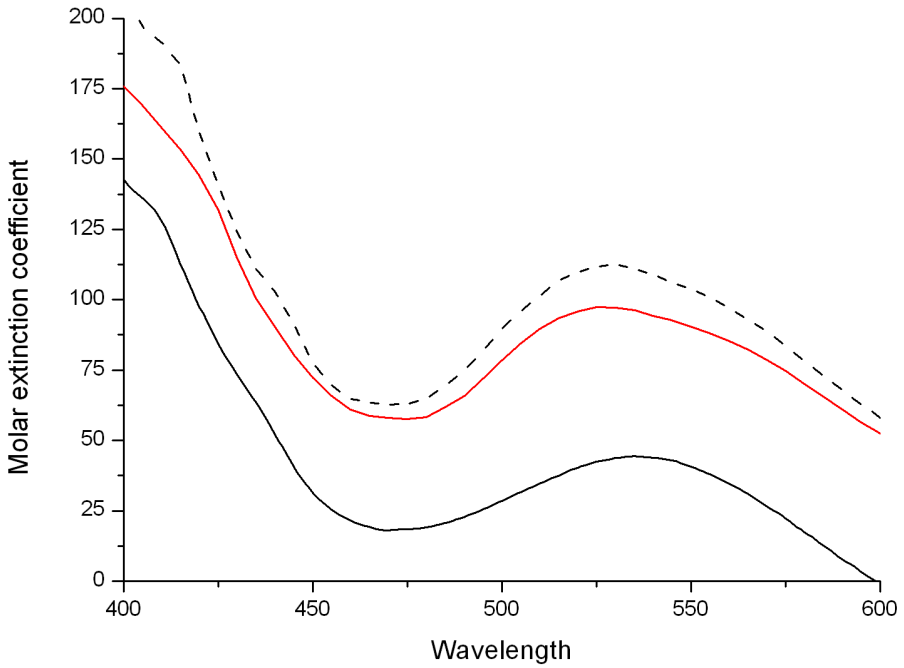

Fig. 4.8. d-d transitions in the studied compounds: compound **7** (dashed black line), compound **8** (red continuous line), compound **9** (black continuous line).

Compound **9** was considered for further analysis due to its better solubility. The Beer-Lambert plot showed that no aggregation was present at the working concentrations for compound **9**.

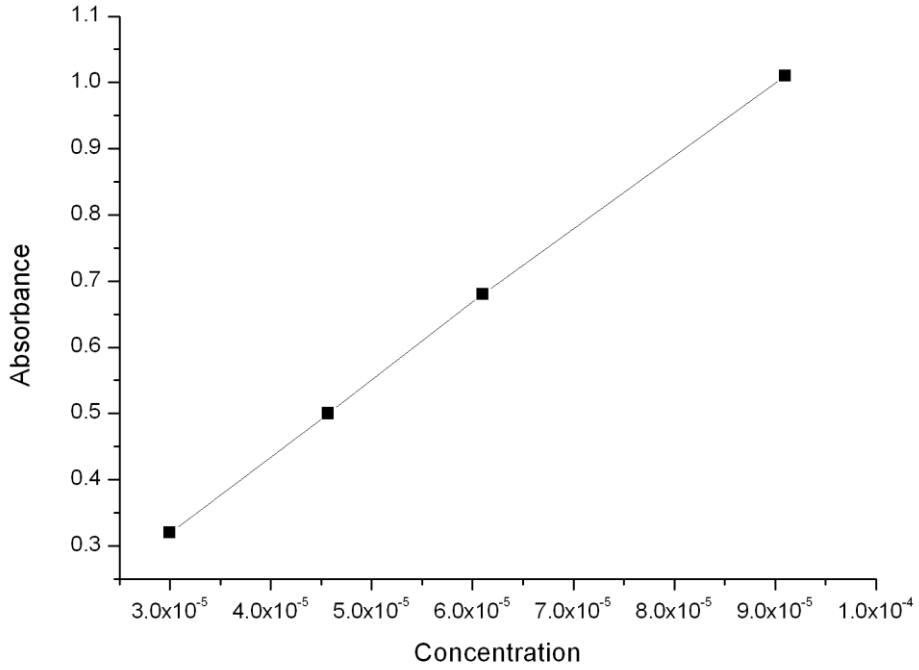

Fig. 4.9. Beer-Lambert plot for compound **9** at 300nm.

The complex was also included in an organic soluble polymer, PMMA (polymethyl methacrylate), in order to investigate the behaviour of the complex in a rigid system and to study the complex in the context appropriate to LSC or LDS applications. The polymer is a transparent plastic material often used as a substitute for glass, with its refractive index of 1.4.

PMMA is not soluble in ethanol or methanol but our chromium compound is, so it was dissolved in chloroform and mixed with a concentrated solution of compound **9** in methanol. The shape of absorption spectrum in PMMA is similar to that in methanol but slightly blue shifted in its absorption peak maxima (277 nm, compared

to 300 nm in methanol solution). It was not possible to observe light absorption in the visible region in PMMA.

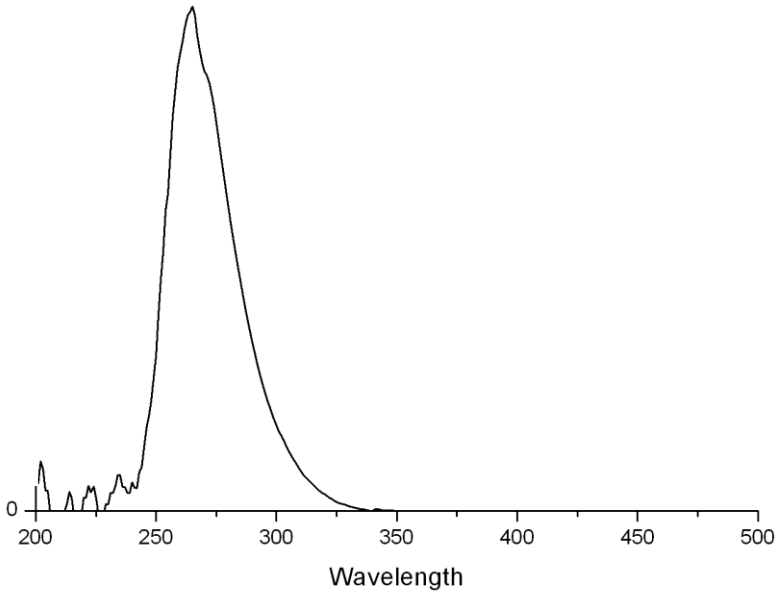

Fig. 4.10. Absorption spectrum of compound **9** in PMMA.

4.2.2 Photoluminescence Studies

Luminescence measurements of frozen samples were taken for each complex. Each complex was also investigated in degassed fluid solution at room temperature, however in all cases no emission at room temperature was observed. We note that complex **7** and **8** possess low solubility and quantitative comparison of their emission spectra is not possible.

The spectra were obtained exciting at 530 nm (18800 cm^{-1}) and showed a narrow emission peak at 730 nm (13700 cm^{-1}), providing a large pseudo-Stokes' shift of about 200 nm. Emission was recorded at different excitation wavelengths and it was always observed at 730 nm, indicating that the photons emitted come from the same excited level.

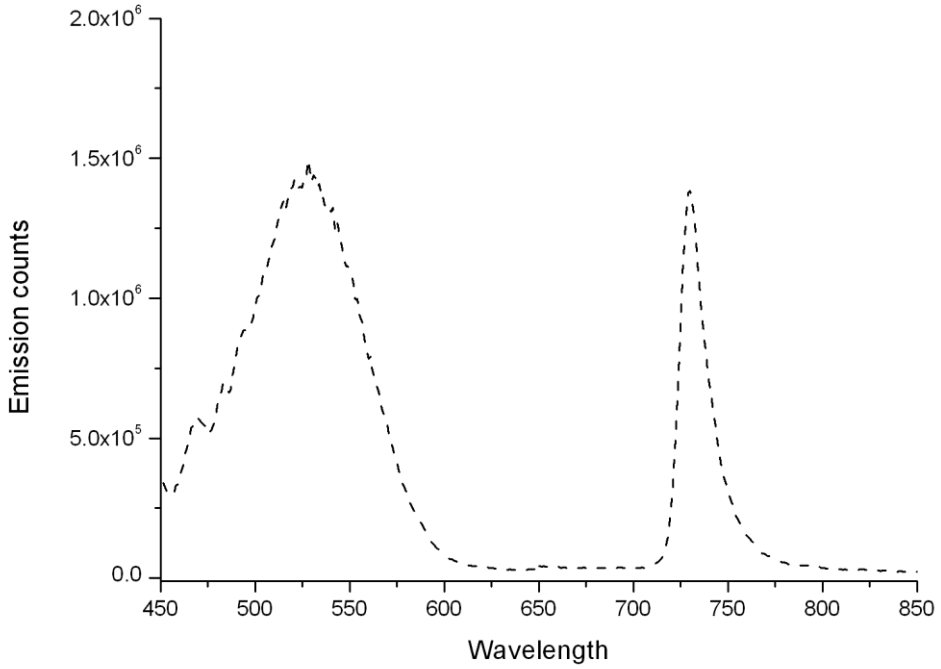

Fig. 4.11. Excitation and emission spectra of **7** at a concentration of $6.1 \cdot 10^{-4}$ M (low solubility).

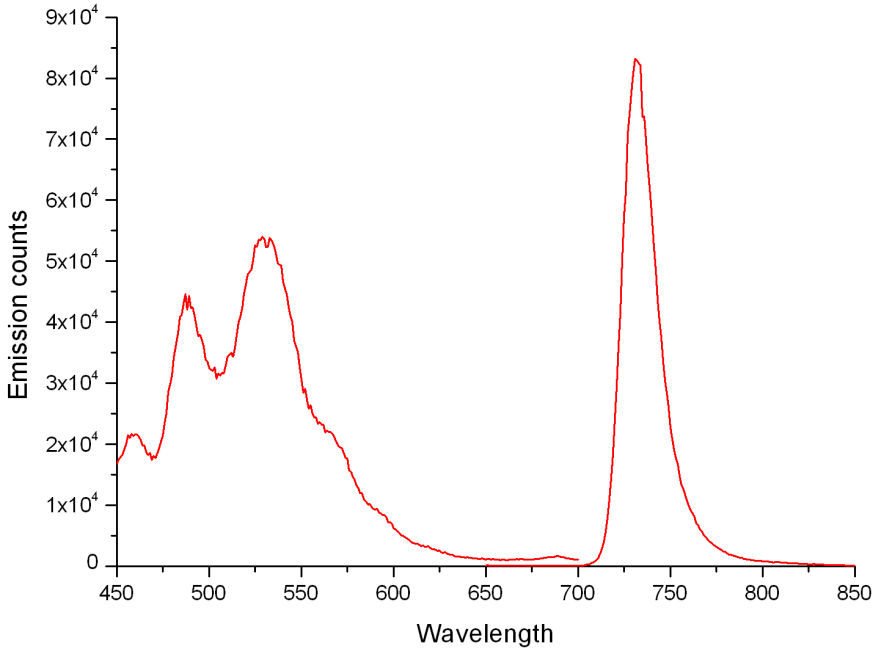

Fig. 4.12. Excitation and emission spectra of **8** at a concentration of $6.1 \cdot 10^{-4}$ M (low solubility).

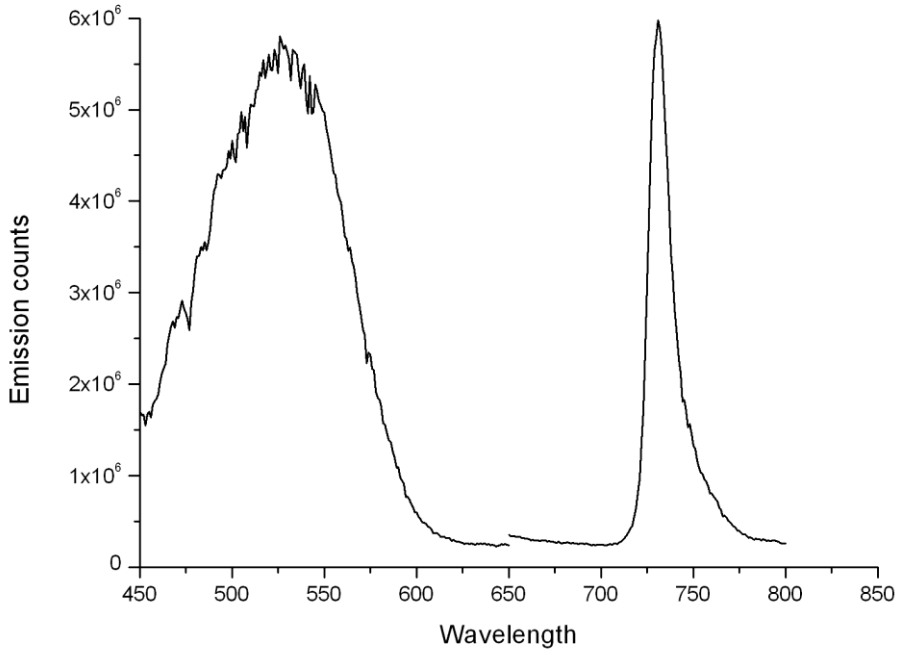

Fig. 4.13. Excitation and emission spectra of **9** at a concentration of $6.1 \cdot 10^{-4}$ M (good solubility).

Luminescence of chromium (III) complexes observed in this study is at low temperature and can be attributed to phosphorescence from $^2E_g \rightarrow {}^4A_{2g}$, typically observed as a sharp peak in a wavelength range from 660 nm to 830 nm (12000 cm^{-1} – 15000 cm^{-1}).[12] Fluorescence normally occurs at longer wavelengths and it is generally broader, and is rarely observed as shown in previous studies in the literature.[16, 29] After initial population of the $^4T_{1g}$ state, there is a rapid relaxation by vibration to the $^4T_{2g}$ excited state which rapidly undergoes intersystem crossing to E_{2g}. This accounts for the lack of any observed emission from $^4T_{2g}$. Population of one level with respect to the other depends on different factors. Ligand field strength is critical in determining population of the $^4T_{2g}$ level. For example, when Dq is small enough, fluorescence is mostly observed. This situation occurs when weak- field ligands are present around Cr(III), such as oxide and fluoride matrices.[5,30] When strong-field ligands, such as bipyridine, are bonded to Cr(III), the energy gap between $^4T_{2g}$ and ^2E_g increases because a large Δ will shift $^4T_{2g}$ states to higher energy. E_g will be significantly populated leading to typical Cr(III) red phosphorescence.[30] The E_g doublet excited state is instead more sensitive to the nephelauxetic effect, which is the magnitude of interelectronic repulsion between the d electrons. The smaller the repulsion, the lower the energy level is.[30] Our complexes - having bpy/phen as ligands – are affected by a certain degree of nephelauxetic effect due to low-lying π^* antibonding orbitals. Accordingly, based on literature precedent, we can conclude that the π-acceptor character of the bpy/phen ligand favours E_g as the lowest excited state, leading to sharp emission.[12]

In order to further probe the nature of this luminescence, lifetime measurements were carried out the three chromium complexes. Data were recorded in degassed frozen methanol solutions and we can assign the emission as phosphorescence, because the lifetime is in the millisecond range.[16, 31]

Table 2 Lifetime of the investigated compounds in methanol at fixed wavelength of emission and excitation

compound	$\lambda_{exc\ (nm)}$	$\lambda_{em\ (nm)}$	Lifetime (ms)
Compound **7**	530	730	1.4
Compound **8**	530	730	1.3
Compound **9**	530	730	1.4

The sharp emission band can be attributed to the fact that $^4A_{2g}$ and ^2E_g are nested one on top of each other with little geometric displacement. The long luminescence lifetime can be attributed primarly to the spin-forbidden nature of the transition and the nested states also play a role in reducing the non-radiative decay rate of the excited state.

Compound **9** was also included in PMMA to measure its emission in the solid state, however no emission was observed. This further analysis gives more information about the luminescence process: observation of emission from the ^2E_g state in the frozen sample can not be attributed solely due to the rigidity of the glassy sample, since a similar effect would be expected in PMMA, but to the temperature at which the complex was measured. Low temperature minimises quenching of the emission

due to back energy transfer to the quartet excited state, avoiding the thermal relaxation from the $^4T_{2g}$ level.

As we mentioned earlier in the chapter, lanthanide ions such as Nd and Yb have low-lying energy levels to accept energy from the higher chromium doublet excited level. The long lifetime of the Cr(III) emissive state in **7**, **8** and **9** is an advantage for an efficient energy transfer to the Ln(III). A preliminary study *in situ* was performed to understand whether a possible energy transfer could occur from Cr(III) to Ln(III). A solution of compound **9** was mixed in a 1:2 ratio with $[Yb(hfac)_3(H_2O)_2]$ in methanol. The experiment aimed to investigate a possible decrease of Cr(III) emission due to energy transfer to the Ln(III) ion at low temperature. Fig. 4.14 shows the outcome of the experiment. Cr(III) emission of compound **9** mixed with $Yb(hfac)_3(H_2O)_2$ in different ratio.

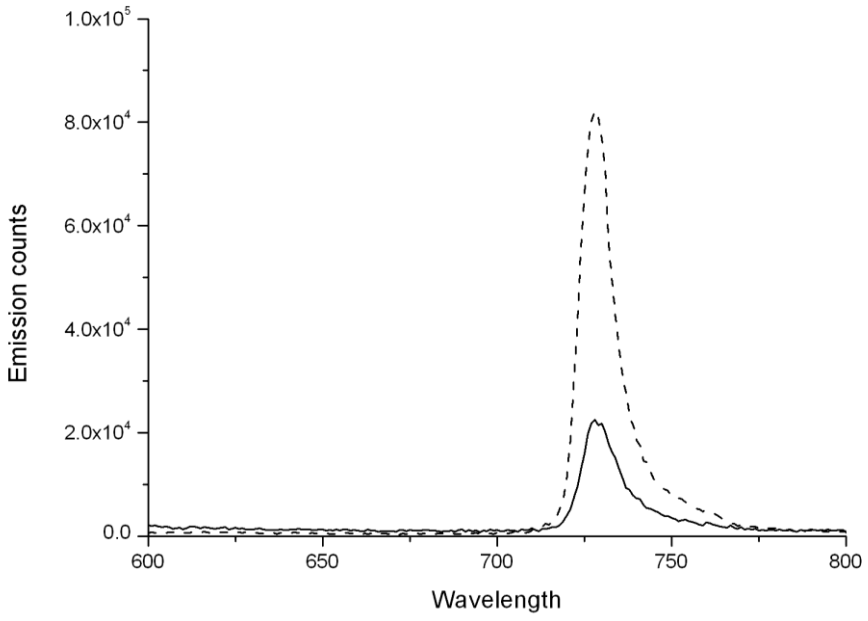

Fig. 4.14. *In situ* emission of compound **9** and $[Yb(hfac)_3(H_2O)_2]$ at 77K. Cr:Yb, 1:0.1(dash line); Cr:Yb, 1:2 (solid line).

Table 3 Concentration and ratio used for compounds for *in situ* emission experiment at 77K.		
ratio	1:0.1 (dash line)	1:2 (solid line)
Compound **9**	$9.16 \cdot 10^{-4}$ M	$9.16 \cdot 10^{-4}$ M
$[Yb(hfac)_3(H_2O)_2]$	$9.16 \cdot 10^{-5}$ M	$1.8 \cdot 10^{-3}$ M

As we can see from the figure, Cr(III) emission peak in the mixed Cr-Yb solution excited at 530 nm (77K) decreased its intensity by more than 50% with respect to the emission of compound **9** in 1:0.1 ratio with Yb. It was not possible to check lanthanide emission with the same experiment because the instrument does not have NIR detector. We could have measured Yb emission with the Edinburgh Instruments FS920 – which has a NIR detector - but the instrument does not have a cryostast necessary to detect Cr(III) emission.

The experiment was significant because at this stage we can see how a mixed Cr-Ln complex can have a good absorption range around 500 nm and emission in the NIR region, which is good for LSC application. At the present however, Cr emission and energy transfer to Yb can only be observed at low temperature. A practical system therefore needs a larger energy gap between E_g and T_{2g} in the Cr complex to avoid back energy transfer to T_{2g}. Hence the Cr-Ln system has interesting possibilities for LSC technology but new design of the Cr complex is needed to give larger ligand field splitting.

4.3 Conclusions

In this chapter we synthesised and analysed three chromium compounds by absorption and emission spectroscopy in order to understand their behaviour in solution, frozen glassy solution and polymer.

Cr(III) photochemistry is strictly related to the lowest quartet and doublet excited states that, according to Kasha's rules, are the most important levels in luminescence. We showed that the observed emission is phosphorescence from the ^2E_g state, evidenced by the long-lived excited state in the range of ms for each of the three complexes and the narrow emission band. The possibility of charge transfer between Cr(III) and Yb(III) was shown by an *in situ* emission experiment which suggests the possibility of making new Cr-Ln polynuclear complexes suitable for LSC applications.

4.4 Experimental section

Materials

All chemicals used were purchased from Aldrich, Alfa Aesar and Acros chemical companies and were not further purified, unless otherwise stated. All the complexes were synthesised based on a procedure reported by Lescouëzec *et al*.[28] with a modification in counterion for **7** and **8**, and in ligand for NH_4[Cr(4,4′-dinonyl-2,2′-bipyridine)$(ox)_2$]·H_2O (**9**).

Synthesis of PPh_4[Cr(2,2′-bipyridine)$(ox)_2$]·H_2O (7)

An aqueous suspension (35 ml) of chromium chloride hexahydrate (2 mmol, 533 mg) and bipyridine (2 mmol, 312 mg) was refluxed for 30 minutes until a green solution was formed. 4 mmol (536 mg)of sodium oxalate were added to the solution and it was refluxed for 30 minutes under continuous stirring to afford a red/violet solution. The resulting solution was filtered to collect a violet powder, which was discarded. A concentrated warm aqueous solution of tetraphenylphosphonium chloride (2 mmol, 838 mg) was added to the clear red solution previously filtrated to afford red crystals, leaving the solid to crystallise at room temperature for 3 days. Yield: 44% (652 mg).

Elemental analysis calc. for $C_{38}H_{30}CrN_2O_9P$: C, 61.54; H, 4.08; N, 3.78. Found: C, 61.55; H, 3.97; N, 3.69.

Synthesis of $PPh_4[Cr(2,2'\text{-phenanthroline})(ox)_2]\cdot H_2O$

The procedure followed was the same as above. Yield: 24% (182 mg).

Elemental analysis calc. for $C_{40}H_{30}CrN_2O_9P$: C, 62.75; H, 3.95; N, 3.66. Found: C, 62.90; H, 3.86; N, 3.52.

Synthesis of $NH_4[Cr(4,4'\text{-dinonyl-}2,2'\text{-bipyridine})(ox)_2]\cdot H_2O$

Equimolar quantities (0.9 mmol, 250 mg) of chromium trichloride hexahydrate and 4,4'-dinonyl-2,2'-bipyridine (0.9 mmol, 383 mg) were stirred under reflux in aqueous concentrated solution (35 ml). A concentrated solution DMF:water (1:1) of sodium oxalate (1.9 mmol, 250 mg) was added to the resulting solution and refluxed for other 30 minutes. The resulting solution was filtered while hot and the precipitate was discarded.

Ammonium hexafluorophosphate was added to the filtrate and two layers were formed. The solution was decanted and the oily residue was left to dry for 4 days, until a dark purple solid was formed.

The solid was refluxed in water for an hour and filtrated. Yield: 28.40% (72 mg).

Elemental analysis calc. for $C_{32}H_{50}CrN_3O_9$: C, 57.13; H, 7.49; N, 6.25. Found: C, 58.82; H, 7.47; N, 6.37.

Photoluminescence and lifetime details

Emission spectra and lifetime measurements were recorder using a FluoroMax-P (Jobin Yvon – HORIBA). All of the emission spectra were recorded at 77K in methanol and the solutions were degassed to minimise the presence of oxygen inside the sample tube.

Excited-state lifetime data in the visible were measured using a Fluoromax-P spectrofluorimeter (Horiba-Jobin-Yvon) in DCM (77 °K) and fitted to exponential functions using an iterative non-linear least squares algorithm in the 'Solver' facility in Microsoft Excel.

PMMA was prepared using 100 mg in 1ml of chloroform and stirred until dissolved. Chromium complexes were dissolved in methanol and mixed in a ratio 1:1 with PMMA in chloroform, then spin coated in 1 step for 1 minute at 1000 RPM.

4.5 References

1. Endicott, J.F., Ramasami, T., Tamilarasan, R., Lessard, R.B., Ryu, C.K., and Brubaker, G.R., *Coord. Chem. Rev.*, 1987. **77**: p. 1.
2. Gudel Hans, U., *Excited States of Mononuclear and Dinuclear Chromium(III) Complexes*, in *Excited States and Reactive Intermediates*. 1986, American Chemical Society. p. 1.
3. Serpone, N., Jamieson, M.A., Sriram, R., and Hoffman, M.Z., *Inorg. Chem.*, 1981. **20**(11): p. 3983.
4. Cantuel, M., Bernardinelli, G., Imbert, D., Bunzli, J.-C.G., Hopfgartner, G., and Piguet, C., *Dalton Trans.*, 2002(9): p. 1929.
5. Shen, Y., Riedener, T., and Bray, K.L., *Phys. Rev. B: Condens. Matter Mater. Phys.*, 2000. **61**(Copyright (C) 2012 American Chemical Society (ACS). All Rights Reserved.): p. 11460.
6. Forster, L.S., *Coord. Chem. Rev.*, 2002. **227**(1): p. 59.
7. Kirk, A.D., *Chem. Rev.*, 1999. **99**(6): p. 1607.
8. Balzani, V., Campagna, S., and Kane-Maguire, N., *Photochemistry and Photophysics of Coordination Compounds: Chromium*, in *Photochemistry and Photophysics of Coordination Compounds I*. 2007, Springer Berlin / Heidelberg. p. 37.
9. Becquerel, E., *La lumiere, ses causes et ses effets*.1867, Paris: Firmin Didotfreres, fils et cie.
10. Finkelstein, R. and Vleck, J.H.V., *J. Chem. Phys.*, 1940. **8**(10): p. 790.
11. Forster, L.S. and DeArmond, K., *J. Chem. Phys.*, 1961. **34**: p. 2193.
12. Schläfer, H.L., Gausmann, H., and Witzke, H., *J. Chem. Phys.*, 1967. **46**: p. 1423.
13. Watson, W.M., Wang, Y., Yardley, J.T., and Stucky, G.D., *Inorg. Chem.*, 1975. **14**(10): p. 2374.
14. Kane-Maguire, N.A.P., Phifer, J.E., and Toney, C.G., *Inorg. Chem.*, 1976. **15**(3): p. 593.
15. Porter, G.B. and Schläfer, H.L., *Zeitschrift für Physikalische Chemie*, 1963. **37**(1_2): p. 109.
16. Rojas, G.E., Dupuy, C., Sexton, D.A., and Magde, D., *J. Phys. Chem.*, 1986. **90**(1): p. 87.
17. Juban, E.A. and McCusker, J.K., *JACS*, 2005. **127**(18): p. 6857.
18. Maestri, M., Bolletta, F., Moggi, L., Balzani, V., Henry, M.S., and Hoffman, M.Z., *JACS*, 1978. **100**(9): p. 2694.
19. Bolletta, F., Maestri, M., Moggi, L., Jamieson, M.A., Serpone, N., Henry, M.S., and Hoffman, M.Z., *Inorg. Chem.*, 1983. **22**(18): p. 2502.
20. Conti, C., Castelli, F., and Forster, L.S., *J. Phys. Chem.*, 1979. **83**(18): p. 2371.
21. Sanada, T., Suzuki, T., Yoshida, T., and Kaizaki, S., *Inorg. Chem.*, 1998. **37**(18): p. 4712.
22. Decurtins, S., Gross, M., Schmalle, H.W., and Ferlay, S., *Inorg. Chem.*, 1998. **37**(10): p. 2443.
23. Imbert, D., Cantuel, M., Bunzli, J.-C.G., Bernardinelli, G., and Piguet, C., *JACS*, 2003. **125**(51): p. 15698.
24. Torelli, S., Imbert, D., Cantuel, M., Bernardinelli, G., Delahaye, S., Hauser, A., Bünzli, J.-C.G., and Piguet, C., *Chem. Eur. J.*, 2005. **11**(11): p. 3228.
25. McCleverty, J.A., Meyer, T.J., and Lever, A.B.P., *Comprehensive coordination chemistry II: from biology to nanotechnology*. 2004: Elsevier.

26. Motson, G.R., Fleming, J.S., and Brooker, S., *Adv. Inorg. Chem.* 2004, p. 361.
27. Tanabe, S., *Comptes Rendus Chimie*, 2002. **5**(12): p. 815.
28. Lescouëzec, R., Marinescu, G., Vaissermann, J., Lloret, F., Faus, J., Andruh, M., and Julve, M., *Inorg. Chim. Acta*, 2003. **350**: p. 131.
29. Juban, E.A. and McCusker, J.K., *JACS*, 2005. **127**(18): p. 6857.
30. Forster, L.S., *Chem. Rev.*, 1990. **90**(2): p. 331.
31. Camassei, F.D. and Forster, L.S., *J. Chem. Phys.*, 1969. **50**(6): p. 2603.

Chapter 5: $[Tb(pobz)_3(hacim)_2]$ and $[Tb(bz)_3(hacim)_2]$ complexes

5.1 Introduction

This chapter contains work carried out in collaboration with Valentina Utochnikova (Lomonosov Moscow State University – Russia). The complexes had been initially characterised by UV/Vis and steady-state emission and we further analysed them as potential candidates for luminescent downshifting materials (LDS). Therefore, we studied their absorption and emission properties, lifetime and photoluminescence quantum yield (PLQY) in several environments.

We studied two lanthanide compounds: $[Tb(pobz)_3(hacim)_2]$ – compound **10** and $[Tb(bz)_3(hacim)_2]$ – compound **11**, (Hpobz = phenoxybenzoic acid; Hbz = benzoic acid; Hacim = acetylacetone imine). Both complexes were studied at Lomonosov University as emitting materials for vapour deposited organic light-emitting devices (OLEDs) and a first communication has been published by Utochnikova[1] in 2012.

Materials for electroluminescent (EL) devices have been known since 1963[2] in which luminescence from anthracene crystals was studied. Thereafter, great interest for luminescent materials increased because of their application in telecommunication, lighting and bioanalytical tools.[3-5] Vapour-deposited organic light-emitting diodes

(OLEDs) have been pointed out as a valid alternative to liquid-crystal-based flat panel displays.[6] Although synthesis and characterisation are easy, there are still some problems related to recrystallisation and thermal stability.[3] Also new technologies like coloured electronic magazines and newspapers take advantage of highly efficient blue, red and green emitters.[7] The lighting market is also trying to improve the production of efficient lighting at lower cost using white organic light-emitting devices (WOLEDs).[8] In order to be used in OLED vapour deposition, the material needs to satisfy different characteristics. It needs to be isolable, highly efficient in solid state fluorescence, able to transport electrons and thermally stable.[9]

Compounds containing lanthanide ions have been widely investigated in this context because of their narrow emission bands discussed earlier.[10] Different classes of ligands were explored as possible candidates to form good light-emitting compounds. β-diketonates and pyrazolonates have been studied as promising ligands suitable for chemical vapour deposition and with tunable high efficiency emission.[11, 12] Unfortunately their practical application is limited due to their poor photo- and chemical stability. Aromatic carboxylate ligands have also been studied[9, 12] but not a great amount of attention has been paid to them since these ligands have poor solubility in most organic solvents and are non-volatile, hence give poor quality thin amorphous films. Nevertheless, lanthanide aromatic carboxylates have good thermal stability and high luminescence efficiency.[13] A compound studied by Bünzli, $Tb(bz)_3$, showed a quantum yield of 100% as a solid.[14] Such a large value

occurs because the triplet excited state of the ligand is close to the highest emissive level of the lanthanide ions, but is far enough to avoid back energy transfer.

For this reason, new techniques have been explored in order to overcome these disadvantages, such as the formation of mixed-ligand complexes (MLCs) in solution that are able to be deposited as a thin film and decompose into the desired compound after film annealing.[15] Utochnikova followed up with work focused on transformation of the insoluble $Tb(pobz)_3$ into a more soluble compound, by adding a neutral donor ligand such as acetylacetone imine (Hacim).[15] The resulting soluble compound was then processed into a thin film directly from solution and annealed in order to remove the hacim ligand and obtain $Tb(pobz)_3$ again. Success of the annealing process was proved by comparison between excitation spectra of Tb(pobz) before and after the treatment.

The ultimate goal of the work described in this chapter concerns inclusion of terbium aromatic carboxylate complex in EVA polymer (ethylvinyl acetate) and attempts to anneal the spin coated films and measure their PLQY, which has not been done before. This study relates to the luminescent downshifting process (LDS) first proposed by Hovel,[16] to improve the poor response at short wavelength of solar cells, which therefore cannot effectively use the UV range of the spectrum. The LDS layer will reemit the photons at a longer wavelength more usable for energy conversion by the solar cell. For this purpose, Tb compounds – with their emission wavelength at 543 nm - could be possible candidates for luminescent downshifting

conversion. Moreover, reducing cost of manufacturing is one of the most important aspects, therefore the use of EVA - a cheap material already used as an encapsulant for solar cells - is certainly appealing.

5.2 Results and discussion

The compounds used for these analysis were made and given to us by Valentina Utochnikova, following the procedure reported by Utochnikova *et al*.[1] Firstly, the insoluble $Tb(pobz)_3$ and $Tb(bz)_3$ are obtained[17] and then mixed with a neutral organic donor ligand (in our case Hacim, which is an acetylacetone imine, Schiff base prepared from acetylacetone and ammonia) in order to form the mixed-ligand compound (MLC), more soluble than the precursor, namely compounds **10** and **11**.

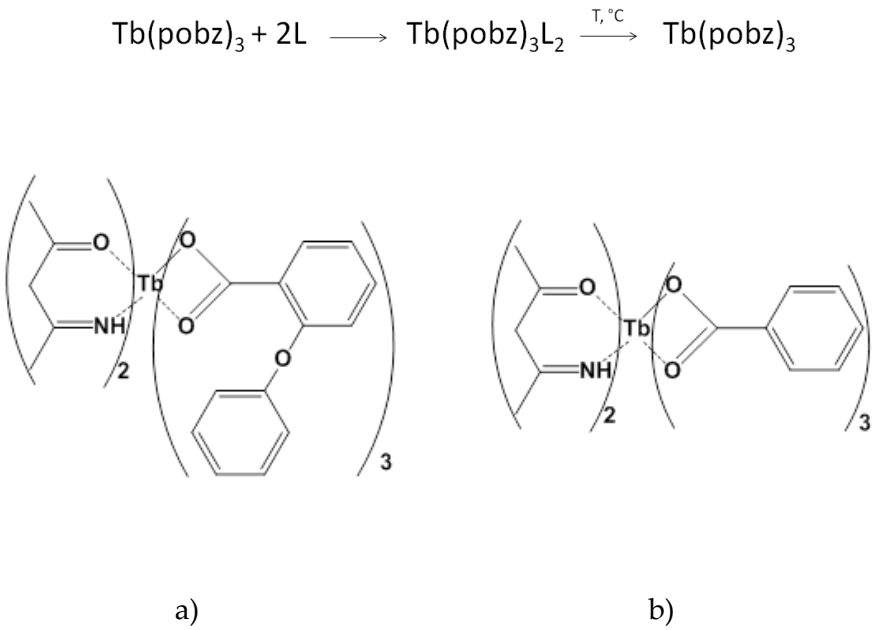

a) b)

Fig. 5.1. Reaction scheme and structural formula of a) compound **10**; b) compound **11**.

Originally in Utochnikova's work, these two complexes were deposited directly from an EtOH:C_6H_6 solution of the MLCs on the glass/ITO substrate by spin-coating. Annealing of the film at low pressure at 100-110 °C led to loss of the neutral Hacim and hence reformation of the original $Tb(pobz)_3$ and $Tb(bz)_3$.

In our work we have included complex **10** in ethylvinyl acetate (EVA), used as host material for our luminescent complexes. EVA will act as substrate for compound **10** because of its good optical qualities: it is a soft and flexible poymer, which possesses good clarity and resistance to UV radiation. This polymer has been already used successfully as a matrix for luminescent down-shifting materials[18, 19] We first proceeded to measure the UV/Vis spectroscopy, photoluminescence and lifetime measurements that had only been studied previously in room temperature solutions. Frozen measurements and quantum yield of the solutions were additionally carried out before including the compounds in EVA.

5.2.1 UV/Vis Absorption Spectroscopy

Solutions in acetonitrile (Fig. 5.2) and 1-propanol (Fig. 5.3) were used to measure the UV/Vis spectra, at the concentration of $2 \cdot 10^{-5}$ M.

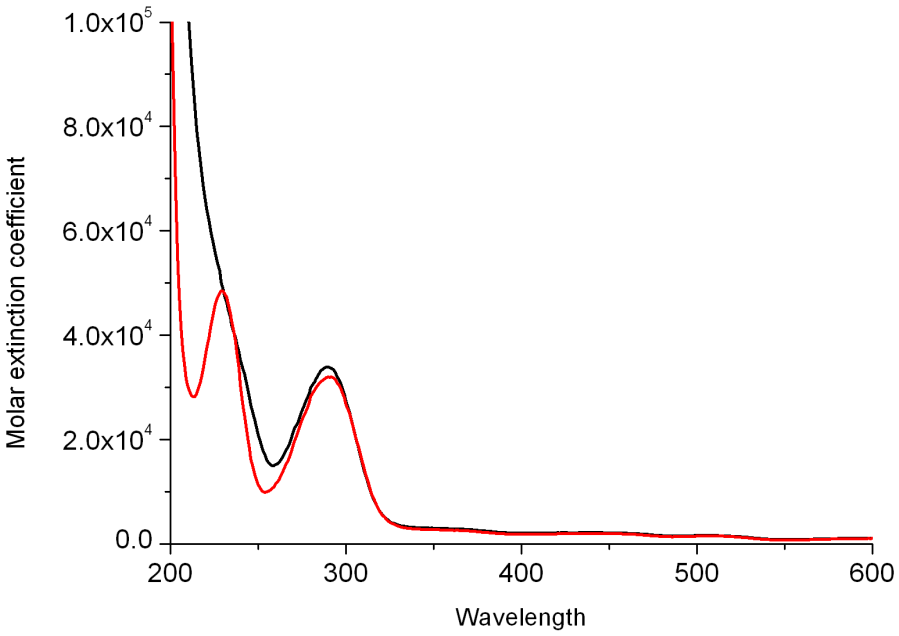

Fig. 5.2. Absorption spectra of compound **10** (black line) and compound **11** (red line) in acetonitrile.

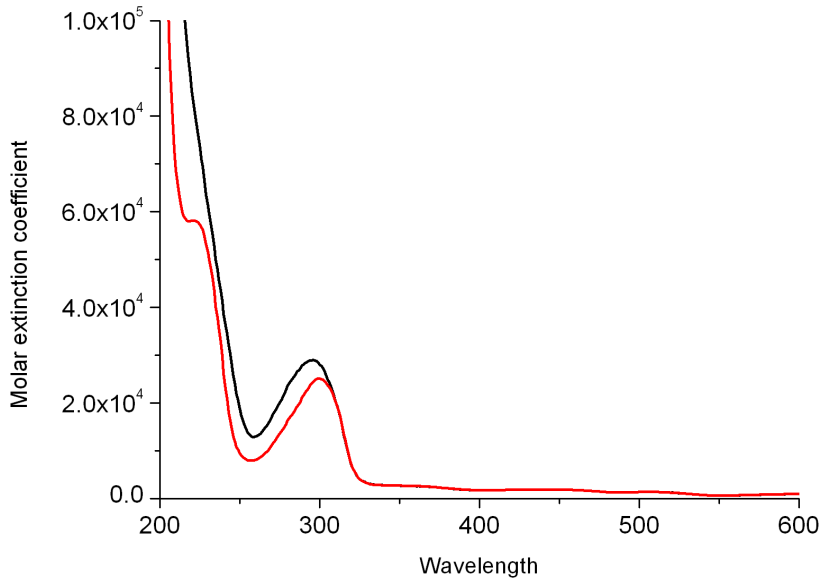

Fig. 5.3. Absorption spectra of compound **10** (black line) and compound **11** (red line) in 1-propanol.

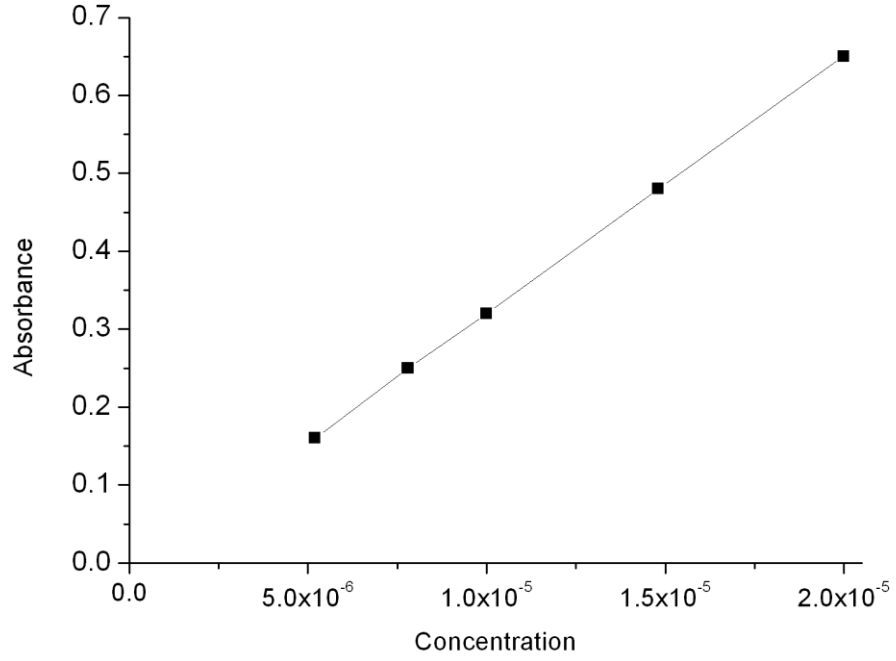

Fig.5.4. Beer-Lambert plot in acetonitrile for compound **10**.

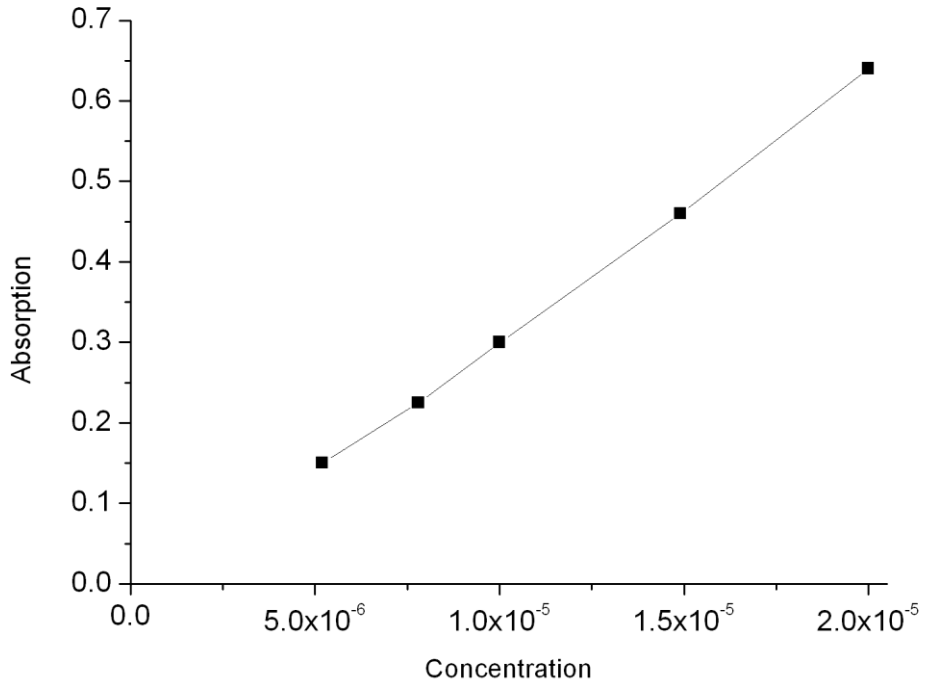

Fig. 5.5. Beer-Lambert plot in 1-propanol for compound **10**.

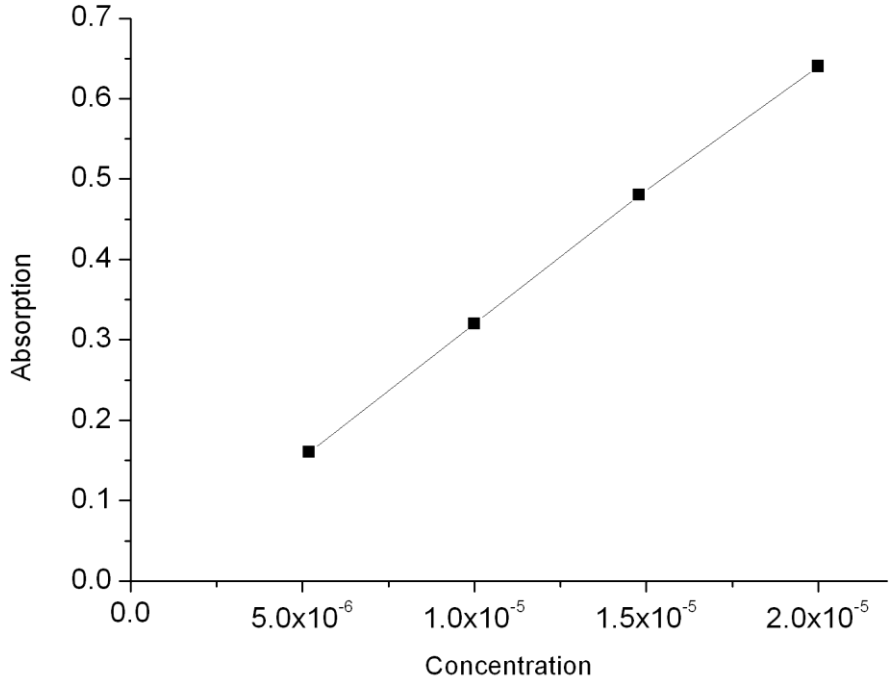

Fig. 5.6. Beer-Lambert plot in acetonitrile for compound **11**.

In acetonitrile solution, both complexes show an absorption peak at 290 nm (34500 cm^{-1}) with a molar extinction coefficient (ε) of 33900 M^{-1} cm^{-1} for compound **10** and 31900 M^{-1} cm^{-1} for compound **11**. An additional absorption peak was also observed for compound **11** in the UV region around 229 nm (43400 cm^{-1}), with ε = 48500 M^{-1} cm^{-1}. Acetonitrile is not appropriate for emission studies at 77 K as it is not a very good solvent to create glassy samples, hence the absorption spectra were also studied in 1-propanol. A slight difference was observed in the absorption peaks of compound **10,** which changed from 290 nm (34500 cm^{-1}) to 295 nm (33900 cm^{-1}). The molar extinction coefficient decreased from 33900 M^{-1} cm^{-1} to 28900 M^{-1} cm^{-1}. Compound **11** was not fully dissolved due to its lower solubility and we show its

spectrum only as a qualitative comparison. Despite its poor solubility in 1-propanol we can still notice a change in the absorption wavelength value with a small positive solvatochromism effect due to the lower polarity of 1-propanol with respect to acetonitrile. The table below summarises the data obtained. From the Beer-Lambert plot we can see that no aggregation was detected at these concentrations.

Table 1 Absorption wavelength and molar absorptivity of the studied compounds

Compound	λ_{max}-ε in acetonitrile	λ_{max}-ε in 1-propanol
Compound **10**	290 nm - 33900 M^{-1} cm^{-1}	295 nm - 28900 M^{-1} cm^{-1}
Compound **11**	290 nm - 33900 M^{-1} cm^{-1} 229 nm - 48500 M^{-1} cm^{-1}	not accurate due to poor solubility

5.2.2 Photoluminescence studies

Both complexes were characterised in terms of their excitation/emission spectra in solution and frozen glass, including excited state lifetime and photoluminescence quantum yield (PLQY). We mentioned already that compound **11** showed lower solubility properties compared to compound **10**. The solution was heated and sonicated but a white deposit was constantly present in it, so it was not possible to include compound **11** in EVA. The films obtained by spin coating mixing the complex in a solution of EVA in toluene were not homogeneous at all and the light scattering was too high for measuring any emission spectrum. Studies in EVA are therefore limited to compound **10**.

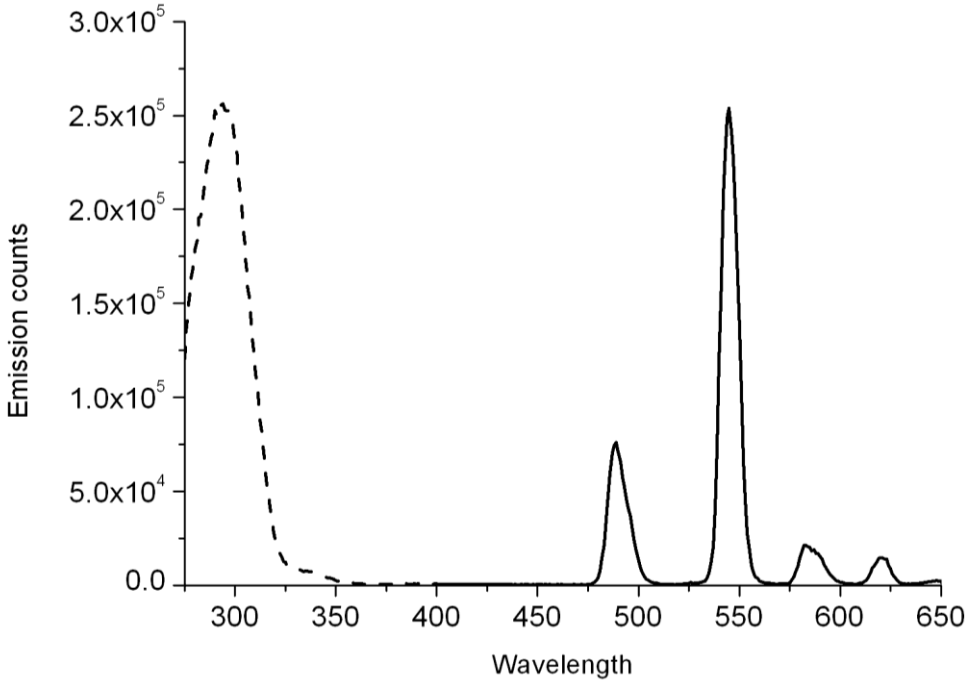

Fig. 5.7. Excitation/Emission spectra of compound **10** at RT in acetonitrile (λ_{ex}= 296 nm).

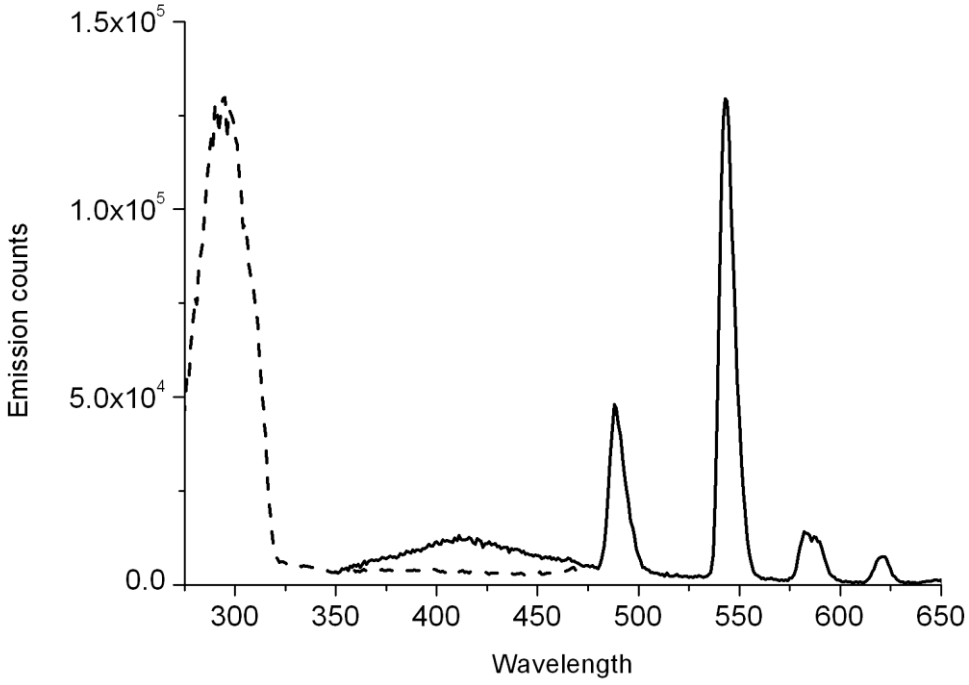

Fig. 5.8. Excitation/Emission spectra of compound **10** at 77K in 1-propanol (λ_{ex}= 296 nm).

Emission spectra of compound **10** both in acetonitrile (Fig. 5.7 - room temperature) and in 1-propanol (Fig. 5.8 - 77K) were obtained exciting at 296 nm (33800 cm^{-1}) showing Tb-like emission with luminescence attributed to $^5D_4 \rightarrow {}^7F_j$ (with j = 6,5,4,3): 20400 cm^{-1} (488 nm), 18400 cm^{-1} (544 nm), 17200 cm^{-1} (581 nm), 16100 cm^{-1} (619 nm). In the same conditions, compounds **11** was analysed both in acetonitrile (Fig. 5.9) and 1-propanol (Fig.5.10 – 77K).

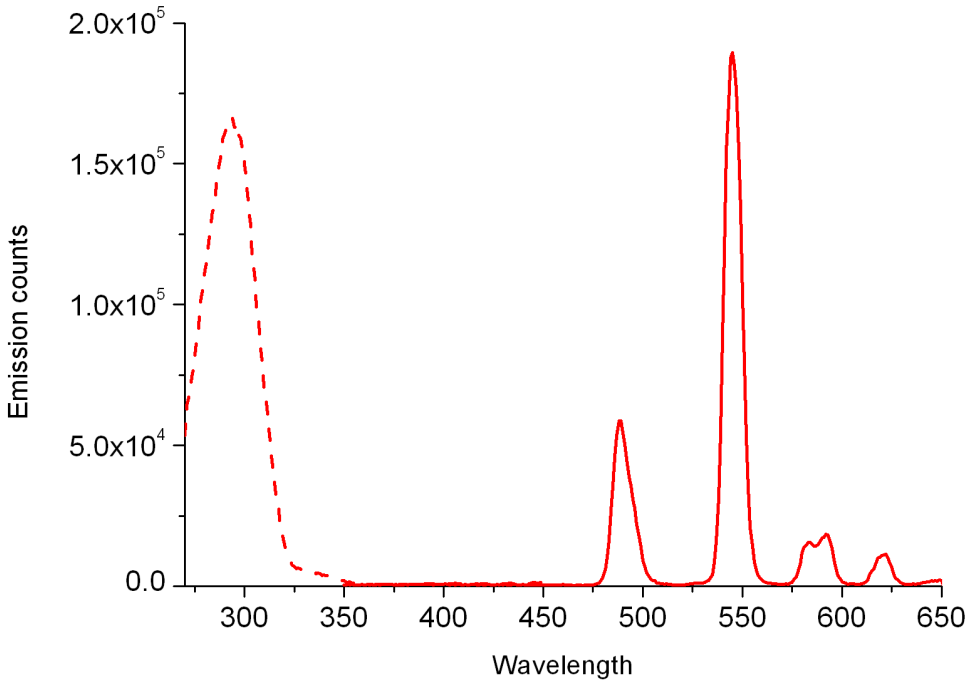

Fig. 5.9. Excitation/Emission spectra of compound **11** at RT in acetonitrile (λ_{ex}= 296 nm).

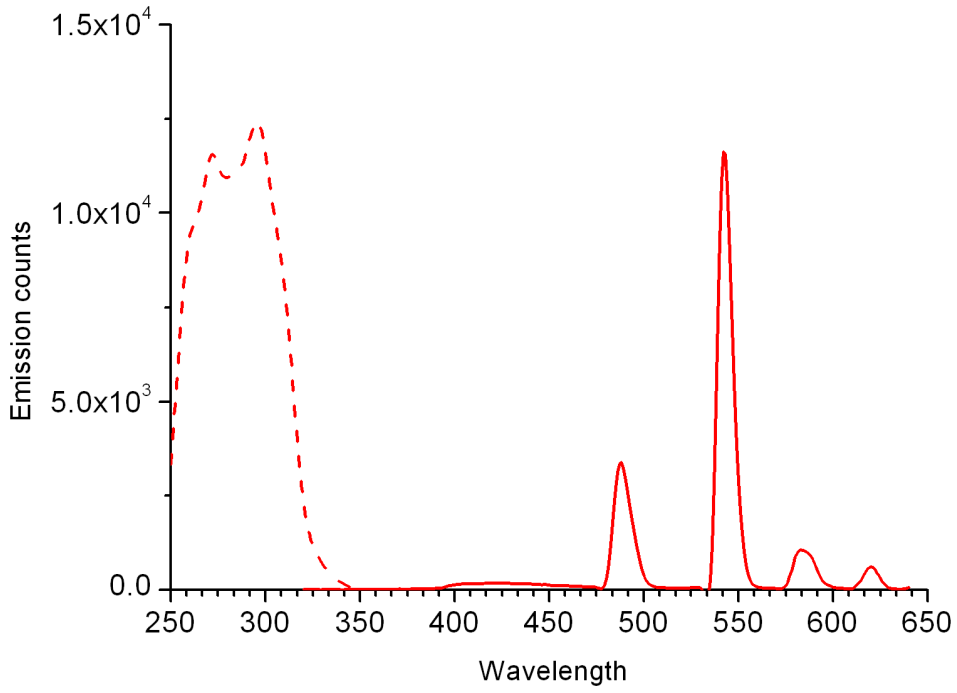

Fig. 5.10. Excitation/Emission spectra of compound **11** at 77K in 1-propanol (λ_{ex}= 296 nm).

Although not observed in the solution emission measurements, the frozen emission of both complexes showed a band centred around 410 nm attributed to general ligand emission (compound **10** more than compound **11** – Fig. 5.11). This is not observed at room temperature mostly likely due to collisional quenching.

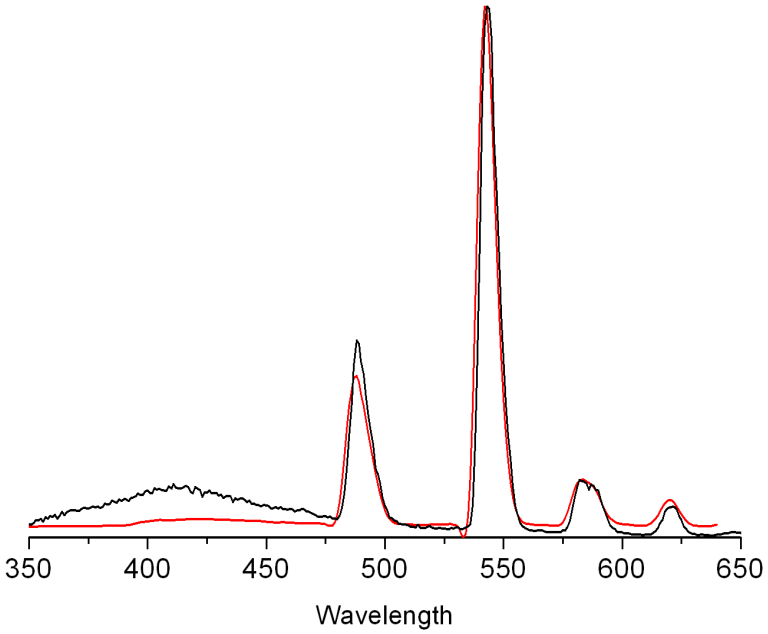

Fig. 5.11. Normalised emission spectra of compound **10** (black line) and compound **11** (red line) at 77K in 1-propanol (λ_{ex}= 296 nm).

Lifetime measurements and PLQY are summarised in Table 2 for both compound **10** and **11**. Data were obtained in acetonitrile at room temperature and 1-propanol at 77K (because it was not possible to obtain a good glassy sample using acetonitrile). Lifetime data in acetonitrile solution were in accordance with that measured by Kotova *et al*.[20] for the mixed ligand compound **10**, whereas frozen lifetime and PLQY were not measured before.

Table 2 Photoluminescence details of the investigated compounds at fixed wavelength of emission and excitation

compound	$\lambda_{exc\ (nm)}$	$\lambda_{em\ (nm)}$	Lifetime (ms) acetonitrile	Lifetime (ms) 1-propanol	PLQY acetonitrile	PLQY 1-propanol
compound **10**	296	543	1.04	1.02	4.86%	4.83%
compound **11**	296	543	0.98	Not accurate	4.48%	Not accurate

Before trying the annealing process in the EVA polymeric film, a solution in acetonitrile of compound **10** was prepared (Abs = 0.1 at 290 nm) and a series of measurements were taken after heating steps at 110°C. The purpose of this approach is to mimic the annealing process carried out by Utochnikova, which was done at the same temperature of 110°C, and detect the outcome of the experiment via PLQY measurements. The PLQY was measured after each heat treatment:

- room temperature: 5%
- after 15 minutes: 5%
- after 40 minutes: 4.4%
- after 60 minutes: 4.4%
- after 75 minutes: 3.9%
- after 90 minutes: 3.1%

What we expected to see was an increment of PLQY along with the longer heating treatment, meaning that the Hacim ligand had been removed. On the contrary, a constant decrease of PLQY is observed in solution sample emission. A possible explanation of these results is that the compound is not stable enough in solution at this high temperature for such long time and further degradation occurs.

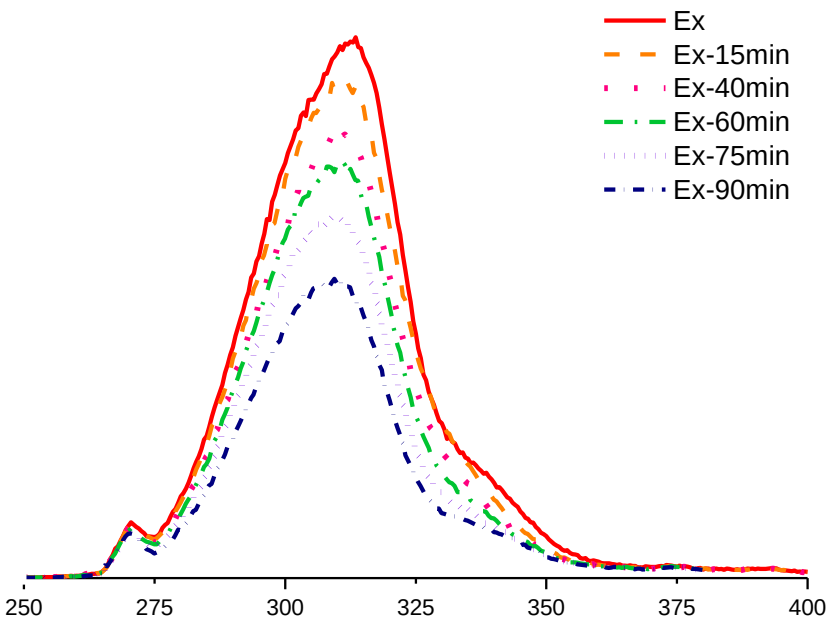

Fig. 5.12. Excitation spectra of compound **10** in acetonitrile during heating treatment (λ_{em}= 545nm).

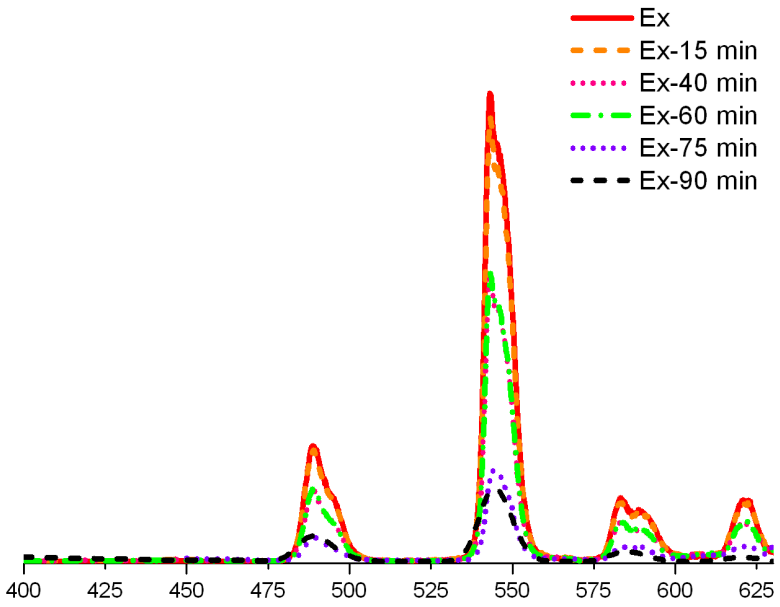

Fig. 5.13. Emission spectra of compound **10** in acetonitrile during heating treatment (λ_{ex}= 310nm)

Measuring EVA films of the compounds was our prime objective because of their potential application in LDS devices. The procedure we adopted consists of

dissolving the EVA pellets in toluene under continuous stirring at 110 °C. Once the polymer is well dissolved, the compound can be added.

Small portions of the solution were taken out at different intervals to prepare the films by pouring 100 µL of the solution in round moulds and leaving them to dry in the open air under the fume hood.

The PLQY was measured for each sample:

- immediately after addition: 31%
- after 15 minutes: 31%
- after 30 minutes: 31%
- after 40 minutes: 27%
- after 50 minutes: 22%
- after 60 minutes: 25%

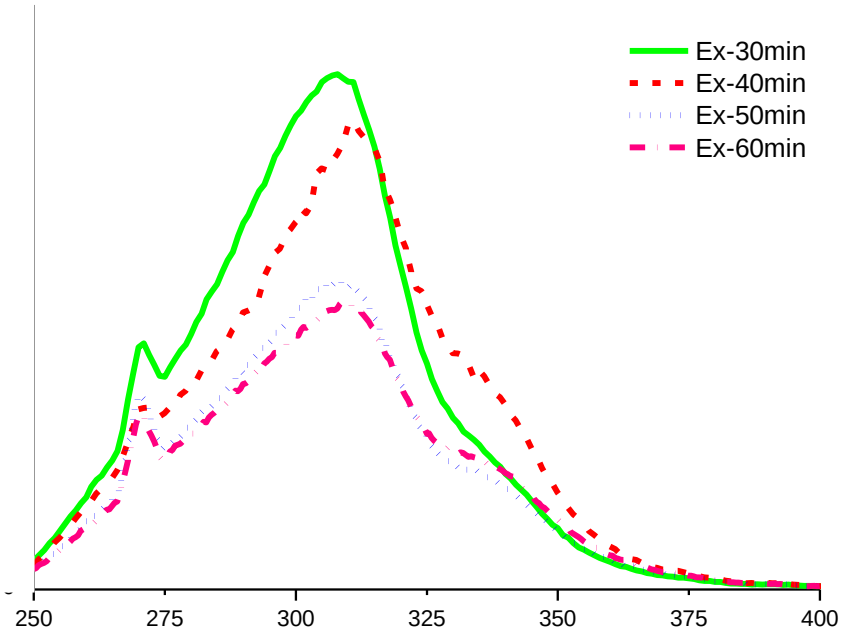

Fig. 5.14. Excitation spectra of compound **10** in EVA during heating treatment (λ_{ex}= 545nm).

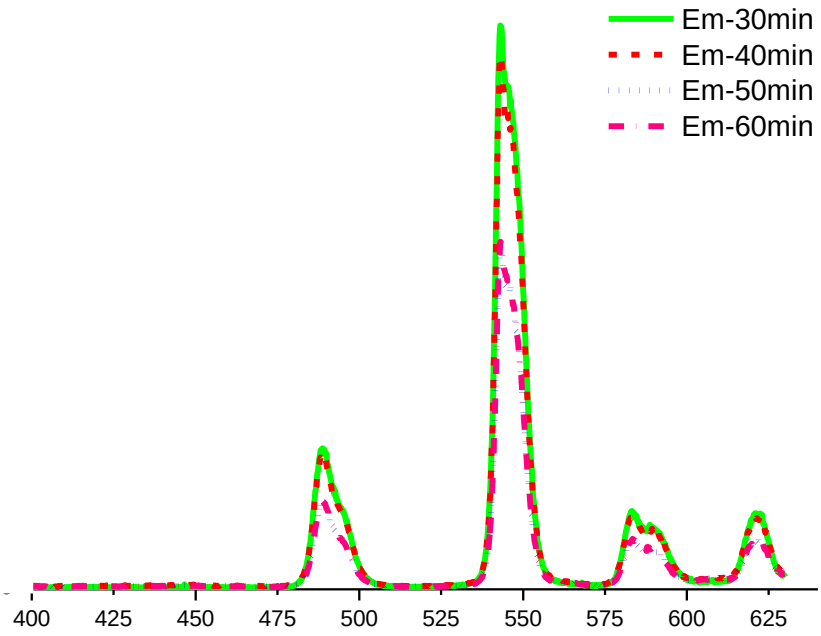

Fig. 5.15. Emission spectra of compound **10** in EVA during heating treatment(λ_{ex}= 310nm).

EVA film excitation spectra showed us the sequence of chemical transformation happening during heating, by the appearance of a shoulder in the excitation spectrum of compound **10** (red dashed line)**.** PLQYs are also affected from the heating time of the precursor solutions and a consistent decrease in yield was observed. Only a small increase was observed after 60 minutes, which stayed constant after 70 minutes, at a value of 25%. An improvement from 5% PLQY in solution to 25% PLQY in EVA was obtained, highlighting the polymer effect on the compound properties. The presence of EVA gave a more rigid environment to compound **10**, likely reducing vibrational deactivation and solvent or collisonal quenching.

Utochnikova[1] showed in her paper that during the annealing process of her films, differences in the excitation spectra were observed. In particular, an extra excitation band appeared in $Tb(pobz)_3(hacim)_2$ and then disappeared, showing the reformation of $Tb(pobz)_3$ as a free complex without the neutral organic ligand attached. In our case, the shoulder peak at 335 nm could be assigned to a related annealing chemical transformation. The PLQY continuously decreases until 50 minutes of heat treatment. From this point forward, two further films were possible to measure, one at 60 minutes of heating and another one at 70 minutes of heating but the PLQY was always 25%. Any further films prepared by heating for longer than 70 minutes were not good enough for emission measurements. The films were not clear and transparent anymore and possible scattering of light caused no detection of emission.

Once the films were measured a further processing and analysis was attempted. The films obtained were heated again on a steel plate in an oven at 110 °C to test their stability and to check whether the annealing process could be successfully pushed forward in order to achieve higher quantum yields. Unfortunately the films were not resistant to the treatment and after 15 minutes a mass reduction of the films was observed with consequent impossibility to obtain any further measurements.

5.3 Conclusions

This chapter describes work on two terbium mixed ligand compounds. $[Tb(pobz)_3(hacim)_2]$ (compound **10**) and $[Tb(bz)_3(hacim)_2]$ (compound **11**). More attention was paid to compound **10** because of its better solubility, hence higher possibility to prepare good films in EVA polymer.

PLQY in solution and EVA film was measured. The compound **10** solutions showed a low quantum yield compared to the EVA film probably due to the rigid environment of the polymer. Within the film measurements, some changes to the excitation spectrum were observed suggesting that the annealing mechanism occurred to give ligand loss. Although this suggests that the heating process did remove the neutral ligand (hacim), with extended treatment in time no further improvements were observed.

Improvements in film fabrication are possible. It could be possible to include the EVA film in a sandwich-shape mould, able to create a film thick enough not to contract under high temperature. Within the current approach however, PLQY of around 30% is not sufficient for practical application in LDS.

5.4 Experimental section

Absorption spectra were recorded with a Cary Varian UV/Vis spectrophotometer.

Emission spectra for the room temperature solutions were measured by an Edinburgh Instrument FS920 spectrometer. Excitation light was delivered with a 450W Xenon lamp via double monochromators to the sample chamber and the emission was detected by a Peltier cooled R2658P Hamamatsu photomultiplier.

The photoluminescence quantum yield measurements were performed at room temperature in air-equilibrated acetonitrile solution (reagent grade from Fischer Scientific).

Frozen emission measurements were measured by Fluoromax-3 in 1-propanol (reagent grade from Alfa Aesar).

EVA (DuPont™ Elvax® PV 1650) was purchased from DuPont™ in pellets.

Inclusion of compound 10 in EVA polymer

0.200 g of EVA were dissolved in 2 ml of toluene under continuous stirring at 110°C for half an hour. Compound **10** (2.5 mg) was dissolved in the minimum amount of toluene and added to the EVA solution. Part of the solution was poured into a mould to obtain disk-shape solid sample. The same procedure was used every 10 minutes step until 70 minutes.

5.5 References

1. Utochnikova, V., Kalyakina, A., and Kuzmina, N., *Inorg. Chem. Comm.*, 2012. **16**(0): p. 4.
2. Pope, M., Kallmann, H.P., and Magnante, P., *J. Chem. Phys.*, 1963. **38**(8): p. 2042.
3. Segura, J.L., *Acta Polym.*, 1998. **49**(7): p. 319.
4. Baldo, M.A., O'Brien, D.F., and Forrest, S.R., *Structure for high efficiency electroluminescent device*. 2000, Google Patents.
5. Bünzli, J.C.G. and Piguet, C., *Chem. Soc. Rev.*, 2005. **34**(12): p. 1048.
6. So, F., Kido, J., and Burrows, P., *MRS bulletin*, 2008. **33**(07): p. 663.
7. D'Andrade, B.W. and Forrest, S.R., *Adv. Mater.*, 2004. **16**(18): p. 1585.
8. Sun, Y., Giebink, N.C., Kanno, H., Ma, B., Thompson, M.E., and Forrest, S.R., *Nature*, 2006. **440**(7086): p. 908.
9. Chen, C.H. and Shi, J., *Coord. Chem. Rev.*, 1998. **171**(0): p. 161.
10. Bünzli, J.C.G., Andre, N., Elhabiri, M., Muller, G., and Piguet, C., *J. Alloys Compd.*, 2000. **303**: p. 66.
11. Zhao, Q., Jiang, C.-Y., Shi, M., Li, F.-Y., Yi, T., Cao, Y., and Huang, C.-H., *Organometallics*, 2006. **25**(15): p. 3631.
12. Katkova, M.A. and Bochkarev, M.N., *Dalton Trans.*, 2010. **39**(29): p. 6599.
13. Kido, J. and Okamoto, Y., *Chem. Rev*, 2002. **102**(6): p. 2357.
14. Eliseeva, S.V. and Bünzli, J.C.G., *Chem. Soc. Rev.*, 2010(39): p. 189.
15. Kotova, O., Utochnikova, V., Samoilenkov, S., and Kuzmina, N.P., *ECS Trans.*, 2009. **25**(8): p. 1107.
16. Hovel, H.J., Hodgson, R.T., and Woodall, J.M., *Sol. Energy Mater.*, 1979. **2**(1): p. 19.
17. Gmelin, I. and Berlin-Heidelberg-N.-Y.-Tokyo, *Handbook of Inorganic Chemistry*. Vol. 39. 1984. 95.
18. Klampaftis, E., Ross, D., McIntosh, K.R., and Richards, B.S., *Sol. Energy Mater.*, 2009. **93**(8): p. 1182.
19. Czanderna, A.W. and Pern, F.J., *Sol. Energy Mater.*, 1996. **43**(2): p. 101.
20. Kotova, O.V., Utochnikova, V.V., Samoylenkov, S.V., Rusin, A.D., Lepnev, L.S., and Kuzmina, N.P., *J. Mater. Chem.*, 2012.

Chapter 6: Potassium Coronene Tetracarboxylate and its interaction with Europium (III)

6.1 Introduction

The work described in this chapter concerns the analysis in solution, in the solid state and as a ligand for Eu(III), of a coronene salt, potassium coronene tetracarboxylate (from now on called compound **12**), prepared by Ravichandran Shivanna at the Jawaharlal Nehru Center for Advanced Scientific Research laboratories, in India.

Coronene belongs to the polycyclic aromatic hydrocarbons (PAH). PAH are materials really abundant on earth by natural combustion of organic substances, fossil fuels, and they are suspected to be carcinogens and mutagens.[1] PAH are interesting compounds from a photophysical point of view. Their absorption spectrum is usually characterised by very defined vibronic structure, because the carbon skeleton gives rise to symmetric oscillations. Usually their absorption wavelength is related to their π conjugation: the larger the conjugation, the lower is the energy spacing between HOMO and LUMO, hence a more red-shifted absorption spectrum is observed.[2] Fluorescence is typically observed at room temperature and shows quite defined spectra, with broadening occurring in the case of adsorption of the compound onto surface due to aggregation.[3-5] Phosphorescence

is present but usually quenched when compounds are analysed in solution or at room temperature, due to oxygen or collisional quenching, which deactivates the long-lived triplet state. The rigidity of matrix in which the PAH can be included retards the usual non-radiative decay and inhibits oxygen quenching.[6] Coronene and other PAH have been studied for applications in materials science[7] and optical communications[8] because of their intrinsic lifetime of phosphorescence which can last several seconds.[6, 8] With the increasing interest in optically-active devices and solar conversion systems, doped materials with appropriate chromophores are always a significant field of study as reported previously in the Introduction. Its structure with seven aromatic rings gives coronene high stability due to its aromatic delocalization across the six outer rings, and it can be used as a charge-transport material. Coronene is known as an electron rich molecule but its carboxylate derivative is electron deficient and could easily promote charge transfer. Tetracarboxylate coronene has been widely used in donor-acceptor systems as an acceptor to promote charge transfer with high quantum yield.[9, 10]

The decision to study photophysical properties of compound **12** rose looking at its peculiar characteristics, such as its absorption across much of the UV region, its long-lived excited state that increases the opportunity of efficient energy transfer to lanthanide ions, and good anchoring groups like carboxylates, which enable strong bonding to lanthanides.[11, 12] The properties of this compound were studied first in solution then in polymer in order to explore its relevance to Luminescent Down-shifting Technology (LDS).

6.2 Results and discussion

The figure below shows the structure of compound **12** and polyvinyl alcohol (PVA - average MW = 130,000). PVA is a dielectric material that we used to include the compound in order to measure the properties in the solid state, thin-film form that is relevant to LDS applications. Using water as a solvent was the only option available since compound **12** is very hydrophilic, due to the presence of four carboxylate groups, and no other common organic solvents were able to dissolve it. Therefore, the choice of the polymer was also due to the water affinity properties and PVA is the ideal matrix to use. PVA is also optically transparent in the near UV and visible regions and oxygen repellent, which is an important factor for luminescence properties.

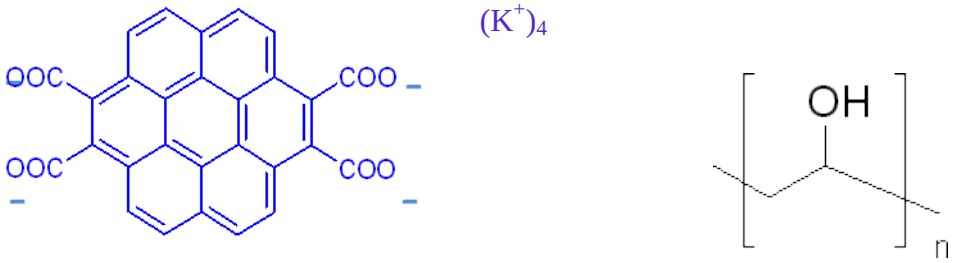

Fig. 6.1. Molecular structure of potassium coronene tetracarboxylate salt (compound **12**) and PVA.

6.2.1 UV/Vis Absorption Spectroscopy

A water solution of compound **12** was prepared (2.8×10^{-3} M) and different dilutions were made to measure the UV/Vis absorption spectrum. From the Fig. 6.2, we can confirm that no aggregation was detected at these concentrations.

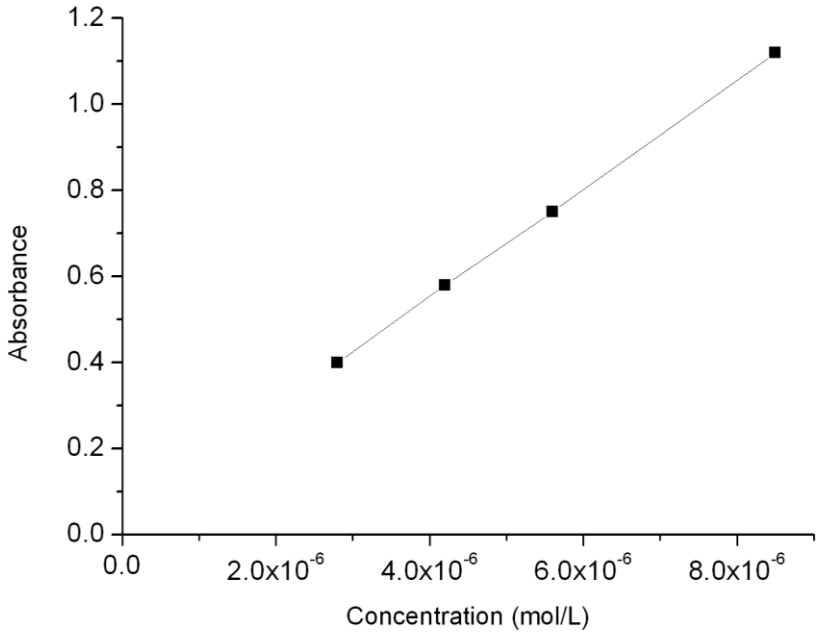

Fig. 6.2 Beer-Lambert plot for compound **12** in water solution.

Two peaks and three shoulders were detected in our compound in the absorption spectrum. Values are shown in Table 1.

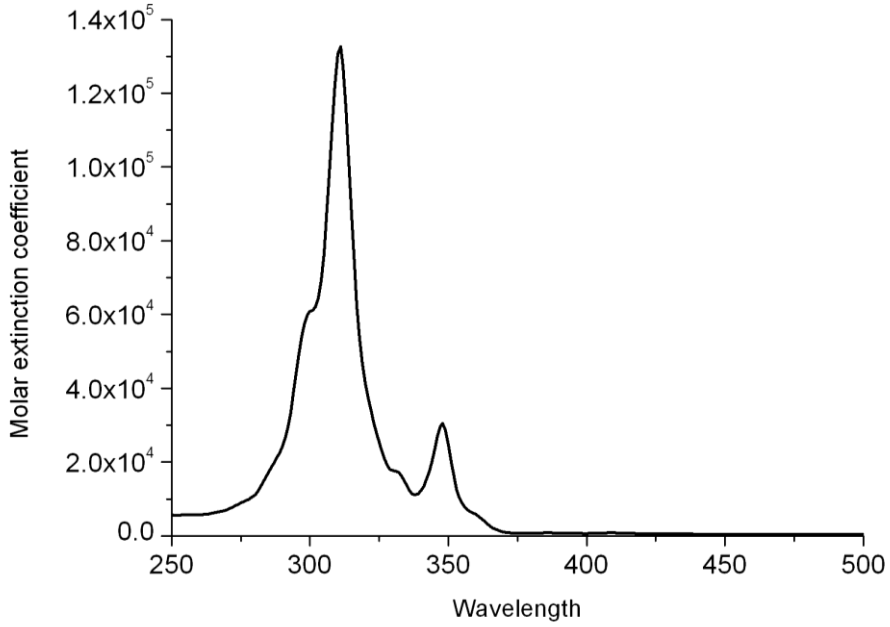

Fig. 6.3. Absorption spectrum of compound **12** in water solution ($8.5 \cdot 10^{-6}$ M).

Table 1 Absorption peaks in water solution and PVA and molar extinction coefficient (ε) in solution.

	λ_{abs} in solution	λ_{abs} in PVA[b]	Molar Extinction Coefficient (ε) in solution
Peak 1	299 nm$^{(sh)}$	304 nm	60000 M^{-1} cm^{-1}
Peak 2	311 nm	316 nm	132000M^{-1} cm^{-1}
Peak 3	331 nm$^{(sh)}$	336 nm	17000 M^{-1} cm^{-1}
Peak 4	348 nm	352 nm	30000 M^{-1} cm^{-1}
Peak 5	360 nm	365 nm	5800 M^{-1} cm^{-1}

Patterson reported the UV/vis spectrum in chloroform of pure coronene, obtaining a value of ε in the order of 270000 M^{-1} cm^{-1} for the absorption peak maxima at 305 nm[13] and Lhoste reported an analogous value for a peak at 300 nm (ε = 250000).[14] The differences we should take into account when analysing these values are the presence of four carboxylate groups in our molecule (whereas in literature it was pure coronene) and the different solvent used (water instead of chloroform).

Spin- coated film was prepared mixing 100 μL of **12** in water solution (2 mM) with 100μL of PVA in water (10 mg/mL). The spin coating was done in one step for 1 minute at 1000 RPM.

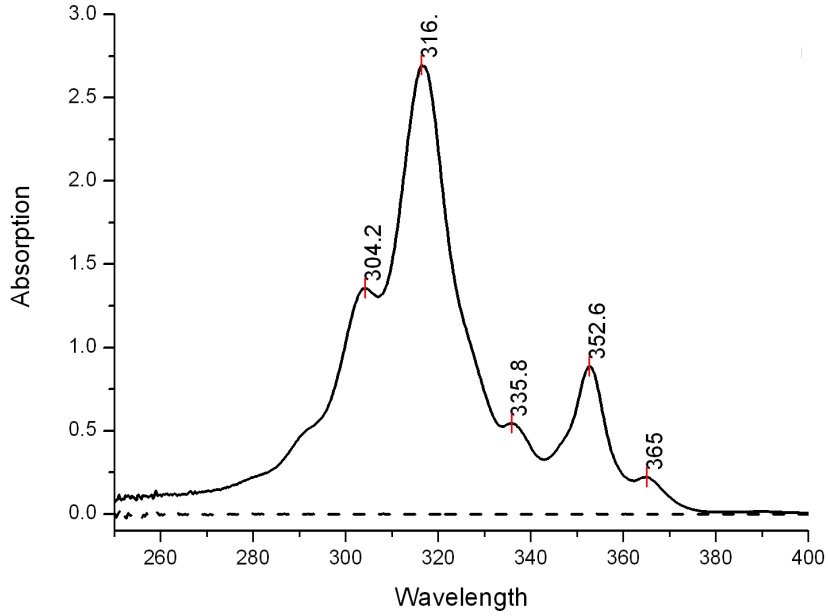

Fig. 6.4. Absorption spectrum of spin-coated compound **12** (2 mM) in PVA matrix.

Fig. 6.4 shows 3 peaks and 3 shoulders, in accordance with the solution absorption. Red shifting of the position of the peaks is observed in the film absorption spectrum compared to the solution one. In fact inclusion in the PVA matrix does affect the compound behaviour, compared to the water solution, but no peaks of PVA itself are detected as shown in Fig. 6.4.

A comparison between the absorption spectrum of compound **12** in PVA film and in water solution was made. Fig. 6.5 below shows that absorption in solution (red line) has sharper structured bands compared to the film (black line). Moreover, the comparison demonstrates that the film spectrum is red shifted with respect to the solution spectrum, indicating possible aggregation of the material in the solid state.

It is worth to point out that the shift to longer wavelength in the film leads to enhanced light harvesting over the UV range.

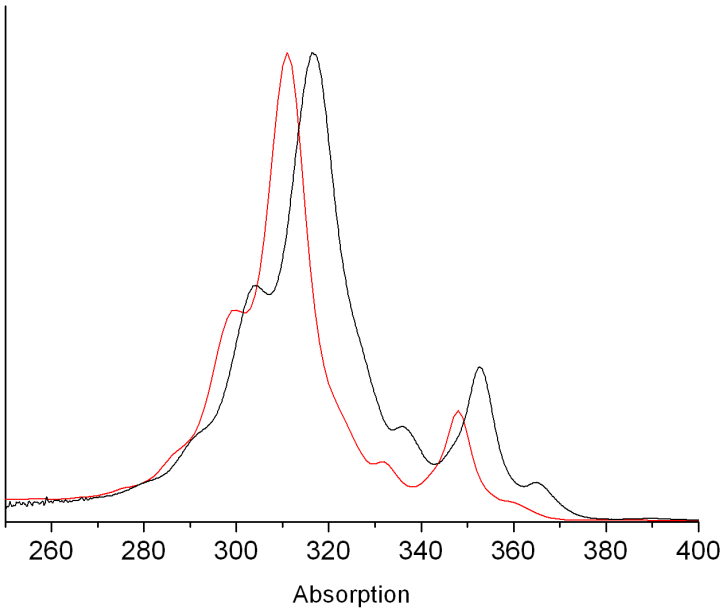

Fig. 6.5. Normalised absorption spectra of **12** in PVA film (black line) and in water solution (red line)

6.2.2 Photoluminescence studies

Emission spectra were recorded for the solution of compound **12** in water and in PVA. A degassed solution of **12** in water with concentration 1.4×10^{-7} M was used for emission spectroscopy. Fig. 6.6 presents the emission spectrum obtained exciting at 311 nm, whereas the excitation spectrum was detected at the emission wavelength of 440 nm. Variation in the range of the excitation wavelength did not affect the shape of the emission spectrum of compound **12**. During the measurements no change in the long-wavelength part of the spectrum was observed, which means that no aggregation occurred at this concentration consistent with the Beer-Lambert plot.

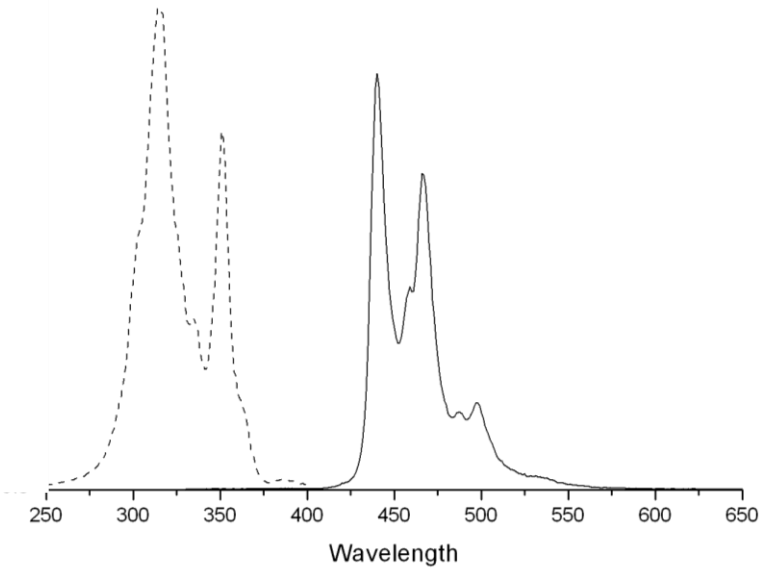

Fig. 6.6. Excitation (dash line) and emission (straight line) spectra of **12** in degassed water solution.

Following study of the luminescence data in water solution, the photoluminescence of compound **12** was further analysed in PVA films. A 2.4×10^{-4} M water solution of compound **12** was prepared and mixed 1:1 with PVA in water (10 mg/mL), then 100μL of the mixture were spin-coated onto clean glass in one step for 1 minute at 1000 RPM.

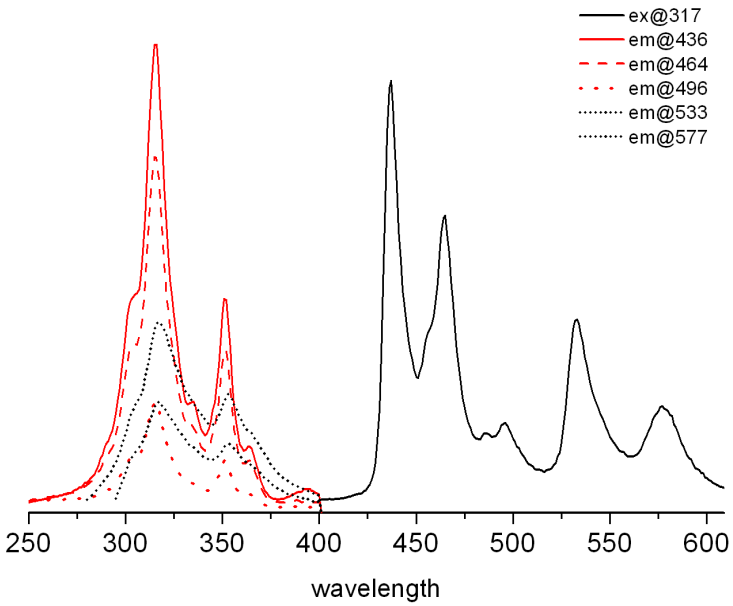

Fig. 6.7. Excitation/emission spectra of **12** in PVA.

Fig. 6.7 above shows the emission spectrum of the compound **12** film in PVA excited at 317 nm. The emission spectrum is divided in two areas: the first one covers 425 to 520 nm (23500 to 19200 cm^{-1}), and the second one is above 500 nm (20000 cm^{-1}). It is clear that the new bands at 533 nm (18700 cm^{-1}) and 577 (17300 cm^{-1}) nm can be assigned to aggregation of the material in the solid state. The excitation part of the spectrum is marked with two different colours. The black lines were obtained observing emission wavelengths above 500 nm, in the aggregation region, which are definitely less intense and slightly red shifted with a different low-energy features from the red ones. This is clear sign of aggregation of material.

In order to evaluate the efficiency of the luminescence process, we measured the photoluminescence quantum yield (PLQY) of compound **12** in solution and films. The values are displayed in the table below. All the solutions were first degassed before measurements. According to the data, solutions of different concentration maintain the same photoluminescence efficiency.

Table 2 Photoluminescence data of compound **12** in degassed water solution.

	Concentration	λ_{ex}	PLQY
Solution 1	8.5×10^{-5} M	315 nm	2%
Solution 2	5.6×10^{-6} M	315 nm	3%
Solution 3	4.2×10^{-6} M	315 nm	3%
Solution 4	2.8×10^{-6} M	315 nm	3%

Table 3 Photoluminescence data of compound **12** in solid state (giving [PVA] = (10mg/mL).

	Water solution concentration of **12** in spin-coated films in PVA matrix	λ_{ex}	PLQY
Film 1	6×10^{-3} M	315 nm	7%
Film 2	1.5×10^{-3} M	315 nm	17%
Film 3	6×10^{-4} M	315 nm	31%
Film 4	3×10^{-4} M	315 nm	43%
Film 5	1.8×10^{-4} M	315 nm	NA
Film 6	1.2×10^{-4} M	315 nm	NA

Comparison between solution PLQY and solid state PLQY proves that emission in solution, although free from oxygen is rapidly quenched, whereas a rigid matrix prevents this from happening to the same extent. Formation of aggregates,[17] as clearly occurs in the formation of the film, also leads to the quenching of light emission[18] as is shown in the table above. Too dilute concentration (films 5 and 6) were not sufficient to obtain a suitable film for PLQY measurements, because emission counts were too low for accurate data collection. However, the trend showed in the experiment was that the lower the concentration of the film, the higher the PLQY. Values around 65% for coronene films sublimed onto glass plates have been reported in the literature.[19] Spin-coated films in PMMA from high-diluted solutions of coronene gave instead PLQY of about 20%,[20] which is in the range of what we found for PVA films, although significantly lower than our highest values.

Attempts to measure lifetime of compound **12** both in solution and film were made, but when performing the analysis it was not possible to obtain a decay curve. A horizontal line was observed instead. A simple trial was then made in the laboratory. A solution of **12** in water was illuminated with a UV lamp in a dark box and it was possible to observe by eye a residual luminescence coming from the sample. Evidence of long lifetime was also reported by Schulman[6] who reported phosphorescence in the dark for over 5 sec in a sample of 2-napthoic acid when exciting it under an ordinary light.

Further experiments to investigate whether coronene is a suitable ligand for lanthanide sensitisation were carried out. As already mentioned in Chapter Three, it is known that lanthanide ions behave as hard acids with strong affinity for hard bases. The four carboxylate groups present on compound **12** can definitely provide a good bridging site for lanthanide bonding and sensitisation.

In situ emission was studied with **12** used as a sensitising ligand for one of our lanthanide molecules, $[Eu(hfac)_3(H_2O)_2]$. Solutions of **12** and Eu complex in water were prepared ($2.4x10^{-4}$ M), then mixed in a 1:1 ratio of the two to perform emission spectroscopy but no emission was observed in a steady state experiment. Unfortunately coronene salt is not soluble in any solvent except water and the lanthanide molecule emission is highly quenched in this solvent. An attempt to dissolve **12** in different organic solvents (i.e. ethanol, methanol, dichloromethane, benzene, chloroform) using the 18-crown-6 to make it more soluble was unsuccessful, therefore the *in situ* emission was not possible to be measured.

Since the presence of water is a drawback for such experiments, because of its ability to quench luminescence of the lanthanide, measurements were attempted in PVA films. Indeed, measurement in a polymer host is also the experiment directly relevant to application in LDS films. 100μL of **12** and Eu (both $2.4x10^{-4}$ M) were prepared and mixed together with 100μL of PVA in water solution (10mg/mL), then spin coated onto a glass slide in order to remove all residues of solvent possible. A

control sample containing only compound **12** at the same concentration was also measured. Fig. 6.8 below shows the results.

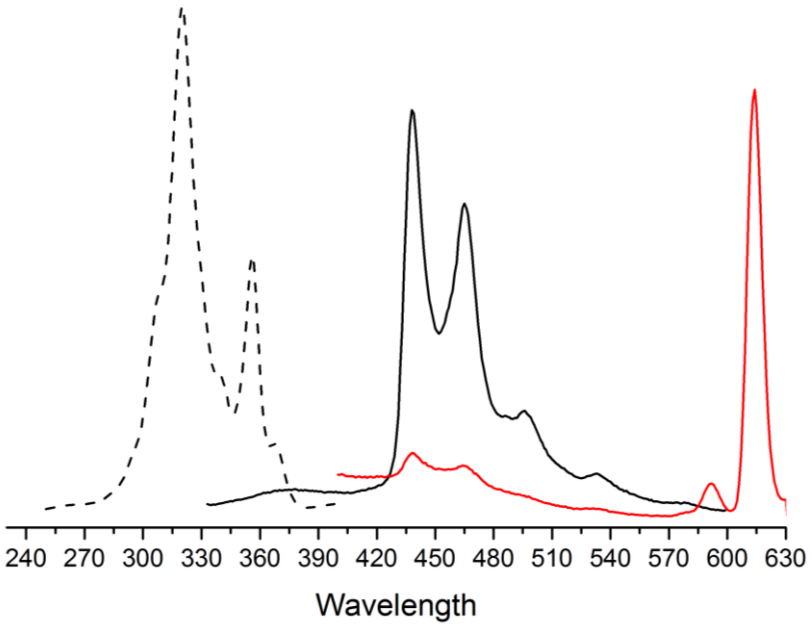

Fig. 6.8. Excitation spectrum of **12** and emission spectra of **12** and Eu in PVA: excitation spectrum (dash line); coronene emission (black line); europium emission (red line).

The film of compound **12** alone was excited at 317 nm to check coronene emission, which was detected as expected at 438 nm, 464 nm, 496 nm and 531 nm, as shown in the Fig. 6.8 above. Secondly, the mixed-complex film was measured again exciting at 317 nm and emission of Europium (613 nm) was detected with the large majority of the coronene emission quenched (low pass filter were not available to avoid the 2nd harmonic peak and the spectrum was cut off before it). Considering that for achieving an efficient sensitisation of Europium we need that the ligand triplet energy level is at least 2500 cm^{-1} higher (at ~19000 cm^{-1}) than the Eu excited state (590

nm, 16900 cm^{-1}), compound **12** has actually a suitable triplet level for energy transfer, which is at about 25000 cm^{-1} (400 nm). The efficient energy transfer is likely due to very long excited state lifetime of coronene, which favours energy transfer and emission from Eu, as this is faster than coronene excited state decay.

6.3 Conclusions

This chapter focused on the photophysical characterisation of potassium coronene tetracarboxylate salt in order to have a better understanding of its properties and its possible further application in material science, in particular as a sensitising ligand for lanthanide emission.

Absorption spectra showed high molar absorptivity and differences between solution and solid state data. Broadness and red shifted spectra in the solid state, indicate aggregation of the material compared to the solution data. This is confirmed by emission spectroscopy with the presence of two new peaks above 500 nm. Aggregation in PVA films at higher concentrations give rise to reabsorption effects and quenching of luminescence, as shown in the analysis of PLQY. Decrease in luminescence efficiency is proportional to the increase in concentration of the solution used for spin coating.

Qualitative measurements of energy transfer between coronene and europium compound showed successful energy transfer leading to a Eu emission peak when exciting at coronene absorption wavelength. It was confirmed that coronene ligand is better than DPEPO and hfac ligands (studied in Chapter Three) and absorbs across nearly the whole UV region. This can be a starting point for future molecular assemblies in order to design lanthanide complexes with coronene-like ligands to use for LSC technology.

6.4 Experimental section

Absorption spectra were recorded with a UV/Vis/NIR spectrophotometer Jasco V-670. Emission spectra at room temperature in water and in the solid state were measured by FluoroMax-3. Excitation light was delivered with a 150 W Ozone-free xenon arc lamp and the emission was detected by R928P photo counting PMT (185-850 nm).

Emission spectra for the room temperature photoluminescence quantum yield solutions were measured by an Edinburgh Instrument FS920 spectrometer. Excitation light was delivered with a 450W Xenon lamp via double monochromators to the sample chamber and the emission was detected by a Peltier cooled R2658P Hamamatsu photomultiplier. The photoluminescence quantum yields were determined by absolute measurement, by using a Horiba Jobin Yvon integrating sphere.

Solid state films were measured using a solid sample holder and the film angle was at 30° with respect to the incident light.

Spin coating was performed with a Spin Coater by Laurell Technologies (Model WS-65OS-6NPP/LITE).

PVA was used as water-soluble synthetic polymer to prepare compound **12** films.

It was prepared dissolving 10 mg of PVA (Mowiol® 18-88 with MW ~ 131000) in distilled water and left to overnight stirring until dissolution. It was then mixed in

1:1 ratio with the solution of **12** (normally 100 μL of each) and spin coated in one step for 1 minute at 1000 RPM.

6.5 References

1. Nijegorodov, N., Mabbs, R., and Downey, W.S., *Spectroc. Acta Part A*, 2001. **57**(13): p. 2673.
2. Dabestani, R. and Ivanov, I.N., *Photochem. Photobiol.*, 1999. **70**(1): p. 10.
3. Reyes, C., Sigman, M.E., Arce, R., Barbas, J.T., and Dabestani, R., *J. Photochem. Photobiol. A*, 1998. **112**(2): p. 277.
4. Dabestani, R., Nelson, M., and Sigman, M.E., *Photochem. Photobiol.*, 1996. **64**(1): p. 80.
5. Barbas, J.T., Sigman, M.E., and Dabestani, R., *Environ. Sci.Technol.*, 1996. **30**(5): p. 1776.
6. Schulman, E.M. and Walling, C., *J. Phys. Chem.*, 1973. **77**(7): p. 902.
7. Yoshimoto, S., Tsutsumi, E., Fujii, O., Narita, R., and Itaya, K., *Chem. Comm.*, 2005(9): p. 1188.
8. Smith, G.J., Dunford, C.L., Woolhouse, A.D., Haskell, T.G., and Barnes, T.H., *J. Photochem. Photobiol. A*, 2003. **154**(2-3): p. 267.
9. Ghosh, A., Rao, K.V., George, S.J., and Rao, C., *Chem. Eur. J.*, 2010. **16**(9): p. 2700.
10. Rao, K.V., Jayaramulu, K., Maji, T.K., and George, S.J., *Angew. Chem.*, 2010. **122**(25): p. 4314.
11. Couchman, S.M., Jeffery, J.C., Thornton, P., and Ward, M.D., *Dalton Trans.*, 1998(7): p. 1163.
12. Ward, M.D., *Ann. Rep. Sec. A (Inorg. Chem.)*, 2006. **102**: p. 584.
13. Patterson, J.W., *J. Am. Chem. Soc.*, 1942. **64**(6): p. 1485.
14. Lhoste, J.-M., Haug, A., and Ptak, M., *J. Chem. Phys.*, 1966. **44**(2): p. 654.
15. Lhoste, J.-M., Haug, A., and Ptak, M., *J. Chem. Phys.*, 1966. **44**(2): p. 648.
16. Brode, W.R. and Patterson, J.W., *J. Am. Chem. Soc.*, 1941. **63**(12): p. 3252.
17. Seko, T., Ogura, K., Kawakami, Y., Sugino, H., Toyotama, H., and Tanaka, J., *Chem. Phys. Lett.*, 1998. **291**(3â€“4): p. 438.
18. Chan, C.Y.K., Zhao, Z., Lam, J.W.Y., Liu, J., Chen, S., Lu, P., Mahtab, F., Chen, X., Sung, H.H.Y., Kwok, H.S., Ma, Y., Williams, I.D., Wong, K.S., and Tang, B.Z., *Adv. Funct. Mater.*, 2012. **22**(2): p. 378.
19. Inokuchi, H., Harada, Y., and Kondow, T., *J. Opt. Soc. Am.*, 1964. **54**(6): p. 842_1.
20. Fückel, B., Hinze, G., Wu, J., Müllen, K., and Basché, T., *ChemPhysChem*, 2012. **13**(4): p. 938.